Check for updates

Psychometrika (2026), **0**, 1–57
doi:10.1017/psy.2026.10143

PSYCHOMETRIC SOCIETY

THEORY AND METHODS

A Copula-Based Joint Model for Speed and Accuracy

Sunbeom Kwon[1] and Susu Zhang[2]

[1]Psychology, University of Illinois Urbana-Champaign, USA; [2]Psychology; Statistics, University of Illinois Urbana-Champaign, Champaign, USA

Corresponding author: Susu Zhang; Email: szhan105@illinois.edu

(Received 26 October 2025 UTC; revised 30 July 2026 UTC; accepted 30 July 2026 UTC)

Abstract

This study proposes a copula-based model that relaxes the multivariate normality assumption among latent traits in the joint modeling of multimodal data, such as item response and response times. In the structural model, the joint distribution of latent traits is defined via a copula with tail dependence. An expectation–maximization algorithm with stochastic approximation is implemented for parameter estimation. A simulation study evaluates the proposed method's accuracy in ability estimation under various conditions, comparing it to traditional approaches. By better capturing the dependence structure between latent ability and speed, the proposed method outperforms the traditional approach with multivariate normality assumption. Applied to a variety of empirical datasets, the proposed method's flexibility and the improvement in model fit are illustrated. The copula-based latent variable modeling can be generalized to broader applications in psychological testing involving multivariate latent traits.

Keywords: copula theory; hierarchical modeling; item response theory; response times; tail dependence

1. Introduction

In educational testing, item response theory (IRT) models are commonly used to estimate a test-taker's latent ability. With the widespread use of computerized testing, there has been a growing interest in using response time data as collateral information to improve the accuracy of ability estimates in IRT modeling (van der Linden et al., 2010). The most commonly adopted approach is the hierarchical modeling approach (van der Linden, 2007). At the first level, the conditional distributions of observed item responses and response times given the latent ability and speed are defined. At the second level, the latent traits are assumed to follow a multivariate normal (MVN) distribution, a convenient but often unrealistic assumption.

Poor model fit of the hierarchical model to empirical data has been discussed in the literature, suggesting that the dependence between responses and response times is not fully captured by the model (e.g., Bolsinova et al., 2017; Domingue et al., 2022; Liu & Wang, 2024). Alternative modeling approaches have been proposed to address these limitations (e.g., Bolsinova et al., 2017; Braeken et al., 2007; Kang et al., 2023; Liu & Wang, 2024). One line of research relaxes the conditional independence assumption between item responses and response times given the latent traits. For example, Bolsinova et al. (2017) explicitly model the conditional dependence (CD) between item response and response time by incorporating the residual log-response time as a covariate of the IRT model parameters.

© The Author(s), 2026. Published by Cambridge University Press on behalf of Psychometric Society.
This is an Open Access article, distributed under the terms of the Creative Commons Attribution-NonCommercial-ShareAlike licence (https://creativecommons.org/licenses/by-nc-sa/4.0), which permits non-commercial re-use, distribution, and reproduction in any medium, provided the same Creative Commons licence is used to distribute the re-used or adapted article and the original article is properly cited. The written permission of Cambridge University Press or the rights holder(s) must be obtained prior to any commercial use.

Downloaded from https://www.cambridge.org/core. 16 Nov 2026 at 02:13:47, subject to the Cambridge Core terms of use.

Kang et al. (2022, 2023) introduce diffusion IRT (DIRT) models that allow for CD between responses and response times by incorporating within-person variation in cognitive components into traditional IRT models. Another line of research tackles the parametric assumptions of the hierarchical model. For instance, Liu and Wang (2024) propose a semi-parametric factor analysis framework that more flexibly models the joint distribution of responses and response times.

This study addresses the potential violation of the structural multivariate normality assumption for latent traits, particularly when dependence is stronger at one extreme of the distribution. Modeling asymmetry has generated recent interest in the IRT literature, specifically regarding asymmetric item characteristic curves (Bolt & Liao, 2022; Lee & Bolt, 2018). However, this study focuses on the structural asymmetric dependence between latent traits. Asymmetric dependence between speed and accuracy can manifest at two distinct levels: within-person and population. At the within-person level, for instance, Domingue et al. (2022) analyzed 29 empirical cognitive test datasets and found a consistent pattern in the speed–accuracy trade-off. There is a larger variance in the lower tail, that is, individuals who receive lower estimates of ability tend to vary their speed more. On the other hand, at the population level (van der Linden, 2007), asymmetric dependence occurs when the strength of dependence between ability and speed varies across the latent spectrum, in particular, the dependence between speed and ability can be stronger at one extreme of the distribution than the other. The current study focuses on the population level, assuming that while an individual's latent speed is fixed across items, there is an asymmetric dependence between latent speed and ability across the population.

We present a copula-based joint model for speed and accuracy within the IRT framework. Rather than modeling conditional dependency between responses and response times, our approach addresses this model misfit by introducing a more flexible dependence structure between the latent traits themselves. The proposed model uses a copula function to specify the joint distribution of latent ability and speed, allowing for asymmetric, stronger tail-dependence structures as exemplified in Figure 1. This flexibility is expected to yield improved model fit with empirical data compared to the model based on the MVN distribution while preserving the original measurement models for the conditional distributions of item response and response times (e.g., two-parameter logistic model [2PL] and log-normal model).

Copula-based dependence models, particularly asymmetric and heavy-tailed copulas, have become powerful tools in econometrics, finance, and survival analysis, addressing limitations of traditional multivariate modeling approaches (see reviews by Genest et al., 2024 and Ghosh et al., 2020). In finance, for instance, copulas have been used to model default dependence between financial institutions (Zhang et al., 2024) and among bundled insurance risks (Shi & Zhao, 2024). Similarly, in survival analysis, they have been applied to model the dependence between tumor progression and patient mortality (Emura et al., 2017). A seminal turning point was the 2008 global financial crisis, which exposed critical flaws in relying on Gaussian copulas to model dependencies such as those among corporate defaults (Donnelly & Embrechts, 2010). During financial crises, corporate defaults occur in clusters, meaning the default of one company significantly increases the likelihood of defaults among interconnected companies. However, a key limitation of the Gaussian copula is its assumption of asymptotic independence in the extreme ends (Donnelly & Embrechts, 2010), meaning it is mathematically structured to model only weak or nonexistent relationships between variables at their most extreme values. This led to a systemic underestimation of joint risk, as empirical evidence showed strong tail dependencies during market collapses. In response, researchers increasingly adopted flexible copula-based models (e.g., Gumbel, Joe, and Student's t copulas; Demarta & McNeil, 2005; Gumbel, 1960; Joe, 1997, 2014; Nelsen, 2006) that can model tail dependence and joint extremes more accurately.

Due to their ability to flexibly model complex dependence structures, copulas offer considerable potential for psychometrics and latent variable modeling by addressing three key challenges: (1) capturing asymmetric tail dependencies, (2) modeling non-normal joint distributions, and (3) preserving marginal distributions while modeling flexible dependence structures that better reflect empirical data. Despite their substantial impact in other fields, applications of copulas in psychometrics remain limited. This study contributes to bridging this gap by adopting a copula-based approach within the context

Downloaded from https://www.cambridge.org/core. 16 Nov 2026 at 02:13:47, subject to the Cambridge Core terms of use.

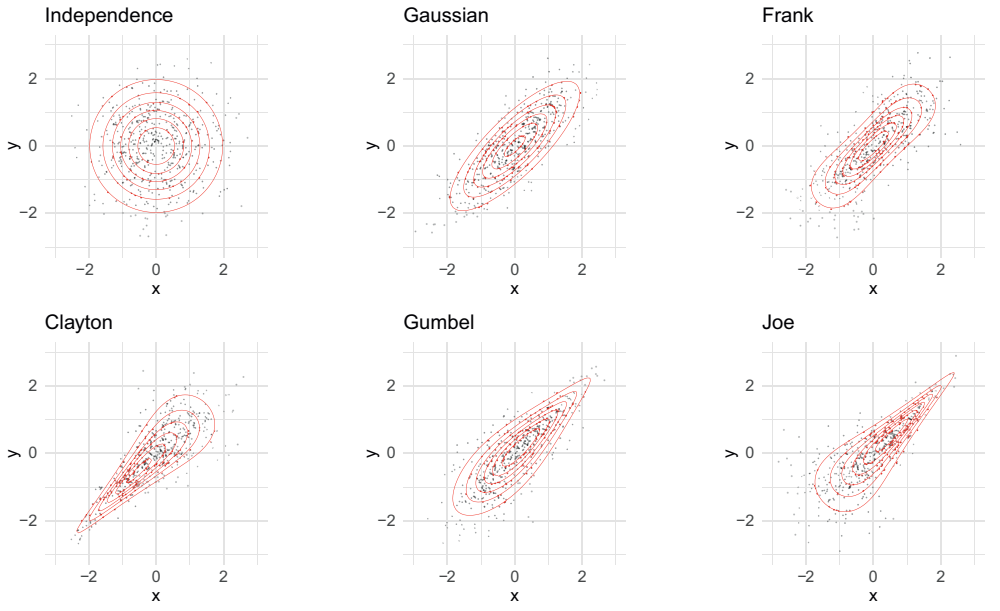


Figure 1. Bivariate distributions constructed with copula functions and standard normal margins.
Note: *X* and *Y* were simulated using a bivariate copula with standard normal marginal distributions. The red contours represent the bivariate density, and the dots indicate the randomly simulated data points.

of IRT. Recent methodological developments have begun to demonstrate the advantages of integrating copula theory into latent variable contexts. The following provides an overview of key studies that have applied copula methods in latent variable modeling.

The application of copula theory in latent variable modeling has developed along two main lines of research. One of the earliest uses of the copula in psychometric modeling focused on modeling local item dependencies that violate the conditional independence assumptions. Braeken et al. (2007) introduced copula-based methods for modeling residual dependencies between item responses in the Rasch model. Copula functions are used to model the residual dependencies within subsets of items. This copula-based approach for modeling residual dependency has been extended to structural equation modeling (SEM) with categorical indicators (Braeken et al., 2013) and to the deterministic input, noisy "and" gate (DINA; Haertel, 1989; Junker & Sijtsma, 2001) model for cognitive diagnosis (Fu et al., 2019). A key distinction of the current study is its application of copula functions to model the dependence between latent traits themselves, rather than between residuals.

Another line of research incorporating copulas into latent variable modeling focuses on dependence structures between item responses and latent traits within the traditional factor analysis framework. In their paper, Krupskii and Joe (2013) introduced a factor copula model where bivariate copulas are used to link continuous observed variables to uniformly distributed latent variables. They demonstrate that the classical factor model based on multivariate normality is a special case of their approach when the Gaussian copula is used. The copula factor model framework was extended to multivariate discrete data, such as item responses, in Nikoloulopoulos and Joe (2015). More recent work has further extended this framework to accommodate complex latent structures, such as bi-factor and second-order models using vine copulas (Kadhem & Nikoloulopoulos, 2023a, 2023b).

Our proposed work differs from prior work in that we use copulas to model the dependence between latent traits, rather than between the observed responses, while allowing each trait to follow its own distinct marginal distribution. A computational challenge in estimating copula-based latent variable models is the intractability of the marginal likelihood functions, with many prior works using

Downloaded from https://www.cambridge.org/core. 16 Nov 2026 at 02:13:47, subject to the Cambridge Core terms of use.

two-stage estimation methods, where parameters for the marginal distributions are estimated first and held fixed in the second step when estimating copula parameters (Kadhem & Nikoloulopoulos, 2023a, 2023b; Nikoloulopoulos & Joe, 2015). We propose an expectation–maximization (EM) algorithm (Dempster et al., 1977) with stochastic approximation (Robbins & Monro, 1951) that allows full-information marginal maximum likelihood (MML) estimation and direct derivation of joint posterior estimates of person-level latent traits, accompanied by a model selection method.

The remainder of this article is organized as follows. The next section provides a brief introduction to copula theory. It is followed by the proposed copula-based joint model for speed and accuracy. A Monte Carlo simulation study evaluates how the copula-based approach compares to the traditional hierarchical modeling approach with normal assumption under various dependency conditions. The proposed approach is illustrated with a variety of empirical cognitive test datasets. Next, we provide a theoretical and empirical comparison of the proposed model with the CD model. Finally, the implications and future directions are discussed.

2. Copula theory

Copula theory allows us to flexibly model a joint distribution of random variables by "coupling" together arbitrary univariate margins. A copula function C is a multivariate cumulative distribution function (CDF) defined on the unit cube:

$$C : [0,1]^J \to [0,1], \quad C(\mathbf{u}) = C(u_1, \ldots, u_J) = P(U_1 \le u_1, \ldots, U_J \le u_J), \tag{1}$$

where each U_j follows a standard uniform distribution, $\text{Uniform}(0,1)$. Sklar's theorem (Sklar, 1959) enables extending copula functions beyond uniformly distributed random variables using the fact that any univariate CDF is defined on the $[0,1]$ interval. Specifically, the theorem states that any multivariate CDF $F_{\mathbf{Y}}$ with univariate marginal CDFs, $F_{Y_1}, \ldots, F_{Y_J}$ can be reformulated by these marginal CDFs and a copula function C as

$$F_{\mathbf{Y}}(y_1, \ldots, y_J) = C\big(F_{Y_1}(y_1), \ldots, F_{Y_J}(y_J)\big). \tag{2}$$

In the continuous case, the reformulation of a multivariate CDF in Equation (2) is unique; in contrast, in the discrete case, it is uniquely defined only on the range of the margins.

The theorem also states that a new multivariate distribution can be constructed from a given set of univariate margins $F_{Y_1}, \ldots, F_{Y_J}$, coupled together through a copula function C to define the joint CDF. Therefore, a modeling approach can begin by choosing univariate margins that are well-suited to the problem, and then constructing a joint dependence structure by coupling these margins with an appropriate copula function. This is possible because copula constructions preserve the univariate margins as below:

$$C(1, \ldots, 1, F_{Y_j}, 1, \ldots, 1) = F_{Y_j}. \tag{3}$$

Then, under the copula framework, the multivariate probability density function (PDF) can be factorized as a product of univariate PDFs and the copula density:

$$f(\boldsymbol{Y}) = c(F_{Y_1}, \ldots, F_{Y_J}) \prod_{j=1}^{J} f(Y_j), \tag{4}$$

where the copula density function c is

$$c = \frac{\partial^J C}{\partial F_{Y_1} \ldots \partial F_{Y_J}}. \tag{5}$$

Further details on the properties and construction of copula functions can be found in Joe (2014) and Nelsen (2006).

Downloaded from https://www.cambridge.org/core. 16 Nov 2026 at 02:13:47, subject to the Cambridge Core terms of use.

Table 1. Examples of copula functions

Copula	$C(\mathbf{u};\cdot)$
Independence	$C(\mathbf{u}) = \prod_{j=1}^{J} u_j$
Gaussian	$C(\mathbf{u};\Sigma) = \Phi_{\Sigma}^{J}\left(\Phi^{-1}(u_1),\ldots,\Phi^{-1}(u_J)\right)$
Frank ($\delta \neq 0$)	$C(\mathbf{u};\delta) = -\frac{1}{\delta}\log\left(1-\frac{\prod_{j=1}^{J}\left(1-e^{-\delta u_j}\right)}{\left(1-e^{-\delta}\right)^{J}}\right)$
Clayton ($\delta > 0$)	$C(\mathbf{u};\delta) = \left(\sum_{j=1}^{J} u_j^{-\delta} - J + 1\right)^{-1/\delta}$
Gumbel ($\delta \geq 1$)	$C(\mathbf{u};\delta) = \exp\left(-\left[\sum_{j=1}^{J}(-\log u_j)^{\delta}\right]^{1/\delta}\right)$
Joe ($\delta \geq 1$)	$C(\mathbf{u};\delta) = 1-\left[1-\prod_{j=1}^{J}\left(1-(1-u_j)^{\delta}\right)\right]^{1/\delta}$

Note: δ denotes the dependence parameter for Archimedean copulas, and Σ denotes the correlation matrix for the Gaussian copula. Φ is the CDF of the univariate standard normal distribution, and Φ_{Σ}^{J} is the CDF of the J-variate normal distribution with correlation matrix Σ.

Some examples of popular copula functions are provided in Table 1. The independence copula represents an independent case where the multivariate CDF is the product of the marginal CDFs. All other copulas include a dependence parameter δ that determines the strength of dependence between the random variables. As an illustration, Figure 1 displays bivariate distributions of x and y with different copulas with standard normal margins. In this figure, data were simulated so that Kendall's τ equals 0.6 for each case. In the bivariate case, δ and Kendall's τ are in one-to-one correspondence. Note that the Gaussian copula combined with univariate normal marginals yields the bivariate normal distribution with correlation matrix Σ. As an illustration, let X and Y be univariate normal random variables, $X \sim \mathcal{N}(\mu_X, \sigma_X^2); Y \sim \mathcal{N}(\mu_Y, \sigma_Y^2)$. Their respective marginal CDFs are defined using the CDF of the standard normal distribution Φ as $u_1 = F_X(x) = \Phi(\frac{x-\mu_X}{\sigma_X})$ and $u_2 = F_Y(y) = \Phi(\frac{y-\mu_Y}{\sigma_Y})$. Plugging in the marginal CDFs into a bivariate copula from Table 1, the joint CDF of X and Y is

$$\Phi_{\Sigma}^{2}\left(\Phi^{-1}\left[\Phi\left(\frac{x-\mu_X}{\sigma_X}\right)\right], \Phi^{-1}\left[\Phi\left(\frac{y-\mu_Y}{\sigma_Y}\right)\right]\right) = \Phi_{\Sigma}^{2}\left(\frac{x-\mu_X}{\sigma_X}, \frac{y-\mu_Y}{\sigma_Y}\right), \tag{6}$$

which is a bivariate normal distribution with means μ_X, μ_Y, variances σ_X^2, σ_Y^2, and correlation matrix Σ.

The shape of the Frank copula is similar to the Gaussian copula, as both have symmetric dependence, that is, the dependence structure is the same in the lower and upper tails of the distribution. Both copulas exhibit no tail dependence, which makes them less suitable for modeling dependencies in the extreme ends of the distribution. On the other hand, the Gumbel and Joe copulas have asymmetric dependencies with larger variance in one tail, and such a joint distribution modeling could better explain the relationship between the latent ability and the speed.

3. A copula-based joint model for speed and accuracy

This section presents the proposed copula-based joint model for speed and accuracy. As an alternative to the conventional hierarchical approach (van der Linden, 2007) with joint normality assumptions, the proposed model employs a copula function to flexibly model tail dependence between latent ability and speed at the second level. The following details the model specification and an MML estimation via an EM algorithm with stochastic approximation, followed by standard error and ability estimation.

Downloaded from https://www.cambridge.org/core. 16 Nov 2026 at 02:13:47, subject to the Cambridge Core terms of use.

3.1. Model specification

At the first level, the conditional distributions of the observed item responses and response times given the latent traits are specified. The choice of the measurement model is flexible. Here, we assume that the probability that examinee p answers item i correctly, given latent ability θ_p follows the 2PL model:

$$P(Y_{pi} = 1|\theta_p, a_i, b_i) = \frac{1}{1 + \exp\big(-a_i(\theta_p - b_i)\big)}. \tag{7}$$

And the observed response time T_{pi} of person p on item i follows a log-normal distribution with an item time intensity parameter β_i and time discrimination α_i, conditional on latent speed τ_p:

$$T_{pi} \sim \log\mathcal{N}(\beta_i - \tau_p, \alpha_i^{-2}), \tag{8}$$

with density

$$f(t_{pi}) = \frac{\alpha_i}{t_{pi}\sqrt{2\pi}} \exp\Big\{-\frac{1}{2}\big[\alpha_i(\log t_{pi} - (\beta_i - \tau_p))\big]^2\Big\}. \tag{9}$$

Item responses and response times are assumed to be independent conditional on the latent traits (θ_p, τ_p).

At the second level, we assume that the marginal distributions of the latent ability and speed factors follow normal distributions:

$$\begin{aligned} \theta_p &\sim \mathcal{N}(\mu_\theta, \sigma_\theta^2), \\ \tau_p &\sim \mathcal{N}(\mu_\tau, \sigma_\tau^2). \end{aligned} \tag{10}$$

For identifiability of the model, we set $\mu_\theta = \mu_\tau = 0$ and $\sigma_\theta^2 = 1$. The joint distribution of (θ_p, τ_p) is defined via a copula function C with a dependence parameter δ to model the asymmetric dependence between the latent ability and speed. Let F_θ and F_τ denote the CDFs of θ and τ. The joint CDF of θ and τ is

$$F_{(\theta,\tau)} = C(F_\theta, F_\tau; \delta). \tag{11}$$

For instance, if we employ a Gumbel copula to model upper-tail dependence, its copula function in the bivariate case (Table 1) is

$$C(u, v; \delta) = \exp\{-([-\log u]^\delta + [-\log v]^\delta)^{1/\delta}\}, \quad u, v \in [0, 1], 1 \le \delta < \infty. \tag{12}$$

Setting, $x = -\log u, y = -\log v$, the copula density is

$$c(u, v; \delta) = \exp\{-[x^\delta + y^\delta]^{1/\delta}\}[(x^\delta + y^\delta)^{1/\delta} + \delta - 1][x^\delta + y^\delta]^{1/\delta - 2}(xy)^{\delta-1}(uv)^{-1}. \tag{13}$$

From Equations (4) and (5), the joint PDF of (θ, τ) is

$$f_{\theta,\tau}(\theta, \tau \mid \sigma_\tau^2, \delta) = c(F_\theta(\theta), F_\tau(\tau) \mid \delta) f_\theta(\theta) f_\tau(\tau \mid \sigma_\tau^2), \tag{14}$$

where f_θ and f_τ denote the respective normal density functions.

Note that the traditional hierarchical model with multivariate normality assumption can be seen as a special case of the proposed framework when the marginal distributions of the latent traits are normal, and their joint distribution is defined via a Gaussian copula. In fact, this framework is general and supports a wide range of copula and marginal specifications. The Gumbel copula could be replaced with the Joe copula to model even stronger upper-tail dependence as detailed in Appendix B and implemented in this study. Alternatively, the Student's t copula could reflect symmetric tail dependence at both extremes. Similarly, the latent trait marginals are not restricted to a normal distribution. One might assume, for instance, a gamma distribution for speed to account for skewness (Maris, 1993), or any other form that best fits the data.

An EM algorithm (Dempster et al., 1977) with stochastic approximation (Robbins & Monro, 1951) for maximum marginal likelihood estimation is used. Details of the estimation algorithm and inference are described in Appendix A.

Downloaded from https://www.cambridge.org/core. 16 Nov 2026 at 02:13:47, subject to the Cambridge Core terms of use.

3.2. Rotated copulas

The standard Gumbel and Joe copulas only model positive association with upper-tail dependence. However, in practice, the association between latent traits could reflect a negative association (e.g., speed–accuracy trade-off) or lower-tail dependence, or both. In order to model different types of dependence structure, we use rotated copulas (Nelsen, 2006) as illustrated in Figure 2. For instance, rotating a Gumbel copula by 90° creates a negative association with lower-tail dependence, while a 270° rotation also creates a negative association but with upper-tail dependence.

Rotated copulas can be implemented by transforming the arguments u and v within the original copula functions, typically by replacing them with $1-u$ or $1-v$. For instance, a 270°-rotated copula, $C_{270}(u,v)$, is derived from its original copula function $C(u,v)$ as follows (Nelsen, 2006):

$$C_{270}(u,v) = u - C(u,1-v). \tag{15}$$

The corresponding copula density, $c_{270}(u,v)$, is then given by

$$c_{270}(u,v) = \frac{\partial^2}{\partial u \partial v} C_{270}(u,v) = \frac{\partial^2}{\partial u \partial v}\left[u - C(u,1-v)\right] = c(u,1-v). \tag{16}$$

Similarly, the 90°- and 180°-rotated copula functions are

$$\begin{aligned} C_{90}(u,v) &= v - C(1-u,v), \\ C_{180}(u,v) &= u + v - 1 + C(1-u,1-v), \end{aligned} \tag{17}$$

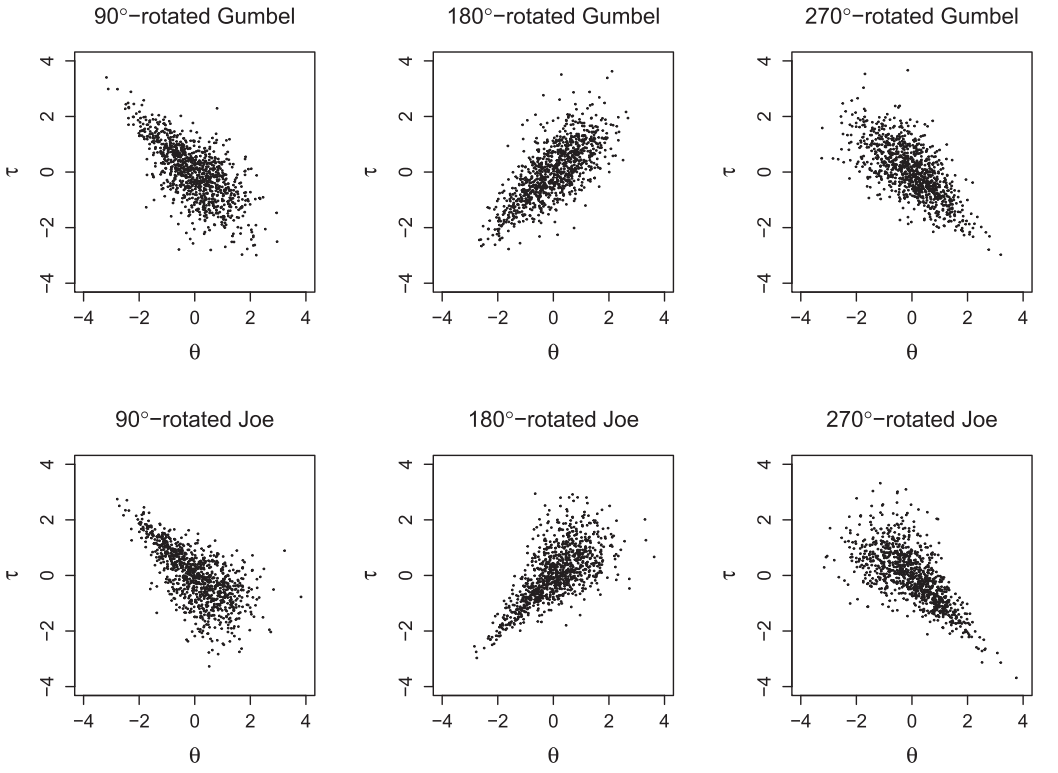


Figure 2. Bivariate distributions of latent traits under rotated copulas.
Note: The marginal distributions of θ and τ are standard normal, and the joint distributions are defined using rotated copulas.

Downloaded from https://www.cambridge.org/core. 16 Nov 2026 at 02:13:47, subject to the Cambridge Core terms of use.

with their respective densities being

$$\begin{aligned} c_{90}(u,v) &= c(1-u,v), \\ c_{180}(u,v) &= c(1-u,1-v). \end{aligned} \tag{18}$$

The gradients of the joint log-likelihood for the EM algorithm are derived for each rotated copula, as detailed in Appendix C. For model selection, likelihood-based criteria such as Akaike's information criterion (AIC; Akaike, 1998) or the Bayesian information criterion (BIC; Schwarz, 1978) can be used. However, because each bivariate copula in this framework has the same number of parameters, comparing their marginal likelihoods is sufficient to find the best-fitting model.

3.3. Functional complexity of bivariate copulas

Although the number of unknown parameters is equal between the MVN and the copula models, the complexity of the models can be explained beyond counting the number of parameters. This section compares the functional complexities of the bivariate copulas considered in this study. Specifically, we compare the bivariate Gaussian, Gumbel, and Joe copulas using the functional complexity penalty derived from the minimum description length (MDL; Hansen & Yu, 2001; Rissanen, 2002). MDL is defined as

$$\text{MDL} = -\ln(f(y \mid \hat{\Delta})) + (k/2)\ln(n/2\pi) + \ln \int_{\Delta} \sqrt{\det(I(\Delta))}\, d\Delta, \tag{19}$$

where Δ is the model parameter vector, $\hat{\Delta}$ represents the parameter values maximizing the likelihood, and $I(\Delta)$ is the Fisher information matrix. MDL accounts for three dimensions of model complexity: the number of parameters, sample size, and functional form (Pitt & Myung, 2002). The last term in Equation (19) quantifies this functional complexity. To compare the MVN and copula models, we calculate this term for the bivariate Gaussian, Gumbel, and Joe copulas with uniform margins. Because evaluating the full joint model for speed and accuracy is computationally intensive, we focus on the bivariate copulas, as they represent the only structural differences between the full joint models.

For a bivariate copula with copula density c and dependence parameter δ, the Fisher information is

$$I(\delta) = E\left[\left(\frac{\partial}{\partial\delta}\ln c(u,v;\delta)\right)^2\right] = \int_0^1\int_0^1 \left(\frac{\partial}{\partial\delta}\ln c(u,v;\delta)\right)^2 c(u,v;\delta)\,du\,dv. \tag{20}$$

For each bivariate copula, we calculated the complexity term:

$$\ln \int_{\delta} \sqrt{\det(I(\delta))}\, d\delta. \tag{21}$$

The integration domain depends on the parameter space of each copula: $\rho \in (-1, 1)$ for the Gaussian, and $\delta \in [1, \infty)$ for the Gumbel and Joe copulas. Analytical expressions for the Fisher information of bivariate Gaussian and Gumbel copulas are available (Schepsmeier & Stöber, 2014) but not for the Joe copula. In this analysis, the integrals in Equations (20) and (21) were approximated using numerical integration to maintain consistency across copulas. As a result, the functional complexity for the bivariate Gaussian copula was 1.99, while the complexities for the Gumbel and Joe copulas were 1.02 and 1.11, respectively. These results indicate that the functional form of the bivariate Gaussian copula is approximately twice as complex. The result is expected, as the bivariate Gaussian copula allows for both negative and positive dependence, whereas the Gumbel and Joe copulas only allow for positive dependence, doubling the fitting propensity of the Gaussian copula. Although the proposed copula-based approach involves a model selection step among rotated copulas, the final model used for parameter estimation employs a single bivariate copula. Admittedly, the process of evaluating multiple rotated models to determine the appropriate dependence direction increases the overall modeling complexity. However, because the evaluated copulas have a lower functional complexity than the Gaussian copula, any observed improvements in model fit of a final selected copula model over the MVN model cannot be merely

Downloaded from https://www.cambridge.org/core. 16 Nov 2026 at 02:13:47, subject to the Cambridge Core terms of use.

a byproduct of functional flexibility. Rather, such improvements would indicate that the selected copula captures the true underlying dependence structure.

4. Monte Carlo simulation study

In a simulation study, we compare the proposed copula-based models for speed and accuracy with the conventional model with MVN assumption (van der Linden, 2007) in terms of the accuracy of ability estimates. Random test data are generated under various conditions, including true dependence structure (asymmetric copulas vs. MVN), strength of dependence between latent traits, sample size, and test length. We evaluate the accuracy of the likelihood-based model selection in identifying the true data-generating model. The ability estimation accuracy is evaluated based on bias, root mean squared error (RMSE), and Pearson correlation with true abilities.

4.1. Simulation design

In $R = 500$ replications, the true latent ability θ_p and speed τ_p for N persons were randomly generated from a Gumbel or Joe copula (both with normal margins) or an MVN distribution. The marginal distribution of θ_p was a standard normal, and the marginal distribution of τ_p was a normal with mean 0 and variance $\sigma_\tau^2 = 0.25$ as in Guo et al. (2022). Two levels of latent trait dependence were considered, corresponding to Kendall's $\tau = 0.3$ and 0.5, representing moderate and strong dependence, respectively. The transformations to the copula dependence parameters (Joe, 1997, 2014) are as follows. For the Gumbel copula,

$$\delta = -1/(\text{Kendall's } \tau - 1). \tag{22}$$

That is, Kendall's τ values of 0.3 and 0.5 correspond to dependence parameter values $\delta = 1.43$ and $\delta = 2$, respectively. For the Joe copula, there is no closed-form expression for $\delta(\tau)$. Instead, one finds δ numerically by solving

$$\text{Kendall's } \tau = 1 + 2(2-\delta)^{-1}[\text{digamma}(2) - \text{digamma}(2/\delta + 1)], \tag{23}$$

where $\text{digamma}(z) = \frac{d}{dz}\log\Gamma(z)$. This is implemented in the `copula` R package (Hofert et al., 2025). Kendall's τ values of 0.3 and 0.5 correspond to $\delta = 1.77$ and $\delta = 2.86$, respectively, under the Joe copula. For the Pearson correlation ρ in a bivariate normal distribution, we have

$$\rho = \sin\left(\frac{\pi}{2}\text{Kendall's } \tau\right). \tag{24}$$

Figure 3 displays the bivariate distributions of the latent traits randomly generated under each dependence condition.

Item responses and response times on I items, conditional on the latent traits, were randomly generated from a 2PL model in Equation (7) and a log-normal model in Equation (8), respectively. The number of persons was $N = 500$ or $1,000$, and the number of items was $I = 10$ or 20. The true item parameter values were set according to the parameter estimates from the empirical data on the 2018 Programme for International Student Assessment (PISA) science assessment reported in Guo et al. (2022) and were held fixed across replications (Table 2). In the $I = 10$ condition, the first 10 items were used. In summary, the simulation design resulted in 24 conditions, including three dependence types (Gumbel, Joe, and MVN), two dependence strengths (Kendall's $\tau = 0.3, 0.5$), two sample sizes ($N = 500, 1,000$), and two test lengths ($I = 10, 20$).

Three models were fit to the data in each replication: the conventional hierarchical model with a multivariate normality assumption (MVN), the Gumbel copula model, and the Joe copula model. The EM algorithm with stochastic approximation, as described in the previous section, was used to obtain the MML parameter estimates for the copula-based models. For the conventional

Downloaded from https://www.cambridge.org/core. 16 Nov 2026 at 02:13:47, subject to the Cambridge Core terms of use.

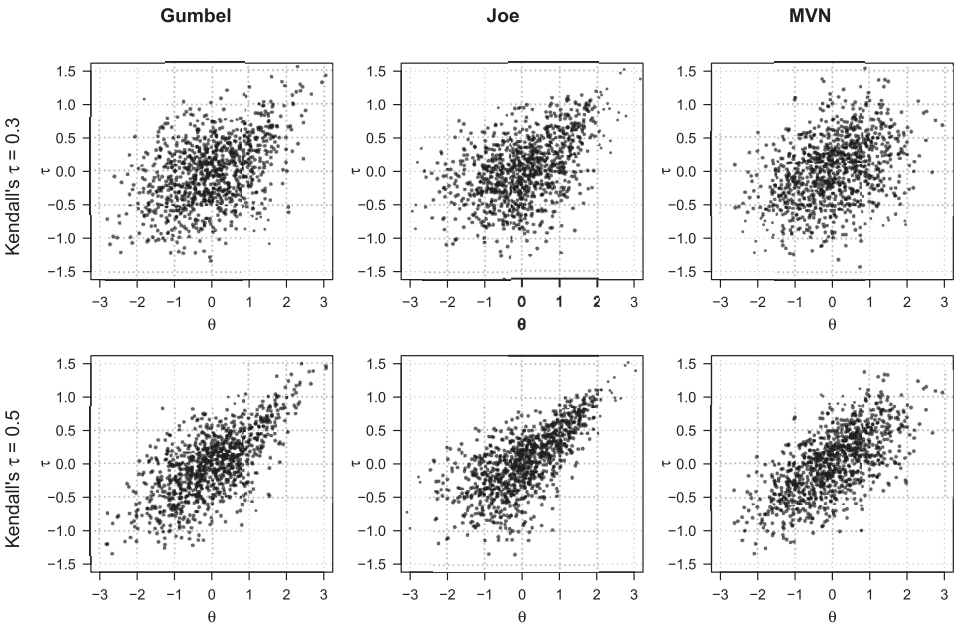


Figure 3. Bivariate distributions of latent ability and speed under different dependence conditions.

Table 2. True item parameter values in the simulation

Item	a	b	α	β
1	0.76	0.43	2.87	0.29
2	0.18	0.05	2.41	0.00
3	1.10	−0.98	2.37	0.81
4	1.00	−2.86	2.59	0.64
5	0.82	0.08	2.40	0.77
6	1.40	−0.85	3.11	0.72
7	0.70	−0.47	2.61	0.52
8	1.47	0.17	2.23	0.12
9	1.05	−0.69	2.14	0.32
10	1.56	−0.62	2.21	0.52
11	1.66	−3.27	2.69	0.10
12	1.11	−0.58	2.81	0.27
13	1.15	−1.72	2.76	0.20
14	1.24	0.71	2.22	0.77
15	1.18	1.89	2.25	0.40
16	0.92	−2.51	2.93	−0.32
17	0.70	−0.04	3.12	0.27
18	1.03	−0.22	2.43	0.10
19	0.96	−0.78	1.96	−0.60
20	1.32	−1.10	2.54	0.37

Downloaded from https://www.cambridge.org/core. 16 Nov 2026 at 02:13:47, subject to the Cambridge Core terms of use.

model, parameter estimates were obtained using an EM algorithm described in Glas and van der Linden (2010). Model convergence was monitored using the change in average individual marginal log-likelihood ($< 10^{-4}$). The standard errors of the parameter estimates were obtained from the approximate information matrix. The 95% confidence intervals were then constructed as

$$\hat{\boldsymbol{\eta}} \pm 1.96 \cdot \mathrm{SE}(\hat{\boldsymbol{\eta}}), \tag{25}$$

where $\hat{\boldsymbol{\eta}}$ denotes the vector of model parameter estimates and $\mathrm{SE}(\hat{\boldsymbol{\eta}})$ represents their corresponding standard errors. Model selection was evaluated by comparing the marginal log-likelihoods of the fitted models. For each condition, the proportion of replications in which the proposed model yielded the highest marginal log-likelihood over the other models was computed. As a baseline, EAP estimates of latent ability were also obtained from the independence 2PL model (Indep) without response time data. All simulations were conducted in R, using the `copula` and `mirt` (Chalmers, 2012) R packages, and custom functions.

The bias, mean absolute deviance (MAD), and RMSE for the item parameters, structural parameters, and ability estimates were calculated as follows:

$$\begin{aligned}
\mathrm{Bias}(\eta) &= \frac{1}{R}\sum_{r=1}^{R}(\hat{\eta}^{(r)} - \eta), \\
\mathrm{MAD}(\eta) &= \frac{1}{R}\sum_{r=1}^{R}(|\hat{\eta}^{(r)} - \eta|), \\
\mathrm{RMSE}(\eta) &= \sqrt{\frac{1}{R}\sum_{r=1}^{R}(\hat{\eta}^{(r)} - \eta)^2},
\end{aligned} \tag{26}$$

where $\hat{\eta}^{(r)}$ is the estimate at the r-th iteration, and η is the true parameter value. To evaluate the accuracy of standard error estimates, the ratio between the average standard error estimates and the empirical standard deviation of the estimates was computed. For a given parameter η, this ratio is defined as

$$\mathrm{SE\ Ratio}(\hat{\eta}) = \frac{\frac{1}{R}\sum_{r=1}^{R}\mathrm{SE}(\hat{\eta}^{(r)})}{\sqrt{\frac{1}{R}\sum_{r=1}^{R}\left(\hat{\eta}^{(r)} - \bar{\hat{\eta}}\right)^2}}, \tag{27}$$

where $\mathrm{SE}(\hat{\eta}^{(r)})$ denotes the standard error estimate in the r-th replication, and $\bar{\hat{\eta}} = \frac{1}{R}\sum_{r=1}^{R}\hat{\eta}^{(r)}$ is the average estimate across replications. The 95% coverage rate was computed as the proportion of replications in which the true parameter value fell within the 95% confidence interval:

$$95\%\ \mathrm{C.R.}(\eta) = \frac{1}{R}\sum_{r=1}^{R}\mathbb{I}\left\{\eta \in \left[\hat{\eta}^{(r)} - 1.96 \cdot \mathrm{SE}(\hat{\eta}^{(r)}),\ \hat{\eta}^{(r)} + 1.96 \cdot \mathrm{SE}(\hat{\eta}^{(r)})\right]\right\}, \tag{28}$$

where $\mathbb{I}$ is the indicator function.

In general, when the true latent traits are generated under strong upper-tail dependence (i.e., Gumbel or Joe copula), the copula models are expected to outperform the conventional model. Conversely, when the data are generated under the MVN distribution, the conventional model is expected to yield better performance than the copula models. The marginal likelihood-based model selection is expected to perform well in identifying the true data-generating models.

4.2. Simulation results

4.2.1. Model selection

Table 3 shows the proportion of replications in which each of the three fitted models yielded the highest marginal log-likelihood under each true data-generating condition. The average marginal log-likelihood values are presented in Appendix D (Table D1). The likelihood-based model

Downloaded from https://www.cambridge.org/core. 16 Nov 2026 at 02:13:47, subject to the Cambridge Core terms of use.

Table 3. Marginal likelihood-based model selection result

			True: Gumbel			True: MVN			True: Joe		
N	*I*	τ_K	Gumbel	MVN	Joe	Gumbel	MVN	Joe	Gumbel	MVN	Joe
500	10	0.3	0.69	0.16	0.15	0.13	0.87	0.00	0.16	0.00	0.84
1,000	10	0.3	0.89	0.06	0.05	0.07	0.93	0.00	0.12	0.00	0.88
500	20	0.3	0.77	0.10	0.13	0.07	0.93	0.00	0.12	0.00	0.88
1,000	20	0.3	0.94	0.02	0.04	0.02	0.98	0.00	0.03	0.00	0.97
500	10	0.5	0.77	0.20	0.03	0.06	0.94	0.00	0.19	0.00	0.81
1,000	10	0.5	0.92	0.07	0.00	0.02	0.98	0.00	0.11	0.00	0.89
500	20	0.5	0.90	0.08	0.02	0.05	0.95	0.00	0.04	0.00	0.96
1,000	20	0.5	0.98	0.01	0.01	0.02	0.98	0.00	0.02	0.00	0.98

Note: *N* is the sample size, and *I* is the test length. τ_K denotes Kendall's τ rank coefficient. The main column headings indicate the true dependence structure used to generate the data. The subheadings indicate the fitted models. Values represent the proportion of replications in which a given fitted model was selected as the best-fitting model based on the marginal likelihood.

selection proved effective at correctly identifying the true model. For data generated under the Gumbel and Joe copulas, selection accuracy ranged from 0.69 to 0.98 and 0.84 to 0.98, respectively. When data were generated under the MVN structure, the MVN model was chosen in 0.87–0.98 of the replications. Across all conditions, model selection accuracy improved with larger sample sizes and longer tests.

4.2.2. Model parameter recovery

Table 4 presents the parameter recovery results for the Gumbel copula model, estimated using the EM algorithm with stochastic approximation, when the data were generated from the Gumbel copula dependence structure. Note that the item parameter recovery results presented here are averaged across all items. The full, item-level parameter recovery tables can be found in Appendix D. The proposed estimation algorithm accurately recovered the true parameter values. Across all conditions, bias for item parameters ranged from −0.036 to 0.001 (MAD: 0.016–0.226), while the structural parameter bias ranged from −0.136 to 0.000 (MAD: 0.010–0.146). The RMSE of parameter estimates consistently decreased as sample size N increased. Note that the relatively large RMSE for the item difficulty parameter $\mathbf{b}$ was largely driven by items with low discrimination (Item 2, $a_i = 0.18$) or extreme difficulty (Item 11, $b_i = -3.27$), as shown in Table D5. The 95% coverage rates ranged from 0.72 to 0.98, and the SE ratios ranged from 0.86 to 1.41, indicating that the estimated standard errors generally approximated the empirical standard errors well. The item-level parameter recovery results were highly similar between the Gumbel model and the MVN model, showing the choice of dependence model in the trait level has minimal impact on the item parameter estimates (Appendix D, Tables D5 and D6). The parameter recovery for the Joe copula model was generally as accurate as the Gumbel model, except for the dependence parameter, δ, which was underestimated when dependence was strong (Appendix D, Table D2).

4.2.3. Latent ability estimation accuracy

Table 5 presents the accuracy of the latent ability estimates under Gumbel copula dependence conditions. The correctly specified Gumbel copula model yielded the lowest RMSE and the highest Pearson correlation with the true ability across all conditions. While its bias was slightly higher than misspecified models in some conditions (e.g., $\delta = 2$), its lower RMSE and higher correlation indicate more accurate

Downloaded from https://www.cambridge.org/core. 16 Nov 2026 at 02:13:47, subject to the Cambridge Core terms of use.

Table 4. Parameter recovery under the Gumbel copula dependence condition

Condition			Bias						MAD					
N	I	δ	a	b	α	β	δ	σ_τ	a	b	α	β	δ	σ_τ
500	10	1.43	0.011	−0.025	0.013	0.001	−0.009	−0.001	0.150	0.214	0.072	0.023	0.056	0.013
1,000	10	1.43	0.009	0.019	0.009	0.002	−0.008	0.000	0.107	0.158	0.050	0.016	0.039	0.010
500	20	1.43	0.019	−0.016	0.009	0.001	−0.007	−0.001	0.157	0.221	0.067	0.023	0.048	0.013
1,000	20	1.43	0.009	−0.010	0.006	0.002	−0.003	0.000	0.107	0.136	0.048	0.016	0.034	0.009
500	10	2	0.014	−0.032	0.010	0.003	−0.136	−0.004	0.150	0.218	0.072	0.022	0.146	0.013
1,000	10	2	0.007	0.002	0.006	0.003	−0.132	−0.004	0.107	0.136	0.050	0.016	0.134	0.010
500	20	2	0.022	−0.036	0.009	0.002	−0.084	−0.003	0.159	0.226	0.067	0.023	0.104	0.013
1,000	20	2	0.007	−0.009	0.005	0.002	−0.075	−0.002	0.106	0.133	0.048	0.016	0.082	0.009
Condition			RMSE						95% coverage rate					
N	I	δ	a	b	α	β	δ	σ_τ	a	b	α	β	δ	σ_τ
500	10	1.43	0.197	0.771	0.091	0.028	0.070	0.016	0.91	0.95	0.96	0.97	0.97	0.95
1,000	10	1.43	0.139	1.340	0.064	0.020	0.049	0.012	0.90	0.94	0.95	0.97	0.96	0.96
500	20	1.43	0.263	1.144	0.085	0.029	0.061	0.016	0.96	0.98	0.97	0.96	0.98	0.97
1,000	20	1.43	0.158	0.386	0.060	0.020	0.042	0.012	0.95	0.97	0.96	0.96	0.97	0.96
500	10	2	0.196	1.056	0.091	0.028	0.167	0.017	0.90	0.95	0.96	0.98	0.84	0.94
1,000	10	2	0.140	0.386	0.064	0.020	0.148	0.012	0.88	0.93	0.95	0.98	0.72	0.93
500	20	2	0.287	1.633	0.085	0.028	0.124	0.017	0.95	0.97	0.97	0.97	0.94	0.98
1,000	20	2	0.155	0.254	0.060	0.020	0.098	0.012	0.94	0.97	0.96	0.97	0.90	0.97
Condition			SE ratio											
N	I	δ	a	b	α	β	δ	σ_τ						
500	10	1.43	0.93	1.14	1.04	1.14	1.12	1.08						
1,000	10	1.43	0.90	1.13	1.01	1.12	1.11	1.01						
500	20	1.43	1.07	1.56	1.11	1.08	1.25	1.17						
1,000	20	1.43	1.03	1.34	1.05	1.05	1.20	1.10						
500	10	2	0.88	1.26	1.04	1.25	1.37	1.06						
1,000	10	2	0.86	1.11	1.01	1.20	1.35	1.01						
500	20	2	1.04	1.38	1.11	1.17	1.41	1.22						
1,000	20	2	0.99	1.20	1.05	1.14	1.38	1.21						

Note: N represents the sample size. I represents the test length. $\boldsymbol{a}$, $\boldsymbol{b}$, $\boldsymbol{\alpha}$, and $\boldsymbol{\beta}$ represent item parameters, and δ and σ_τ represent structural parameters.

ability estimation. This general finding was consistent across simulations where the model that matched the true dependence structure consistently outperformed the others in overall accuracy (Table D3).

In addition to evaluating the overall accuracy of ability estimates, the RMSE and bias of θ conditional on the true ability level were computed to assess how estimation accuracy varies across the ability range. The conditional RMSE and bias values were calculated using equally spaced bins of width 0.5, covering the range of θ from −4 to 4. Under the Gumbel copula dependence condition (Figures 4 and 5), the copula models' advantage over both the conventional model and the independence model is most

Downloaded from https://www.cambridge.org/core. 16 Nov 2026 at 02:13:47, subject to the Cambridge Core terms of use.

Table 5. Accuracy of ability estimates under the Gumbel copula dependence condition

Condition			Bias(θ)				RMSE(θ)				Cor($\hat{\theta}$, θ)			
N	*I*	δ	Gumbel	Joe	MVN	Indep	Gumbel	Joe	MVN	Indep	Gumbel	Joe	MVN	Indep
500	10	1.43	0.005	0.007	0.005	0.005	0.564	0.566	0.569	0.598	0.825	0.824	0.821	0.800
1,000	10	1.43	0.001	0.003	0.001	0.000	0.561	0.563	0.566	0.596	0.828	0.826	0.824	0.803
500	20	1.43	0.005	0.004	0.005	0.005	0.459	0.460	0.463	0.480	0.888	0.887	0.886	0.877
1,000	20	1.43	0.000	0.000	0.001	0.000	0.457	0.458	0.461	0.477	0.890	0.889	0.887	0.879
500	10	2	0.009	0.020	0.006	0.005	0.509	0.515	0.516	0.597	0.860	0.857	0.856	0.801
1,000	10	2	0.005	0.017	0.002	0.001	0.507	0.513	0.513	0.596	0.862	0.859	0.858	0.803
500	20	2	0.007	0.011	0.006	0.005	0.424	0.427	0.430	0.480	0.906	0.904	0.902	0.877
1,000	20	2	0.004	0.007	0.002	0.001	0.421	0.425	0.428	0.477	0.907	0.905	0.904	0.879

Note: *N* represents the sample size. *I* represents the test length. The column headers (Gumbel, Joe, MVN, and Indep) indicate the estimating model, while Gumbel was the data-generating model. *Indep* represents the baseline independence 2PL model without response time.

prominent in the upper tail of the θ distribution. This effect is even stronger when the dependence between latent traits increases (Kendall's $\tau = 0.5$). When the true data structure exhibits strong upper-tail dependence, response-time data provide more information about high-ability individuals and less information about low-ability individuals. The copula-based models borrow more information from response times for upper-tail abilities while borrowing less for lower-tail abilities, which aligns better with the true data structure in the simulation. In contrast, the conventional model's MVN assumption implies asymptotic tail independence and therefore borrows less information from the response time data in the upper tail of ability. This discrepancy explains the performance gap in the upper tail between these models. The conditional RMSE shows a similar pattern when data are generated under the Joe copula dependence structure (Figure D1). Latent speed estimation accuracy was highly similar across the different dependence models, with negligible differences in bias, RMSE, and correlation (Table D4 and Figure D2).

When the data were generated under the MVN dependence structure, the conventional MVN model exhibited the smallest overall RMSE and the highest correlation with the true values (Table 6). Similarly, the conditional RMSE was the lowest for the MVN in both the lower tail and the mid-range of θ, although the differences were less substantial than in the Gumbel copula condition (Figure 6). These results confirm that the conventional MVN model provides the most accurate ability estimates when the underlying dependence structure is MVN.

We conducted additional simulations to evaluate model performance using data generated from 270°-rotated Gumbel and Joe copulas, which reflect a negative association with upper-tail dependence. These simulations compared five models, including the two 270°-rotated copulas, their unrotated counterparts, and the MVN model. Parameter recovery for the rotated models was comparable to the unrotated scenarios, showing minimal bias except for an underestimation of the δ parameter for the rotated Joe copula in the strong dependence condition. The marginal likelihood-based model selection effectively selected the true data-generating models, with selection accuracies ranging from 0.71 to 0.99 for the rotated Gumbel and 0.83 to 0.98 for the rotated Joe. Importantly, the misspecified unrotated models (with positive associations) were never selected. In terms of ability estimation, the rotated copula models again yielded the lowest conditional RMSE, particularly in the upper tail, outperforming the MVN model. The baseline independence model and misspecified unrotated copula models were the least accurate. (See Appendix E for full results.)

In summary, model parameters were recovered accurately, and the true data-generating model could be reliably identified using the marginal log-likelihood. Most importantly, the simulation results show that by correctly specifying the dependence structure, particularly tail dependencies, the copula models

Downloaded from https://www.cambridge.org/core. 16 Nov 2026 at 02:13:47, subject to the Cambridge Core terms of use.

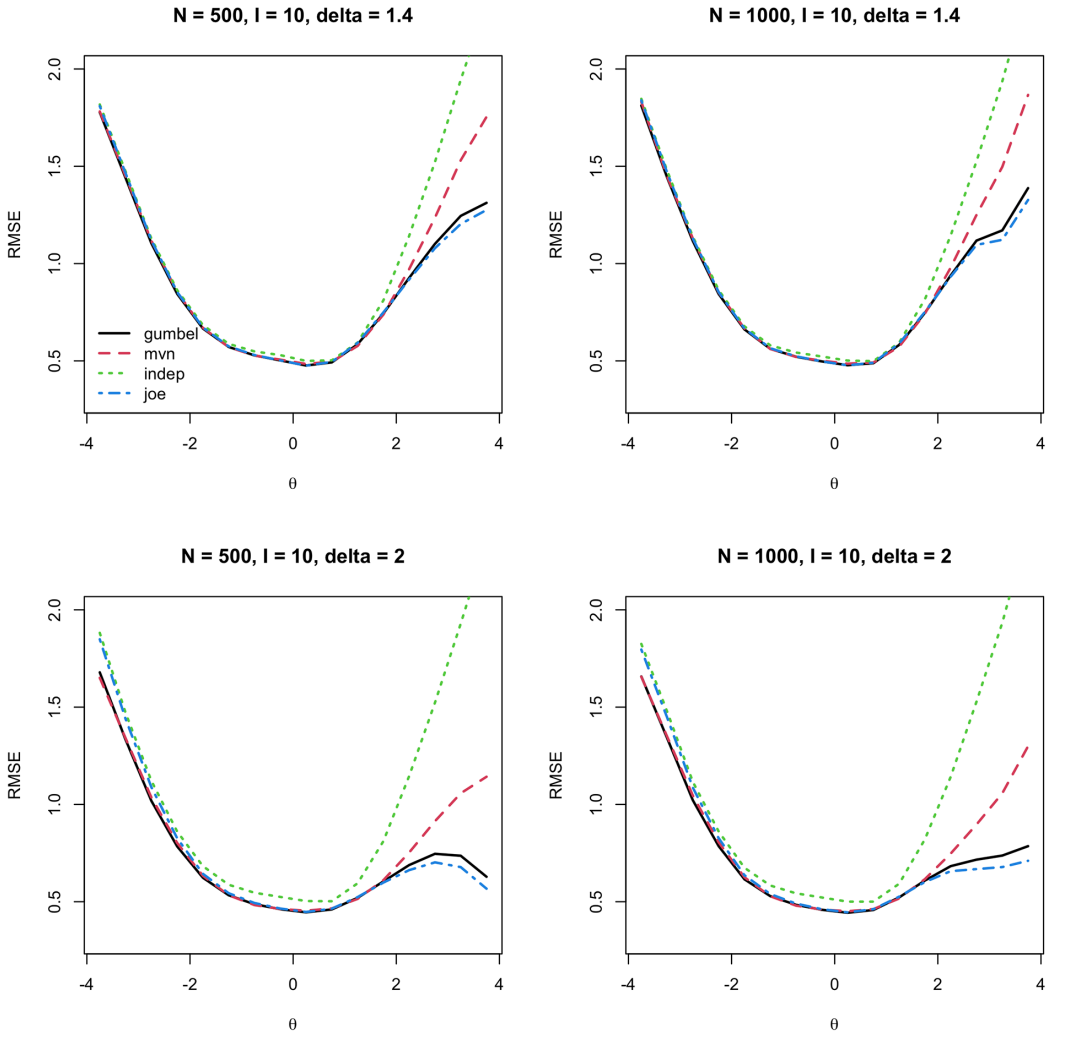


Figure 4. Conditional RMSE of ability estimates under the Gumbel copula dependence condition.

produced significantly more accurate ability estimates than the standard MVN and independence models. This advantage was most pronounced at the extremes of the ability scale, confirming that the model's flexibility improved measurement accuracy.

5. Empirical data illustration

In this section, we apply the proposed copula-based methods to a variety of cognitive test datasets, summarized in Table 7. For a thorough examination of our model's empirical utility across different testing contexts, the datasets span from game-based tests and memory tests to large-scale educational assessments, including the 2018 PISA data on mathematics and science. The sample size (N) for these datasets ranges from 389 to 3,035, and the test length (I) ranges from 10 to 144. These datasets were also analyzed in a meta-analysis of speed and accuracy (Domingue et al., 2022). The data for letterchaos, addition, multiplication, subtraction, and set tasks (Coomans et al., 2016) are available from the Open

Downloaded from https://www.cambridge.org/core. 16 Nov 2026 at 02:13:47, subject to the Cambridge Core terms of use.

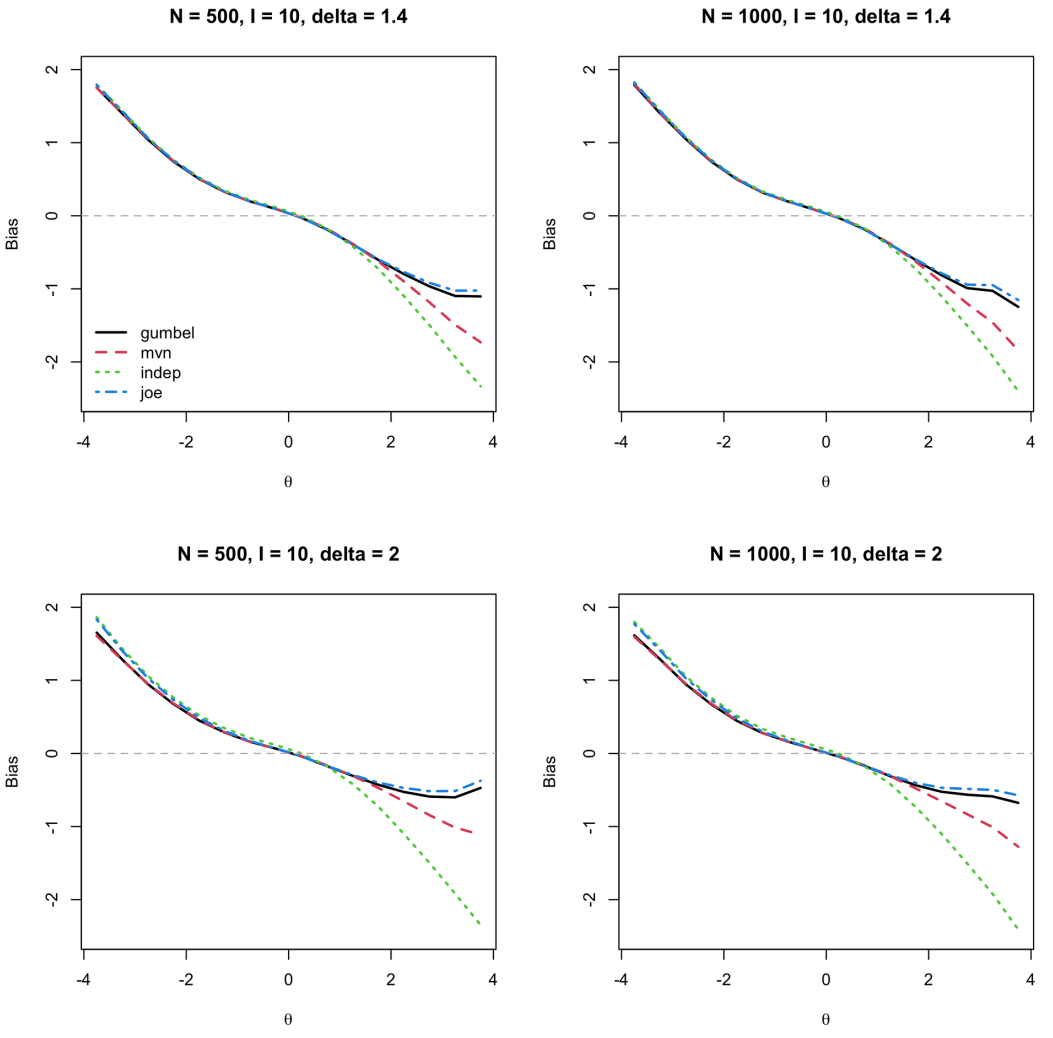


Figure 5. Conditional bias of ability estimates under the Gumbel copula dependence condition.

Table 6. Accuracy of ability estimates under the MVN dependence condition

Condition			Bias(θ)				RMSE(θ)				Cor($\hat{\theta}$, θ)			
N	*I*	ρ	Gumbel	Joe	MVN	Indep	Gumbel	Joe	MVN	Indep	Gumbel	Joe	MVN	Indep
500	10	0.45	−0.004	−0.001	−0.001	−0.001	0.579	0.585	0.575	0.599	0.815	0.811	0.818	0.800
1,000	10	0.45	−0.003	−0.001	0.000	0.000	0.576	0.582	0.572	0.595	0.817	0.812	0.820	0.803
500	20	0.45	−0.004	−0.004	−0.001	−0.001	0.470	0.474	0.467	0.480	0.882	0.880	0.884	0.877
1,000	20	0.45	−0.003	−0.004	0.000	0.000	0.467	0.472	0.464	0.477	0.884	0.881	0.886	0.879
500	10	0.71	0.000	0.013	−0.001	−0.001	0.528	0.541	0.522	0.599	0.849	0.841	0.853	0.800
1,000	10	0.71	0.001	0.014	0.000	0.000	0.526	0.539	0.519	0.595	0.850	0.842	0.854	0.803
500	20	0.71	−0.002	0.002	0.000	−0.001	0.441	0.451	0.436	0.480	0.897	0.892	0.900	0.877
1,000	20	0.71	−0.001	0.002	0.000	0.000	0.438	0.449	0.432	0.477	0.898	0.893	0.901	0.879

Note: *N* represents the sample size. *I* represents the test length. The column headers (Gumbel, Joe, MVN, and Indep) indicate the estimating model, while Gumbel was the data-generating model. *Indep* represents the baseline independence 2PL model without response time.

Downloaded from https://www.cambridge.org/core. 16 Nov 2026 at 02:13:47, subject to the Cambridge Core terms of use.

Table 7. Descriptive statistics of the empirical datasets

Dataset	*N*	*I*	Mean Prop.	Median Time (s)
addition	789	30	0.96	11.70
multiplication	3,035	30	0.97	12.52
set	2,649	10	0.90	11.09
letterchaos	667	10	0.92	6.69
subtraction	2,193	30	0.95	7.71
nomt	389	144	0.75	2.53
pisa_math_C1_DEU	411	12	0.54	91.01
pisa_math_C1_JPN	399	12	0.60	82.62
pisa_math_C1_MEX	567	12	0.31	103.86
pisa_math_C1_NZL	497	12	0.50	85.20
pisa_math_C1_USA	593	12	0.41	83.92
pisa_math_C2_DEU	580	11	0.55	79.34
pisa_math_C2_JPN	633	11	0.57	71.56
pisa_math_C2_MEX	812	11	0.31	95.37
pisa_math_C2_NZL	692	11	0.47	77.87
pisa_math_C2_USA	673	11	0.40	78.03
pisa_math_C3_DEU	525	11	0.60	87.45
pisa_math_C3_JPN	633	11	0.57	82.82
pisa_math_C3_MEX	820	11	0.36	102.14
pisa_math_C3_NZL	680	11	0.59	78.18
pisa_math_C3_USA	673	11	0.46	78.27
pisa_science_C1_DEU	491	20	0.55	63.51
pisa_science_C1_JPN	483	20	0.59	54.54
pisa_science_C1_MEX	735	20	0.30	68.80
pisa_science_C1_NZL	669	19	0.53	58.08
pisa_science_C1_USA	616	20	0.46	55.51
pisa_science_C2_DEU	472	17	0.58	76.82
pisa_science_C2_JPN	595	17	0.59	70.35
pisa_science_C2_MEX	765	17	0.36	83.29
pisa_science_C2_NZL	650	17	0.54	70.61
pisa_science_C2_USA	630	17	0.47	70.39
pisa_science_C3_DEU	422	19	0.67	55.67
pisa_science_C3_JPN	594	19	0.68	41.94
pisa_science_C3_MEX	765	19	0.45	59.22
pisa_science_C3_NZL	652	19	0.63	50.47
pisa_science_C3_USA	608	19	0.58	46.11

Note: *N* is the sample size, and *I* is the test length. Mean Prop. is the mean response proportion correct. Median Time (s) is the median response time in seconds. C1–C3 represent clusters 1–3.

Downloaded from https://www.cambridge.org/core. 16 Nov 2026 at 02:13:47, subject to the Cambridge Core terms of use.

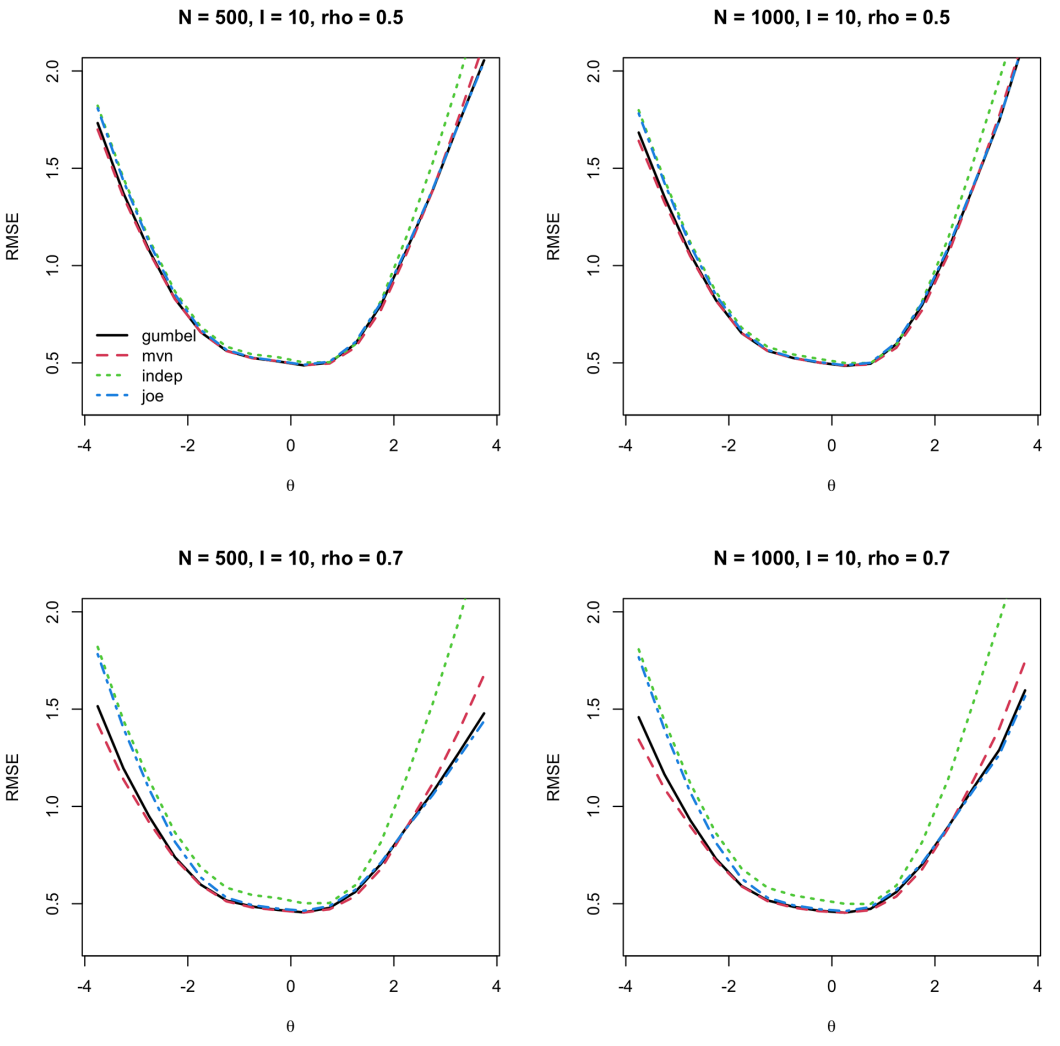


Figure 6. Conditional RMSE of ability estimates under the MVN dependence condition.

Science Framework (OSF).[1] The novel object memory test (nomt; Hooper et al., 2024) data are available from the Item Response Warehouse (IRW; Domingue, Braginsky, et al., 2024).[2] The PISA 2018 data are available from both the OECD website[3] and the IRW.

For data preprocessing, we removed examinees with missing values and items with invariant responses (all correct or incorrect), and we transformed response time data to seconds. For the PISA data, we analyzed the first three clusters from the mathematics and science assessments, respectively, selecting five countries to account for heterogeneity in item response and response time patterns across countries (e.g., Michaelides & Ivanova, 2022; Pohl et al., 2019): Germany (DEU), Japan (JPN), Mexico (MEX), New Zealand (NZL), and the United States (USA). Polytomously scored items in the science

[1] https://osf.io/pbuvj/
[2] https://itemresponsewarehouse.org/
[3] https://www.oecd.org/en/data/datasets/pisa-2018-database.html

Downloaded from https://www.cambridge.org/core. 16 Nov 2026 at 02:13:47, subject to the Cambridge Core terms of use.

Downloaded from https://www.cambridge.org/core. 16 Nov 2026 at 02:13:47, subject to the Cambridge Core terms of use.

Table 8. Model selection results with log-likelihood values from the empirical data analyses

Dataset	Selected model	Log-likelihood								
		MVN	Gumbel	Joe	90G	90J	180G	180J	270G	270J
addition	MVN	**−70,450.8**	−73,712.0	−73,291.0	−72,557.4	−70,470.4	−73,535.6	−73,643.6	−72,856.1	−72,681.0
multiplication	MVN	**−253,762.9**	−262,843.9	−261,468.8	−262,826.3	−262,828.1	−268,265.1	−258,031.1	−257,703.8	−261,450.5
subtraction	MVN	**−197,955.1**	−198,128.1	−198,128.0	−197,990.9	−198,024.1	−198,128.0	−198,128.0	−201,808.9	−202,087.8
set	270G	−75,164.3	−75,193.3	−75,512.4	−75,174.4	−75,179.9	−75,418.2	−75,193.3	**−75,160.3**	−75,475.9
letterchaos	270G	−20,606.5	−20,615.3	−20,615.3	−20,611.7	−20,613.6	−20,615.4	−20,615.4	**−20,603.8**	−20,604.5
nomt	MVN	**−123,058.3**	−125,850.4	−125,541.9	−129,930.9	−126,746.2	−125,647.6	−126,061.5	−125,778.4	−123,106.2
pisa_math_C1_DEU	MVN	**−27,565.9**	−28,702.9	−27,981.1	−27,980.7	−28,719.4	−27,981.1	−27,981.0	−28,718.6	−28,718.4
pisa_math_C1_JPN	MVN	**−26,859.6**	−27,770.3	−27,124.6	−27,124.2	−27,124.1	−27,124.6	−27,124.6	−27,810.6	−27,124.4
pisa_math_C1_MEX	90J	−40,044.2	−40,069.7	−40,069.7	−40,036.8	**−40,033.3**	−40,069.8	−40,069.7	−40,053.7	−40,063.2
pisa_math_C1_NZL	MVN	**−33,770.8**	−35,169.8	−34,316.4	−34,927.8	−34,315.9	−34,316.4	−34,316.5	−34,316.2	−34,583.4
pisa_math_C1_USA	90J	−40,818.3	−40,833.6	−40,833.3	−40,808.7	**−40,806.9**	−40,833.3	−40,833.1	−40,826.0	−40,833.2
pisa_math_C2_DEU	MVN	**−36,001.5**	−36,564.7	−36,564.7	−36,564.2	−36,564.2	−36,564.7	−36,564.7	−37,605.7	−36,564.3
pisa_math_C2_JPN	90J	−39,756.0	−39,793.8	−39,794.0	−39,751.1	**−39,750.4**	−39,792.5	−39,792.7	−39,765.6	−39,785.2
pisa_math_C2_MEX	MVN	**−52,004.8**	−52,026.5	−52,026.5	−52,007.0	−52,009.7	−52,026.5	−52,026.5	−52,012.7	−52,018.8
pisa_math_C2_NZL	MVN	**−43,045.3**	−43,585.8	−43,619.4	−43,523.3	−43,489.6	−43,490.8	−43,487.1	−43,354.2	−43,057.9
pisa_math_C2_USA	90G	−42,629.0	−42,665.5	−42,665.4	**−42,627.7**	−42,629.0	−42,665.4	−42,665.4	−42,641.4	−42,655.8
pisa_math_C3_DEU	MVN	**−32,422.4**	−32,426.0	−32,426.2	−32,645.7	−32,577.0	−32,426.4	−32,425.8	−32,426.4	−32,426.7
pisa_math_C3_JPN	MVN	**−38,920.9**	−39,206.7	−39,377.6	−39,480.6	−39,321.1	−39,198.1	−39,387.9	−39,183.7	−38,939.9
pisa_math_C3_MEX	90J	−52,271.5	−52,280.9	−52,280.9	−52,267.1	**−52,264.5**	−52,280.9	−52,280.9	−52,278.8	−52,280.9
pisa_math_C3_NZL	270G	−41,712.5	−41,713.9	−41,713.7	−41,877.2	−42,031.4	−41,712.9	−41,713.7	**−41,712.1**	−41,714.0

(Continued)

Table 8. Continued

Dataset	Selected model	Log-likelihood								
		MVN	Gumbel	Joe	90G	90J	180G	180J	270G	270J
pisa_math_C3_USA	90J	−41,972.4	−41,990.6	−41,990.4	−41,957.5	**−41,952.2**	−41,990.6	−41,990.5	−41,983.0	−41,990.2
pisa_science_C1_DEU	MVN	**−51,596.9**	−51,620.2	−51,620.1	−52,061.1	−52,322.1	−51,619.8	−51,619.8	−51,610.3	−51,620.7
pisa_science_C1_JPN	90J	−49,983.0	−50,016.9	−50,016.8	−49,974.3	**−49,970.2**	−50,016.7	−50,016.7	−49,995.7	−50,012.7
pisa_science_C1_MEX	90J	−78,502.8	−78,525.9	−78,525.9	−78,498.9	**−78,497.5**	−78,525.9	−78,525.9	−78,511.5	−78,519.0
pisa_science_C1_NZL	90J	−66,655.4	−66,688.4	−66,688.3	−66,643.7	**−66,639.6**	−66,688.4	−66,688.4	−66,669.6	−66,685.4
pisa_science_C1_USA	90J	−65,556.4	−65,591.5	−65,591.5	−65,546.8	**−65,541.8**	−65,591.5	−65,591.5	−65,569.9	−65,586.9
pisa_science_C2_DEU	90J	−43,464.3	−43,489.0	−43,489.0	−43,458.4	**−43,456.4**	−43,489.0	−43,489.0	−43,475.1	−43,487.9
pisa_science_C2_JPN	90J	−54,983.2	−55,012.1	−55,011.9	−54,981.6	**−54,979.6**	−55,012.1	−55,012.3	−54,997.2	−55,011.5
pisa_science_C2_MEX	90J	−72,139.6	−72,169.9	−72,169.9	−72,138.2	**−72,137.7**	−72,169.9	−72,169.9	−72,153.5	−72,164.7
pisa_science_C2_NZL	90J	−60,047.0	−60,074.5	−60,074.3	−60,034.9	**−60,030.2**	−60,074.4	−60,074.3	−60,060.3	−60,074.2
pisa_science_C2_USA	90J	−58,852.6	−58,899.3	−58,899.3	−58,844.5	**−58,840.3**	−58,899.3	−58,874.6	−58,899.3	−58,896.0
pisa_science_C3_DEU	90J	−40,631.3	−40,644.1	−40,643.0	−40,626.2	**−40,624.0**	−40,644.1	−40,644.1	−40,638.9	−40,645.0
pisa_science_C3_JPN	90J	−55,177.0	−55,207.8	−55,207.8	−55,167.2	**−55,162.8**	−55,207.8	−55,207.8	−55,193.8	−55,207.4
pisa_science_C3_MEX	90J	−77,565.9	−77,616.8	−77,616.8	−77,560.4	**−77,556.7**	−77,616.8	−77,616.8	−77,585.6	−77,605.8
pisa_science_C3_NZL	90J	−63,354.9	−63,390.1	−63,390.1	−63,342.6	**−63,337.5**	−63,390.2	−63,389.9	−63,370.6	−63,389.5
pisa_science_C3_USA	90J	−59,757.9	−59,821.5	−59,821.5	−59,754.2	**−59,751.3**	−59,821.6	−59,821.6	−59,778.1	−59,808.4

Note: “addition,” “multiplication,” and “subtraction” are basic arithmetic tests. “set” is a card game, and “letterchaos” is a language learning game. “nomt” is a novel object memory test. C1–C3 represent clusters 1–3 of PISA Science and Math Data. Bold values indicate the largest log-likelihood for each row.

Downloaded from https://www.cambridge.org/core. 16 Nov 2026 at 02:13:47, subject to the Cambridge Core terms of use.

assessment were dichotomized by treating only the full score as correct. The code used to preprocess and analyze the data is available on the OSF.[4]

For each of the 36 datasets, we analyzed nine models: the MVN model, the Gumbel and Joe copulas, and their 90°-, 180°-, and 270°-rotated versions. All models were estimated via MML using an EM algorithm. As shown in Table 8, the best-fitting model based on the marginal likelihood was the 90°-rotated Joe (90J) for 19 datasets, the MVN for 13 datasets, the 270°-rotated Gumbel (270G) for three datasets, and the 90°-rotated Gumbel (90G) for one. The association between latent ability and speed was consistently negative, as indicated by the negative Pearson correlation estimates from the MVN model (Appendix F, Table F1). This negative association means that copula models assuming a positive relationship (i.e., the unrotated and 180°-rotated versions) were misspecified. As a result, the dependence parameter (δ) in these models converged to its lower bound of 1.00.

For most datasets from the 2018 PISA science assessment, the 90°-rotated Joe copula provided the best fit. This implies a strong tail dependence between the lower tail of ability and the upper tail of speed. In other words, the relationship is strongest at the joint extreme where low ability is associated with highly fast responses, which may indicate behaviors, such as rapid guessing or speededness.

Figure 7 presents scatter plots of the ability and speed estimates for representative datasets from three models. The latent trait distributions from the MVN model (first row) do not show tail dependence. In contrast, the latent trait distributions for the 90°-rotated Joe (second row) and 270°-rotated Gumbel (third row) show stronger lower-tail and upper-tail dependence, respectively. Note that the curvilinear patterns in the bottom row (letterchaos and set) represent examinees who have identical item response patterns, but varying response times. This demonstrates that the conditional expectation of ability is a non-linear function of speed when the joint distribution is constructed with an asymmetric copula.

Focusing on a dataset for which the 90°-rotated Joe copula was selected, we compared the ability estimates from the MVN and the selected model (Figure 8). The largest differences occur in the lower tail, where the MVN model yields higher ability estimates with a maximum difference of 1.16. This is because the 90°-rotated Joe copula, with its stronger lower-tail dependence, penalizes fast responses among low-ability examinees more heavily than the MVN model does. Consequently, both the raw and squared differences between the ability estimates are largest at the low end of the ability distribution (Figure 9). On the other hand, when MVN was the best-fitting model (e.g., Math, Cluster 3, JPN; Figure 10), the 90°-rotated Joe copula model tends to underestimate the latent abilities in the lower tail of the ability distribution.

5.1. Random-split replication analysis

In addition, we conducted a random-split replication analysis to evaluate the replicability of the model selection and to test whether asymmetric tail dependence is consistently observed across the PISA dataset. For both the math and science assessments, we aggregated country data within each cluster and randomly split the students into five folds. As a result, 30 datasets were fit to the same nine models, and the best model was selected based on the highest log-likelihood value. The analysis results suggest that the model selection is consistent within the PISA data, as the 90°-rotated Joe copula model was selected for 28 of the 30 datasets. This provides strong evidence for the presence of asymmetric tail dependence in large-scale educational assessments. The log-likelihood values and selected models are summarized in Appendix F (Table F2).

5.2. Item response-level predictive accuracy

Using the InterModel Vigorish (IMV; Domingue, Kanopka, Kapoor, et al., 2024), the item response-level predictive accuracy of the 90°-rotated Joe copula model and the MVN model was compared. IMV is an index that quantifies the predictive gain of a compared model $M1$ against a baseline model

[4] https://osf.io/48z2k/overview?view_only=0457bfa01f8448a3a36b48fc49cd52ac

Downloaded from https://www.cambridge.org/core. 16 Nov 2026 at 02:13:47, subject to the Cambridge Core terms of use.

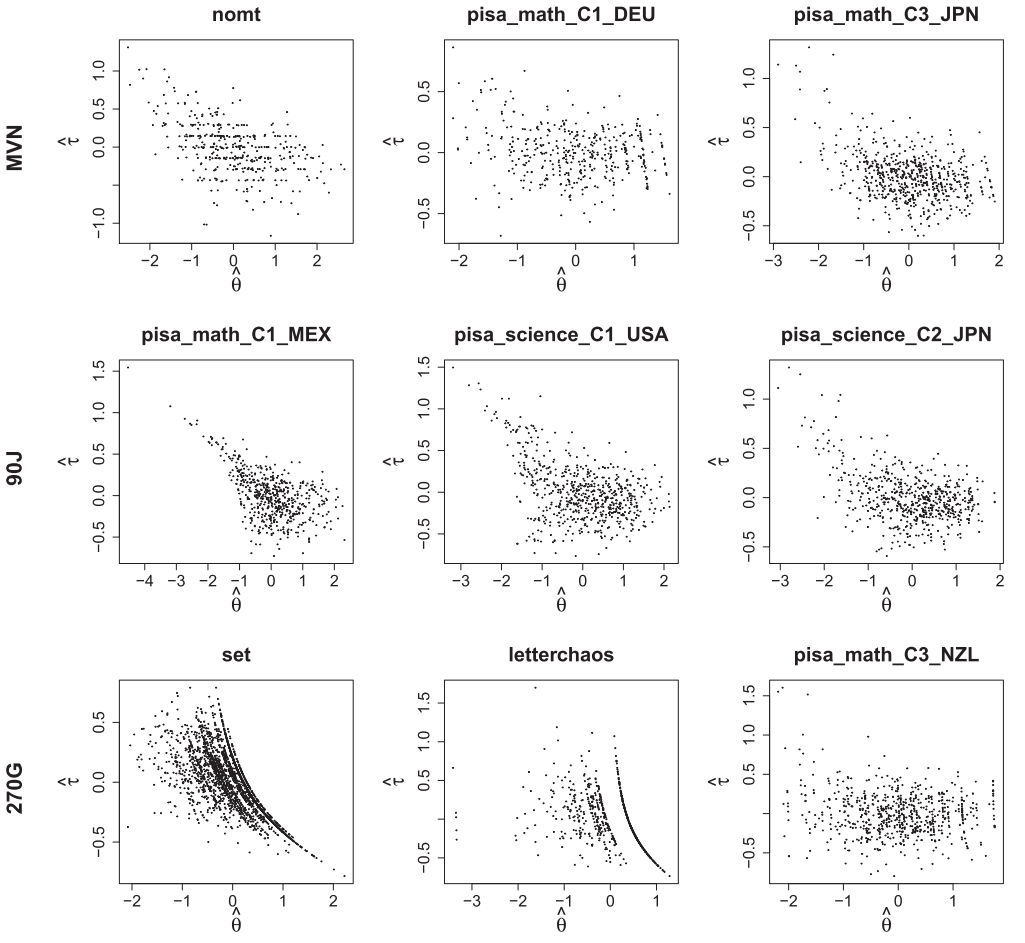


Figure 7. Scatter plots of θ and τ estimates from empirical data analyses.
Note: Each row displays latent trait estimates obtained from the MVN model, the 90°-rotated Joe copula, and the 270°-rotated Gumbel copula.

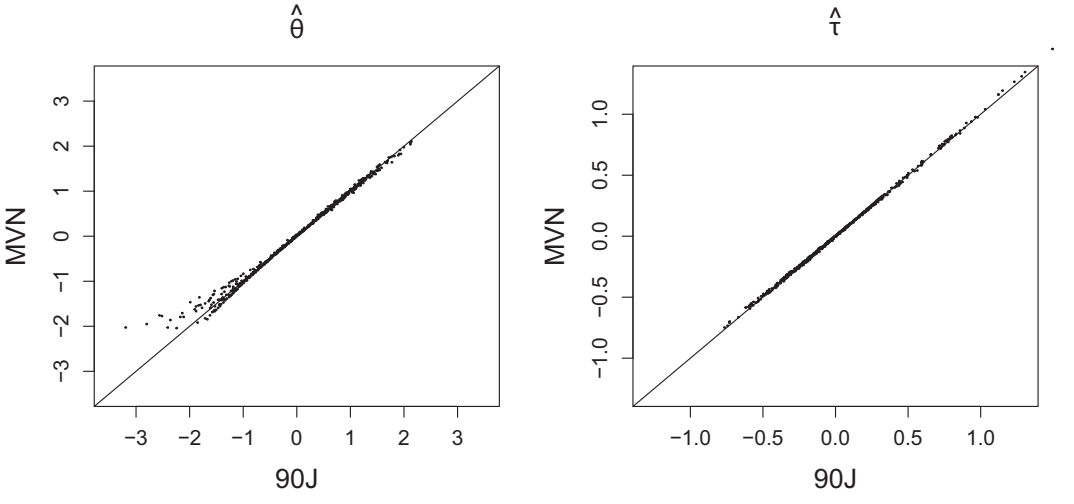


Figure 8. θ and τ estimates of MVN and 90°-rotated Joe from the 2018 PISA Science Data, Cluster 1, USA.

Downloaded from https://www.cambridge.org/core. 16 Nov 2026 at 02:13:47, subject to the Cambridge Core terms of use.

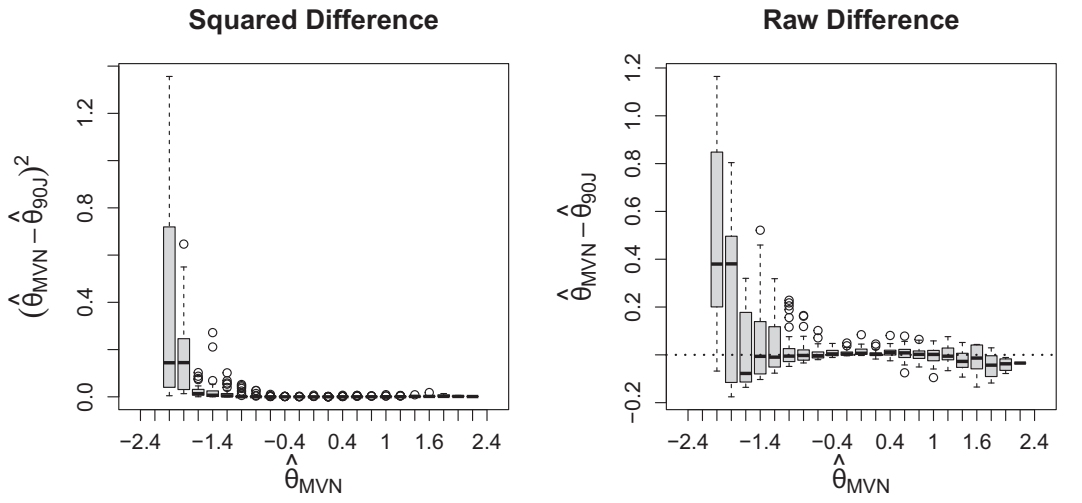


Figure 9. Squared and raw differences in θ estimates between MVN and 90°-rotated Joe from the 2018 PISA Science Data, Cluster 1, USA.

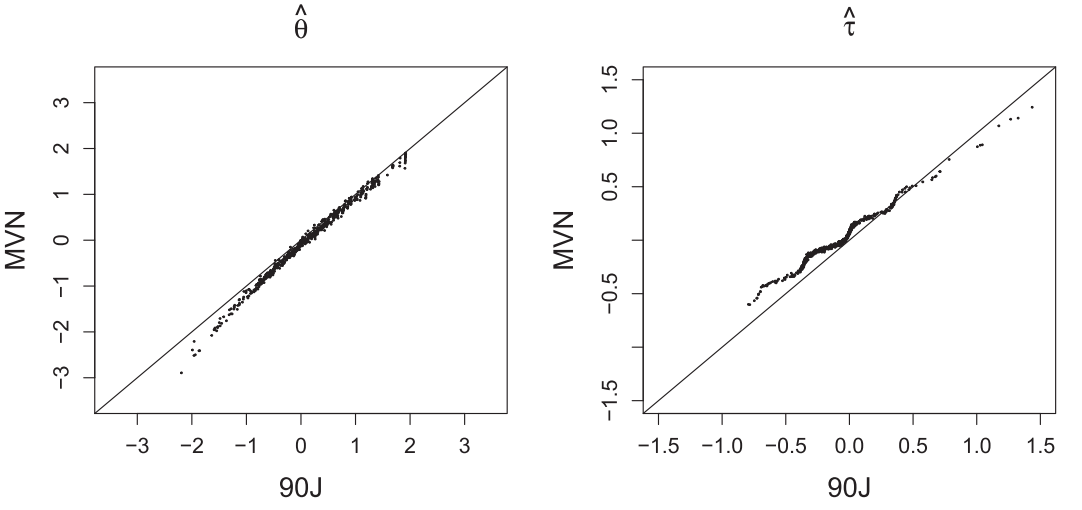


Figure 10. θ and τ estimates of MVN and 90°-rotated Joe from the 2018 PISA Math Data, Cluster 3, JPN.

$M0$ for binary responses. Let $\hat{p}_{pi}$ denote the predicted item response for examinee p and item i from a model. For each prediction model, the uncertainty in binary prediction is quantified by finding a $w \in [0.5, 1]$ value such that

$$w\log(w) + (1-w)\log(1-w) = \log\left(\prod_{p=1}^{N}\prod_{i=1}^{I}\hat{p}_{pi}^{y_{pi}}(1-\hat{p}_{pi})^{1-y_{pi}}\right)^{\frac{1}{N\times I}}. \tag{29}$$

A w value closer to 0.5 indicates higher uncertainty in binary prediction. Then, the IMV is calculated as

$$\text{IMV} = \frac{w_1 - w_0}{w_0}. \tag{30}$$

Downloaded from https://www.cambridge.org/core. 16 Nov 2026 at 02:13:47, subject to the Cambridge Core terms of use.

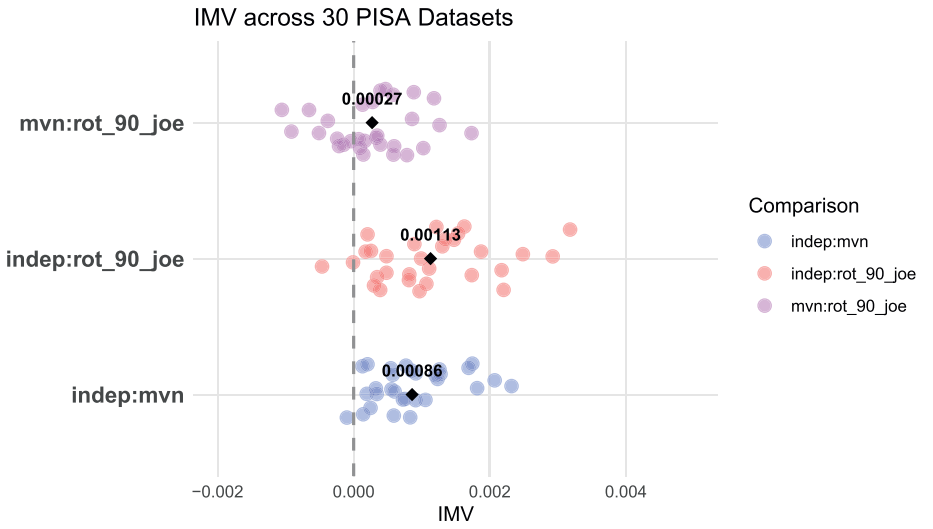


Figure 11. IMV values from the 2018 PISA Math and Science Data.

Here, w_1 and w_0 are the levels of uncertainty in $M1$ and $M0$, respectively. IMV values greater than zero quantify the gain in replacing $M0$ with $M1$ for binary outcome prediction.

To evaluate the out-of-sample prediction accuracy of the models, the "missing response" paradigm was implemented for each of the 30 PISA datasets by randomly splitting the response-level data into five folds. Across five iterations, item responses and response times in each fold were treated as missing, and the models were fit using the remaining data. The predicted values for the missing responses were obtained using the item parameter estimates and the latent ability estimates from the 90J model, the MVN model, and the independence model. For each dataset, the IMV values were averaged across the five folds. Figure 11 shows the IMV values for the 30 PISA datasets, and the black diamonds indicate the average IMV across all 30 datasets. The two panels comparing each model against the independence model show that both hierarchical approaches outperformed the independence model. The average IMV of the 90J model against the MVN model was 0.00027. This suggests a weak improvement in predictive accuracy for the 90J relative to the MVN, a magnitude comparable to the predictive gain of a 3PL model over a 2PL model found in Domingue, Kanopka, Kapoor, et al. (2024).

Figure 12 presents person-level predicted accuracy against the observed accuracy for the 90J, MVN, and independence models across the 30 PISA datasets. For each individual i, the predicted accuracy is the mean of the predicted response probabilities obtained from the five-fold out-of-sample prediction, while the observed accuracy is the proportion of correct responses across the items. Overall, the accuracy of low-performing students tends to be over-predicted, whereas the accuracy of high-performing students is under-predicted. However, the 90J and MVN models mitigate this bias in the lower tail by incorporating response time information. Specifically, the 90J model applies a stronger adjustment to fast-responding examinees within the low-performing group (observed accuracy < 0.3), drawing their predicted accuracy closer to the reference diagonal line. Similarly, Figure 13 plots the person-level predicted median response time against the observed median response time. For each individual, the predicted median response time was calculated as the median of the predicted median response time (i.e., Median$(\hat{\beta}_j - \hat{\tau}_i)$). The 90J model better predicts the median response time for slow-responding examinees (e.g., observed median RT > 150) compared to the MVN model. In terms of item-level accuracy and response time predictions, the two methods showed negligible differences (Appendix F, Figures F1 and F2).

Downloaded from https://www.cambridge.org/core. 16 Nov 2026 at 02:13:47, subject to the Cambridge Core terms of use.

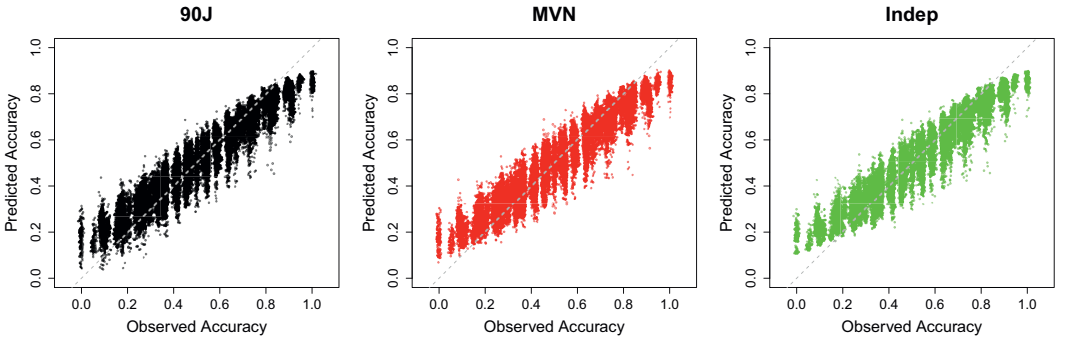


Figure 12. Person-level predicted accuracy versus observed accuracy from the 2018 PISA Math and Science Data.

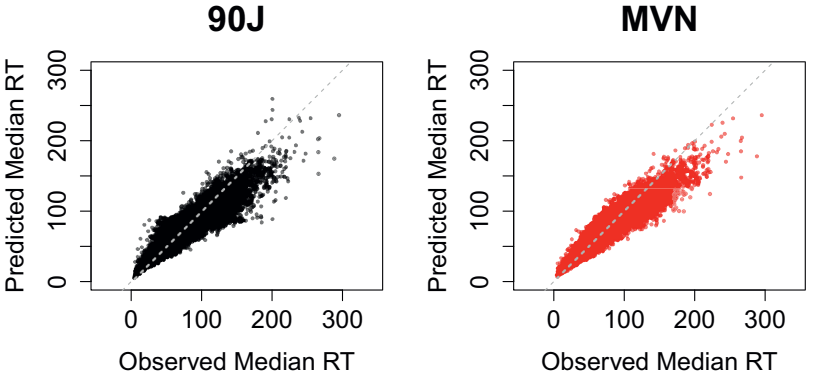


Figure 13. Person-level predicted median RT versus observed median RT from the 2018 PISA Math and Science Data.

6. Comparison to the conditional dependence model

This section compares the copula-based models to the CD model described in Bolsinova et al. (2017), as it is one of the widely used alternative hierarchical models to the MVN model. At the first level, the observed response times are modeled with a log-normal model (Equation (8), and the item parameters for observed responses (Equation (7)) are expressed as a function of the standardized residual log-response time (z_{pi}) of person p and item i as follows:

$$\begin{aligned} a_{pi} &= a_{0i} a_{1i}^{z_{pi}}, \\ b_{pi} &= b_{0i} + b_{1i} z_{pi}, \end{aligned} \tag{31}$$

where $z_{pi} = \alpha_i (\ln t_{pi} - (\beta_i - \tau_p))$. At the second level, the latent speed and latent ability follow an MVN distribution with structural parameters ρ and σ_τ^2. As a result, the CD model consists of six parameters for each item at the first level (a_{0i}, a_{1i}, b_{0i}, b_{1i}, α_i, and β_i) and two structural parameters at the second level. A Markov chain Monte Carlo (MCMC) algorithm is implemented for parameter estimation. See Bolsinova et al. (2017) for full details of the model specification and estimation for the CD model.

Conceptually, the CD model and the copula model capture different aspects of the speed–accuracy relationship. The CD model relaxes the assumption of conditional independence at the first level (the observation level). The measurement model allows CD between the observed responses and response times, after controlling for the latent traits. In contrast, the proposed copula model relaxes the assumption of a symmetric multivariate distribution at the second level (the latent trait level). Therefore, the two models are different approaches for capturing distinct dependence structures at the two levels.

Downloaded from https://www.cambridge.org/core. 16 Nov 2026 at 02:13:47, subject to the Cambridge Core terms of use.

Table 9. Ability estimation accuracy of the Gumbel copula and conditional dependence models

Condition			Bias(θ)		RMSE(θ)		Cor($\hat{\theta}$, θ)	
N	I	True model	Gumbel	CD	Gumbel	CD	Gumbel	CD
500	10	Gumbel	0.005	0.007	0.564	0.572	0.825	0.819
1,000	10	Gumbel	0.001	0.001	0.561	0.569	0.828	0.822
500	20	Gumbel	0.005	0.006	0.459	0.464	0.888	0.885
1,000	20	Gumbel	0.000	0.000	0.457	0.463	0.890	0.887
500	10	CD	−0.003	−0.001	0.740	0.724	0.673	0.690
1,000	10	CD	−0.003	0.000	0.732	0.718	0.680	0.695
500	20	CD	−0.003	0.000	0.628	0.610	0.778	0.792
1,000	20	CD	−0.003	0.000	0.622	0.604	0.782	0.796

We next present a simulation study to provide empirical evidence that the two models represent distinct data-generating processes.

Through simulation studies, we evaluated the performance of the copula-based model compared to the CD model when data were generated under either the Gumbel copula or the CD model. The sample sizes ($N = 500, 1,000$) and the test lengths ($I = 10, 20$) were identical to those in the previous simulation studies. Under the Gumbel copula condition, the true item parameters were set as in Table 2, and the true latent dependence structures were the same as in Section 4. Under the CD model condition, data were generated using the true item parameter and structural parameter distributions given in Table 2 of Bolsinova et al. (2017). The number of replications under each condition was $R = 500$. The CD model was estimated using the MCMC algorithm provided by Bolsinova et al. (2017) with a chain length of 5,000 and a burn-in of 2,500 iterations. The RMSE, bias, and correlation (with the true values) of latent ability estimates were calculated. In addition, we evaluated the model selection accuracy using the model likelihood, AIC, and BIC, given the number of unknown parameters k and sample size N:

$$\begin{aligned} \text{AIC} &= -2 \cdot \text{log-likelihood} + 2k, \\ \text{BIC} &= -2 \cdot \text{log-likelihood} + k \log N. \end{aligned} \tag{32}$$

The model with the lower AIC (or BIC) values was selected. Note that, for calculating the model fit indices of the CD model, EAP estimates were plugged into the likelihood function for fair comparison with the copula model, whose parameters were obtained via an MML estimation.

Table 9 shows the accuracy of ability estimates from the Gumbel copula and CD model. Within each dependence condition (Gumbel or CD), the true data-generating model consistently yielded a lower RMSE and a higher correlation. Table 10 presents the model selection accuracy by the proportion of replications in which the true model was selected based on likelihood, AIC, and BIC. When the data were generated under the CD model, the CD model always produced a higher likelihood. Conversely, the CD model often yielded a higher likelihood than the Gumbel even when the true data-generating model was the Gumbel copula. AIC was a more reliable tool for model selection, identifying the true data-generating model in over 99% of replications. BIC showed lower model selection accuracy than AIC when the true model was CD at $N = 500$. In summary, these results indicate that the two models account for distinct dependence structures between item responses and response times.

When applied to the 36 empirical datasets from the previous section, the estimation algorithm for the CD model resulted in errors in three datasets, potentially due to outliers in response times. Out of the remaining 33 datasets, the CD model yielded the lowest AIC values in 28 datasets, and the 90°-rotated Joe copula model yielded the lowest BIC values in 16 datasets (Appendix F, Tables F3 and F4). This may suggest that the CD model provides a larger improvement in model fit than

Downloaded from https://www.cambridge.org/core. 16 Nov 2026 at 02:13:47, subject to the Cambridge Core terms of use.

Table 10. Model selection results under the Gumbel copula and the CD model

Condition			Model selection accuracy		
N	*I*	True model	Likelihood	AIC	BIC
500	10	Gumbel	0.29	1.00	1.00
1,000	10	Gumbel	0.44	1.00	1.00
500	18	Gumbel	0.66	1.00	1.00
1,000	18	Gumbel	0.72	1.00	1.00
500	10	CD	1.00	0.99	0.49
1,000	10	CD	1.00	1.00	1.00
500	18	CD	1.00	0.99	0.43
1,000	18	CD	1.00	1.00	0.99

Note: Proportions of replications where the true data-generating model is selected using likelihood, AIC, and BIC.

the copula model. However, these two approaches attempt to address distinct sources of model misfit within the hierarchical structure, namely, multivariate normality and CD assumptions. Therefore, the two approaches could be combined, where the measurement model accounts for CD at the observed response level, while asymmetric latent trait dependence is captured at the second level. Future studies should explore the utility of such a unified framework. One challenge in implementation is developing an estimation algorithm that can incorporate both the copula-based joint model structure and the CD parameters, which extends beyond the scope of this article.

7. Discussion

In this study, a copula-based approach is proposed for jointly modeling speed and accuracy. The Gumbel and Joe copulas are adopted to capture the tail dependence between the latent ability and the latent speed. Copula theory was integrated into latent variable modeling, focusing on modeling tail dependence between latent traits within an IRT framework. By allowing for a flexible, tail-sensitive association between latent traits, the proposed framework enhances traditional psychometric models' capacity to represent a wider variety of latent trait relationships.

The simulation results suggest that the proposed framework is robust in both model selection and ability estimation. The results show that the likelihood-based model selection reliably identifies the true data-generating model across various dependence structures. When data were generated with tail dependence, the correctly specified copula models yielded more accurate ability estimates with lower RMSE than the traditional MVN model. This advantage was most prominent in the tails of the ability distribution. The practical consequence of the model misspecification is that the conventional MVN model is likely to misestimate ability for the lowest or the highest performing individuals.

The proposed copula-based models were applied to a variety of empirical cognitive test datasets. The frequent selection of copula models over the MVN model provides strong evidence that the relationship between ability and speed is often asymmetric and characterized by tail dependencies. The prevalence of the 90°-rotated Joe copula, particularly in the PISA science data, suggests that lower-tail dependence is common in large-scale assessments. This captures a scenario where low-ability students are disproportionately likely to respond quickly. While this pattern can sometimes arise due to item difficulty relative to the examinee's ability (Bolsinova et al., 2017), it is also frequently associated with test-taking behaviors like rapid guessing or disengagement. Detecting such behaviors commonly requires mixture models accounting for different latent classes of response processes (e.g., Lu et al., 2023; Ulitzsch et al., 2024). These mixture modeling approaches aim to explain tail variance by identifying

Downloaded from https://www.cambridge.org/core. 16 Nov 2026 at 02:13:47, subject to the Cambridge Core terms of use.

specific latent classes (e.g., rapid guessing). They assume that the heteroskedasticity stems from these discrete classes of pre-specified test-taking behaviors. In contrast, our copula approach does not attempt to reduce unexplained variance by introducing test-taking behavior classes. Instead, it models the asymmetric dependence and controls the magnitude of information borrowing between speed and ability. In regions where tail dependence is weak, the model borrows less information from response times to estimate ability, reflecting higher uncertainty. In regions of strong dependence, it leverages the dependence more heavily. This allows the model to accommodate tail heterogeneity without requiring a priori assumptions about specific aberrant behaviors. Future studies should explore the utility of these different approaches when diverse test-taking behaviors are present.

The choice of the dependence model can impact the accuracy and fairness of student scoring. For instance, as demonstrated in the simulations and Figures 8 and 9, when lower-tail dependence is present but ignored, the MVN model systematically overestimates the ability of low-performing, fast-responding examinees. The better-fitting 90°-rotated Joe copula model corrects for this by more appropriately penalizing these response patterns, leading to more valid ability estimates. Furthermore, the heterogeneity of the best-fitting model across countries underscores that a single model is insufficient for international assessments. The distinct patterns observed (e.g., 90J for USA/MEX vs. MVN for DEU) suggest that speed–accuracy dependence varies across populations, making flexible dependence modeling essential for valid cross-country comparisons.

While the EM algorithm with stochastic approximation demonstrated robust performance, our results suggest a potential area for refinement. We observed a consistent underestimation of the dependence parameter δ for the Joe copula, particularly in the strong dependence condition. We hypothesize that this occurs because the numerical quadrature used to approximate the joint distributions struggles to capture the very strong tail dependence in the Joe copula. Therefore, future research could benefit from exploring alternative estimation techniques. For instance, implementing a Metropolis–Hastings algorithm with a tail-heavy proposal distribution could potentially improve both the efficiency and accuracy of estimation for models with such extreme dependence structures.

In this study, the optimal dependence structure is determined via post-hoc model selection after fitting multiple rotated models. One may consider allowing an arbitrary rotation angle instead of restricting the rotation to perpendicular orientations. Specifically, the rotated latent traits can be defined as

$$\begin{pmatrix} \theta^* \\ \tau^* \end{pmatrix} = R(\omega) \begin{pmatrix} \theta \\ \tau \end{pmatrix}, \tag{33}$$

where

$$R(\omega) = \begin{bmatrix} \cos(\omega) & -\sin(\omega) \\ \sin(\omega) & \cos(\omega) \end{bmatrix} \tag{34}$$

is a rotation matrix with an arbitrary angle $\omega \in [0, 2\pi)$. However, such an arbitrary rotation angle may alter the variances and the interpretation of the latent traits, as the rotated variables become linear combinations of the original latent traits (θ, τ). Alternatively, one could restrict the rotation angle to the discrete set $\omega \in \left\{0, \frac{\pi}{2}, \pi, \frac{3\pi}{2}\right\}$ and estimate ω jointly with the other model parameters. However, this approach would require a grid search over the discrete space. Practically, this is equivalent to our current approach of fitting the models separately and selecting the optimal rotation using log-likelihood.

The copula-based joint model can be generalized and extended in several ways. Future research should evaluate the utility of copula models for modeling the dependence of latent traits other than ability and speed, such as missing propensity (Holman & Glas, 2005; Moustaki & Knott, 2000) as the joint-normality assumption for these traits may be violated. Another natural extension is to computerized adaptive testing (CAT), where a copula-based joint model could be applied to latent ability and speed estimation on-the-fly (Fan et al., 2012; Kern & Choe, 2021). In addition, the copula framework can be extended to SEM to address asymmetric dependencies between latent variables. For instance, copulas could link a latent variable measured by multiple indicators to a dichotomous risk outcome

Downloaded from https://www.cambridge.org/core. 16 Nov 2026 at 02:13:47, subject to the Cambridge Core terms of use.

underlying a continuous latent variable. This approach will provide a novel method for investigating risk-sensitive relationships among constructs that are not adequately modeled under traditional Gaussian assumptions. Lastly, the proposed model assumed that an examinee's latent speed is constant across items. This assumption can be relaxed to allow examinees to vary their speed during a test. For instance, when there is a time constraint, examinees may vary their speed and test-taking strategies depending on the remaining time. Response times under such constraints can have different interpretations, such as omission time (Guo et al., 2025) and power time (Lee & Ying, 2015). Future extensions can explore incorporating these alternative response times into the copula-based joint model framework.

Data availability statement. The data and code that support the findings of this study are available in the Open Science Framework (OSF) repository at https://osf.io/48z2k/overview?view_only=0457bfa01f8448a3a36b48fc49cd52ac.

Funding statement. The research reported here was supported by the Illinois Campus Research Board through award RB25124.

Competing interests. The authors declare that no competing interests exist.

References

Akaike, H. (1998). Information theory and an extension of the maximum likelihood principle. In E. Parzen, K. Tanabe, & G. Kitagawa (Eds.), Selected papers of Hirotugu Akaike (pp. 199–213). Springer.

Bolsinova, M., De Boeck, P., & Tijmstra, J. (2017). Modelling conditional dependence between response time and accuracy. *Psychometrika*, *82*(4), 1126–1148.

Bolt, D. M., & Liao, X. (2022). Item complexity: A neglected psychometric feature of test items? *Psychometrika*, *87*(4), 1195–1213.

Braeken, J., Kuppens, P., De Boeck, P., & Tuerlinckx, F. (2013). Contextualized personality questionnaires: A case for copulas in structural equation models for categorical data. *Multivariate Behavioral Research*, *48*(6), 845–870.

Braeken, J., Tuerlinckx, F., & De Boeck, P. (2007). Copula functions for residual dependency. *Psychometrika*, *72*, 393–411.

Chalmers, R. P. (2012). mirt: A multidimensional item response theory package for the R environment. *Journal of Statistical Software*, *48*(6), 1–29. https://doi.org/10.18637/jss.v048.i06

Coomans, F., Hofman, A., Brinkhuis, M., Van Der Maas, H. L., & Maris, G. (2016). Distinguishing fast and slow processes in accuracy-response time data. *PLoS One*, *11*(5), e0155149.

Demarta, S., & McNeil, A. J. (2005). The t copula and related copulas. *International Statistical Review*, *73*(1), 111–129.

Dempster, A. P., Laird, N. M., & Rubin, D. B. (1977). Maximum likelihood from incomplete data via the EM algorithm. *Journal of the Royal Statistical Society: Series B (Methodological)*, *39*(1), 1–22.

Domingue, B. W., Braginsky, M., Caffrey-Maffei, L., Gilbert, J., Kanopka, K., Kapoor, R., Liu, Y., Nadela, S., Pan, G., Zhang, L., Zhang, S., & Frank, M. C. (2024). Solving the problem of data in psychometrics: An introduction to the item response warehouse (IRW). PsyArXiv. https://doi.org/10.31234/osf.io/7bd54

Domingue, B. W., Kanopka, K., Kapoor, R., Pohl, S., Chalmers, R. P., Rahal, C., & Rhemtulla, M. (2024). The InterModel vigorish as a lens for understanding (and quantifying) the value of item response models for dichotomously coded items. *Psychometrika*, *89*(3), 1034–1054.

Domingue, B. W., Kanopka, K., Stenhaug, B., Sulik, M. J., Beverly, T., Brinkhuis, M., Circi, R., Faul, J., Liao, D., McCandliss, B., Obradovic, J., Piech, C., Porter, T., Project iLEAD Consortium, Soland, J., Weeks, J., Wise, S. L., & Yeatman, J. (2022). Speed–accuracy trade-off? Not so fast: Marginal changes in speed have inconsistent relationships with accuracy in real-world settings. *Journal of Educational and Behavioral Statistics*, *47*(5), 576–602.

Donnelly, C., & Embrechts, P. (2010). The devil is in the tails: Actuarial mathematics and the subprime mortgage crisis. *ASTIN Bulletin: The Journal of the IAA*, *40*(1), 1–33.

Emura, T., Nakatochi, M., Murotani, K., & Rondeau, V. (2017). A joint frailty-copula model between tumour progression and death for meta-analysis. *Statistical Methods in Medical Research*, *26*(6), 2649–2666.

Fan, Z., Wang, C., Chang, H.-H., & Douglas, J. (2012). Utilizing response time distributions for item selection in cat. *Journal of Educational and Behavioral Statistics*, *37*(5), 655–670.

Fu, Z., Su, Y.-H., & Tao, J. (2019). A copula model for residual dependency in DINA model. In M. Wiberg, S. Culpepper, R. Janssen, J. González, & D. Molenaar (Eds), *Quantitative psychology: 83rd annual meeting of the psychometric society, New York, NY, 2018* (pp. 145–156). Springer.

Genest, C., Okhrin, O., & Bodnar, T. (2024). Copula modeling from Abe Sklar to the present day. *Journal of Multivariate Analysis*, *201*, 105278.

Ghosh, S., Sheppard, L. W., Holder, M. T., Loecke, T. D., Reid, P. C., Bever, J. D., & Reuman, D. C. (2020). Copulas and their potential for ecology. In *Advances in ecological research* (pp. 409–468). Elsevier. https://doi.org/10.1016/bs.aecr.2020.01.003

Glas, C. A., & van der Linden, W. J. (2010). Marginal likelihood inference for a model for item responses and response times. *British Journal of Mathematical and Statistical Psychology*, *63*(3), 603–626.

Downloaded from https://www.cambridge.org/core. 16 Nov 2026 at 02:13:47, subject to the Cambridge Core terms of use.

Gumbel, E. J. (1960). Bivariate exponential distributions. *Journal of the American Statistical Association*, *55*(292), 698–707.
Guo, J., Xu, X., Ying, Z., & Zhang, S. (2022). Modeling not-reached items in timed tests: A response time censoring approach. *Psychometrika*, *87*(3), 1–33.
Guo, J., Xu, X., & Zhang, S. (2025). Jointly modeling omitted and not-reached items in time-limit tests: A survival analysis approach. *Journal of Educational and Behavioral Statistics*, https://doi.org/10.3102/10769986251380892
Haertel, E. H. (1989). Using restricted latent class models to map the skill structure of achievement items. *Journal of Educational Measurement*, *26*(4), 301–321.
Hansen, M. H., & Yu, B. (2001). Model selection and the principle of minimum description length. *Journal of the American Statistical Association*, *96*(454), 746–774.
Hofert, M., Kojadinovic, I., Maechler, M., & Yan, J. (2025). Copula: Multivariate dependence with copulas. R package version 1.1-6. https://CRAN.R-project.org/package=copula
Holman, R., & Glas, C. A. (2005). Modelling non-ignorable missing-data mechanisms with item response theory models. *British Journal of Mathematical and Statistical Psychology*, *58*(1), 1–17.
Hooper, M. A., Tomarken, A., & Gauthier, I. (2024). Measuring visual ability in linguistically diverse populations. *Behavior Research Methods*, *57*(1), 36.
Joe, H. (1997). *Multivariate models and multivariate dependence concepts*. CRC Press.
Joe, H. (2014). *Dependence modeling with copulas*. CRC Press.
Junker, B. W., & Sijtsma, K. (2001). Cognitive assessment models with few assumptions, and connections with nonparametric item response theory. *Applied Psychological Measurement*, *25*(3), 258–272.
Kadhem, S. H., & Nikoloulopoulos, A. K. (2023a). Bi-factor and second-order copula models for item response data. *Psychometrika*, *88*(1), 132–157.
Kadhem, S. H., & Nikoloulopoulos, A. K. (2023b). Factor tree copula models for item response data. *Psychometrika*, *88*(3), 776–802.
Kang, I., De Boeck, P., & Ratcliff, R. (2022). Modeling conditional dependence of response accuracy and response time with the diffusion item response theory model. *Psychometrika*, *87*(2), 725–748.
Kang, I., Jeon, M., & Partchev, I. (2023). A latent space diffusion item response theory model to explore conditional dependence between responses and response times. *Psychometrika*, *88*(3), 830–864.
Kern, J. L., & Choe, E. (2021). Using a response time–based expected a posteriori estimator to control for differential speededness in computerized adaptive test. *Applied Psychological Measurement*, *45*(5), 361–385.
Krupskii, P., & Joe, H. (2013). Factor copula models for multivariate data. *Journal of Multivariate Analysis*, *120*, 85–101.
Lee, S., & Bolt, D. M. (2018). Asymmetric item characteristic curves and item complexity: Insights from simulation and real data analyses. *Psychometrika*, *83*(2), 453–475.
Lee, Y.-H., & Ying, Z. (2015). A mixture cure-rate model for responses and response times in time-limit tests. *Psychometrika*, *80*(3), 748–775.
Liu, Y., & Wang, W. (2024). What can we learn from a semiparametric factor analysis of item responses and response time? An illustration with the PISA 2015 data. *Psychometrika*, *89*(2), 386–410.
Lu, J., Wang, C., & Shi, N. (2023). A mixture response time process model for aberrant behaviors and item nonresponses. *Multivariate Behavioral Research*, *58*(1), 71–89.
Maris, E. (1993). Additive and multiplicative models for gamma distributed random variables, and their application as psychometric models for response times. *Psychometrika*, *58*(3), 445–469.
Michaelides, M. P., & Ivanova, M. (2022). Response time as an indicator of test-taking effort in PISA: Country and item-type differences. *Psychological Test and Assessment Modeling*, *64*(3), 304–338.
Moustaki, I., & Knott, M. (2000). Weighting for item non-response in attitude scales by using latent variable models with covariates. *Journal of the Royal Statistical Society Series A: Statistics in Society*, *163*(3), 445–459.
Nelsen, R. B. (2006). *An introduction to copulas*. Springer.
Nikoloulopoulos, A. K., & Joe, H. (2015). Factor copula models for item response data. *Psychometrika*, *80*(1), 126–150.
Pitt, M. A., & Myung, I. J. (2002). When a good fit can be bad. *Trends in Cognitive Sciences*, *6*(10), 421–425.
Pohl, S., Ulitzsch, E., & von Davier, M. (2019). Using response times to model not-reached items due to time limits. *Psychometrika*, *84*(3), 892–920.
Rissanen, J. J. (2002). Fisher information and stochastic complexity. *IEEE Transactions on Information Theory*, *42*(1), 40–47.
Robbins, H., & Monro, S. (1951). A stochastic approximation method. *The Annals of Mathematical Statistics*, *22*(3), 400–407.
Schepsmeier, U., & Stöber, J. (2014). Derivatives and fisher information of bivariate copulas. *Statistical Papers*, *55*(2), 525–542.
Schwarz, G. (1978). Estimating the dimension of a model. *The Annals of Statistics*, *6*(2), 461–464.
Shi, P., & Zhao, Z. (2024). Enhanced pricing and management of bundled insurance risks with dependence-aware prediction using pair copula construction. *Journal of Econometrics*, *240*(1), 105676.
Sklar, M. (1959). *Fonctions de repartition an dimensions et leurs marges* (Vol. *8*, pp. 229–231). Publications of the Institute of Statistical University.
Ulitzsch, E., Zhang, S., & Pohl, S. (2024). A model-based approach to the disentanglement and differential treatment of engaged and disengaged item omissions. *Multivariate Behavioral Research*, *59*(3), 599–619.

Downloaded from https://www.cambridge.org/core. 16 Nov 2026 at 02:13:47, subject to the Cambridge Core terms of use.

van der Linden, W. J. (2007). A hierarchical framework for modeling speed and accuracy on test items. *Psychometrika*, *72*(3), 287–308.

van der Linden, W. J., Klein Entink, R. H., & Fox, J.-P. (2010). IRT parameter estimation with response times as collateral information. *Applied Psychological Measurement*, *34*(5), 327–347.

Zhang, X., Kim, M., Yan, C., & Zhao, Y. (2024). Default dependence in the insurance and banking sectors: A copula approach. *Journal of International Financial Markets, Institutions and Money*, *91*, 101911.

Appendix A. Marginal maximum likelihood estimation for copula-based joint model

The marginal likelihood function of a copula-based joint model is

$$\begin{aligned} &L(\mathbf{a}, \mathbf{b}, \boldsymbol{\alpha}, \boldsymbol{\beta}, \sigma_\tau^2, \delta) \\ &= \prod_{p=1}^{N} \Big\{ \iint \prod_{i=1}^{I} [P(Y_{pi} \mid \theta_p, a_i, b_i) f(T_{pi} \mid \tau_p, \alpha_i, \beta_i)] f_{\theta,\tau}(\theta_p, \tau_p \mid \sigma_\tau^2, \delta) d\theta_p d\tau_p \Big\}. \end{aligned} \tag{A.1}$$

A.1. EM algorithm with stochastic approximation

Let $\boldsymbol{\eta}^{(m)} = (\boldsymbol{\zeta}^{(m)}, \boldsymbol{\psi}^{(m)})'$ denote the parameter estimates at the m-th iteration where $\boldsymbol{\zeta}_i = (a_i, b_i, \alpha_i, \beta_i)'$ and $\boldsymbol{\psi} = (\sigma_\tau^2, \delta)'$. Denote the latent ability and speed of person p as $\boldsymbol{\lambda}_p = (\theta_p, \tau_p)'$.

A.1.1. E-step

In the E-step, based on $\boldsymbol{\eta}^{(m)}$, we compute the expected complete-data log-likelihood given the observed data with respect to the posterior distribution of latent traits:

$$Q(\boldsymbol{\eta} \mid \boldsymbol{\eta}^{(m)}) = E\Big[\log h(\boldsymbol{\eta} \mid \tilde{\mathbf{Y}}, \tilde{\mathbf{T}}, \boldsymbol{\theta}, \boldsymbol{\tau}) \Big| \boldsymbol{\eta}^{(m)}, \tilde{\mathbf{Y}}, \tilde{\mathbf{T}}\Big], \tag{A.2}$$

where

$$h(\boldsymbol{\eta} \mid \tilde{\mathbf{Y}}, \tilde{\mathbf{T}}, \boldsymbol{\theta}, \boldsymbol{\tau}) = \prod_{p=1}^{N} \prod_{i=1}^{I} P(Y_{pi} \mid \theta_p, a_i, b_i) f(T_{pi} \mid \tau_p, \alpha_i, \beta_i). \tag{A.3}$$

The Q-function can be written as

$$Q(\boldsymbol{\eta} \mid \boldsymbol{\eta}^{(m)}) = \sum_{i=1}^{I} Q_i(\boldsymbol{\zeta}_i, \sigma_\tau^2, \delta \mid \boldsymbol{\eta}^{(m)}), \tag{A.4}$$

where

$$Q_i(\boldsymbol{\zeta}_i, \sigma_\tau^2, \delta \mid \boldsymbol{\eta}^{(m)}) = \sum_{p=1}^{N} E\Big\{\log P(Y_{pi} = y_{pi} \mid \theta_p) + \log f(t_{pi} \mid \tau_p) \Big| \boldsymbol{\eta}^{(m)}, \tilde{\mathbf{Y}}, \tilde{\mathbf{T}}\Big\}. \tag{A.5}$$

For person p, the posterior distribution of latent traits is proportional to $L(\boldsymbol{\eta}^{(m)} \mid \tilde{\mathbf{Y}}_p, \tilde{\mathbf{T}}_p, \theta_p, \tau_p)$.

$$p(\theta_p, \tau_p \mid \boldsymbol{\eta}^{(m)}, \tilde{\mathbf{Y}}_p, \tilde{\mathbf{T}}_p) = \frac{L(\boldsymbol{\eta}^{(m)} \mid \tilde{\mathbf{Y}}_p, \tilde{\mathbf{T}}_p, \theta_p, \tau_p)}{\iint L(\boldsymbol{\eta}^{(m)} \mid \tilde{\mathbf{Y}}_p, \tilde{\mathbf{T}}_p, \theta, \tau) d\theta d\tau}, \tag{A.6}$$

where $L(\boldsymbol{\eta}^{(m)} \mid \tilde{\mathbf{Y}}_p, \tilde{\mathbf{T}}_p, \theta_p, \tau_p)$ is

$$\prod_{i=1}^{I} \Big[P(y_{pi} \mid \theta_p, a_i^{(m)}, b_i^{(m)}) f(t_{pi} \mid \tau_p, \alpha_i^{(m)}, \beta_i^{(m)}) f(\theta_p, \tau_p \mid \sigma_\tau^{2(m)}, \delta^{(m)})\Big]. \tag{A.7}$$

We approximate the posterior distribution in Equation (A.6) via numerical integration, using $21 \times 21 = 441$ equally spaced cubature points on the domain $[-4, 4] \times [-4\sigma_\tau^{(m)}, 4\sigma_\tau^{(m)}]$. Let Δ denote the set of cubature points. Then Q_i is approximated by

$$\hat{Q}_i(\boldsymbol{\zeta}_i, \sigma_\tau^2, \delta \mid \boldsymbol{\eta}^{(m)}) = \sum_{p=1}^{N} \sum_{(\theta,\tau)\in\Delta} \Big\{\Big[\log P(Y_{pi} = y_{pi} \mid \theta) + \log f(t_{pi} \mid \tau)\Big] \hat{p}(\theta, \tau \mid \boldsymbol{\eta}^{(m)}, \tilde{\mathbf{Y}}_p, \tilde{\mathbf{T}}_p)\Big\}, \tag{A.8}$$

with

$$\hat{p}(\theta, \tau \mid \boldsymbol{\eta}^{(m)}, \tilde{\mathbf{Y}}_p, \tilde{\mathbf{T}}_p) = \frac{L(\boldsymbol{\eta}^{(m)} \mid \tilde{\mathbf{Y}}_p, \tilde{\mathbf{T}}_p, \theta, \tau)}{\sum_{(\theta_q,\tau_q)\in\Delta} L(\boldsymbol{\eta}^{(m)} \mid \tilde{\mathbf{Y}}_p, \tilde{\mathbf{T}}_p, \theta_q, \tau_q)}. \tag{A.9}$$

Downloaded from https://www.cambridge.org/core. 16 Nov 2026 at 02:13:47, subject to the Cambridge Core terms of use.

Accordingly, the Q-function can be approximated by

$$\hat{Q}(\boldsymbol{\eta} \mid \boldsymbol{\eta}^{(m)}) = \sum_{i=1}^{I} \hat{Q}_i(\boldsymbol{\zeta}_i, \sigma_\tau^2, \delta \mid \boldsymbol{\eta}^{(m)}). \tag{A.10}$$

A.1.2. M-step

In the M-step, the $\hat{Q}$-function is maximized to obtain the parameter estimates for the $(m+1)$-th iteration:

$$\boldsymbol{\eta}^{(m+1)} = \arg\max_{\boldsymbol{\eta}} \hat{Q}(\boldsymbol{\eta} \mid \boldsymbol{\eta}^{(m)}). \tag{A.11}$$

This process consists of two steps, as in Guo et al. (2022). Let $\omega_p(\cdot)$ denote a generic operator for a first-order derivative of $\log P(\boldsymbol{y_p}, \boldsymbol{t_p}, \boldsymbol{\lambda_p}, \boldsymbol{\eta})$ with respect to any subset of parameters in $\boldsymbol{\eta}$. From Fisher's identity, the first-order derivatives of the log marginal likelihood are expressed as the expected first-order derivatives of the complete data log-likelihood. Then

$$\begin{aligned} \frac{\partial}{\partial \boldsymbol{\eta}} L(\boldsymbol{\eta}) &= \sum_{p=1}^{N} E\left[\omega_p(\boldsymbol{\eta}) \middle| \tilde{\mathbf{Y}}_p, \tilde{\mathbf{T}}_p, \boldsymbol{\eta}\right] \\ &= \sum_{p=1}^{N} E\left[\frac{\partial}{\partial \boldsymbol{\eta}} \log P(\tilde{\mathbf{Y}}_p, \tilde{\mathbf{T}}_p \boldsymbol{\lambda_p}, \boldsymbol{\zeta}) \middle| \tilde{\mathbf{Y}}_p, \tilde{\mathbf{T}}_p, \boldsymbol{\eta}\right] \\ &\quad + \sum_{p=1}^{N} E\left[\frac{\partial}{\partial \boldsymbol{\eta}} \log f(\boldsymbol{\lambda}_p \mid \sigma_\tau^2, \delta) \middle| \tilde{\mathbf{Y}}_p, \tilde{\mathbf{T}}_p, \boldsymbol{\eta}\right]. \end{aligned} \tag{A.12}$$

In the first step, the maximum likelihood estimates for the structural parameters $\boldsymbol{\psi}$ are obtained by equating the last term in Equation (A.12) given $\boldsymbol{\eta}^{(m)}$ to zero and solving for $\boldsymbol{\psi}$:

$$\begin{aligned} &\sum_{p=1}^{N} E\left[\frac{\partial}{\partial \boldsymbol{\psi}} \log f(\theta_p, \tau_p \mid \sigma_\tau^2, \delta) \middle| \tilde{\mathbf{Y}}_p, \tilde{\mathbf{T}}_p, \boldsymbol{\eta}^{(m)}\right] \\ &= E\left[\sum_{p=1}^{N} \frac{\partial}{\partial \boldsymbol{\psi}} \log f(\boldsymbol{\lambda}_p \mid \boldsymbol{\psi}) \middle| \tilde{\mathbf{Y}}, \tilde{\mathbf{T}}, \boldsymbol{\eta}^{(m)}\right] = 0. \end{aligned} \tag{A.13}$$

A stochastic approximation (Robbins & Monro, 1951) is used to find the root. Let $g\left(\boldsymbol{\psi}^{(m)}, \boldsymbol{\lambda}^{(m)}\right) = \sum_{p=1}^{N} \left\{ \frac{\partial}{\partial \boldsymbol{\psi}} \log f(\boldsymbol{\lambda}_p^{(m)} \mid \boldsymbol{\psi}^{(m)}) \Big|_{\boldsymbol{\psi}=\boldsymbol{\psi}^{(m)}} \right\}$. Then $\boldsymbol{\psi}$ is updated:

$$\boldsymbol{\psi}^{(m+1)} = \boldsymbol{\psi}^{(m)} - \gamma_m g\left(\boldsymbol{\psi}^{(m)}, \boldsymbol{\lambda}^{(m)}\right), \tag{A.14}$$

where $\boldsymbol{\lambda}^{(m)}$ is randomly sampled from Equation (A.6), and $\gamma_m \propto \frac{1}{m^\kappa}$, $\kappa \in (0.5, 1]$ is the step size at the m-th iteration. $\boldsymbol{\lambda}^{(m)}$ can be generated with an M-H sampler using the fact that the posterior distribution of $\boldsymbol{\lambda}_p$ is proportional to $L(\boldsymbol{\eta}^{(m)} \mid \tilde{\mathbf{Y}}_p, \tilde{\mathbf{T}}_p, \theta, \tau)$ in Equation (A.7). The gradient with respect to $\boldsymbol{\psi}$ is derived in Appendix B.

In the second step, the MML estimates for the item parameters can be updated by maximizing each $\hat{Q}_i$ using a gradient descent with a backtracking line search. For instance, update the slope parameter a_i at each step by

$$a_i^{(m+1)} = a_i^{(m)} + \xi_i^{(m)} \cdot \frac{\partial \hat{Q}_i}{\partial a_i}, \tag{A.15}$$

where $\xi_i^{(m)}$ is the step size determined by backtracking line search. Similarly, update $b_i^{(m+1)}$, $\alpha_i^{(m+1)}$, and $\beta_i^{(m+1)}$ as in Equation (A.15). The partial derivatives in Equation (A.15) are in Appendix B.

A.2. Standard error and latent trait estimation

Standard errors of the parameter estimates are obtained as in Glas and van der Linden (2010) by inverting the approximate information matrix:

$$I(\boldsymbol{\eta}) = \sum_{p=1}^{N} E\left[\omega_p(\boldsymbol{\eta}) \mid \mathbf{y}_p, \mathbf{t}_p, \boldsymbol{\eta}\right] E\left[\omega_p(\boldsymbol{\eta}) \mid \mathbf{y}_p, \mathbf{t}_p, \boldsymbol{\eta}\right]'. \tag{A.16}$$

The standard errors are then given by the square roots of the diagonal elements of the inverse information matrix:

$$\mathrm{SE}(\boldsymbol{\eta}) = \sqrt{\mathrm{diag}\left(I(\boldsymbol{\eta})^{-1}\right)}. \tag{A.17}$$

Downloaded from https://www.cambridge.org/core. 16 Nov 2026 at 02:13:47, subject to the Cambridge Core terms of use.

The expected a posteriori (EAP) estimates of the latent traits of each person, given the parameter estimates $\hat{\boldsymbol{\eta}}$, are computed as follows:

$$\begin{aligned}\hat{\theta}_p &= E[\theta \mid \hat{\boldsymbol{\eta}}, \tilde{\mathbf{Y}}_p, \tilde{\mathbf{T}}_p] \approx \sum_{(\theta,\tau)\in\Delta} \theta \cdot \hat{p}(\theta, \tau \mid \hat{\boldsymbol{\eta}}, \tilde{\mathbf{Y}}_p, \tilde{\mathbf{T}}_p),\\ \hat{\tau}_p &= E[\tau \mid \hat{\boldsymbol{\eta}}, \tilde{\mathbf{Y}}_p, \tilde{\mathbf{T}}_p] \approx \sum_{(\theta,\tau)\in\Delta} \tau \cdot \hat{p}(\theta, \tau \mid \hat{\boldsymbol{\eta}}, \tilde{\mathbf{Y}}_p, \tilde{\mathbf{T}}_p).\end{aligned} \tag{A.18}$$

Appendix B. Gradient of the log joint PDF with Gumbel and Joe copulas

B.1. Gumbel copula

Here, we derive the gradient of the log joint PDF of θ and τ with Gumbel copula with respect to $\boldsymbol{\psi} = (\delta, \sigma_\tau^2)$:

$$\log f(\theta, \tau) = \log c(u, v) + \log f_\theta(\theta) + \log f_\tau(\tau), \tag{B.1}$$

where $u = F_\theta(\theta)$ and $v = F_\tau(\tau)$.

The partial derivative of $\log f(\theta, \tau)$ with respect to δ is

$$\begin{aligned}\frac{\partial \log f(\theta,\tau)}{\partial \delta} &= \frac{\partial \log c(u,v)}{\partial \delta}\\ &= \Big[-1 + \frac{1}{A+\delta-1} + \frac{1-2\delta}{A}\Big]\frac{\partial A}{\partial \delta} + \frac{1}{A+\delta-1} - 2\log A + \log x + \log y,\end{aligned} \tag{B.2}$$

where $x = -\log u$, $y = -\log v$, and $A = (x^\delta + y^\delta)^{1/\delta}$ with

$$\frac{\partial A}{\partial \delta} = \frac{A}{\delta}\left(\frac{x^\delta \log x + y^\delta \log y}{x^\delta + y^\delta} - \log A\right). \tag{B.3}$$

The partial derivative of $\log f(\theta, \tau)$ with respect to σ_τ^2 is

$$\begin{aligned}\frac{\partial \log f(\theta,\tau)}{\partial \sigma_\tau^2} &= \frac{\partial \log c(u,v)}{\partial \sigma_\tau^2} + \frac{\partial \log f_\tau(\tau)}{\partial \sigma_\tau^2}\\ &= \frac{\partial \log c(u,v)}{\partial v}\frac{\partial v}{\partial \sigma_\tau^2} + \frac{\partial \log f_\tau(\tau)}{\partial \sigma_\tau^2},\end{aligned} \tag{B.4}$$

where

$$\frac{\partial \log c(u,v)}{\partial v} = \Big[-1 + \frac{1}{A+\delta-1} + \frac{1-2\delta}{A}\Big]\frac{\partial A}{\partial v} - \frac{\delta-1}{yv} - \frac{1}{v}, \tag{B.5}$$

with $\frac{\partial A}{\partial v} = -\frac{1}{v}A^{1-\delta}y^{\delta-1}$, and

$$\frac{\partial v}{\partial \sigma_\tau^2} = \frac{\partial F_\tau(\tau)}{\partial \sigma_\tau^2} = -\frac{\tau}{2(\sigma_\tau^2)^{3/2}}\phi\left(\frac{\tau}{\sqrt{\sigma_\tau^2}}\right), \tag{B.6}$$

with $\phi()$ being the PDF of the standard normal distribution. The last term in Equation (B.4) is

$$\frac{\partial \log f_\tau(\tau)}{\partial \sigma_\tau^2} = \frac{\tau^2 - \sigma_\tau^2}{2\sigma_\tau^4}. \tag{B.7}$$

B.2. Joe copula

Let $u = F_\theta(\theta)$ and $v = F_\tau(\tau)$. The copula density of the bivariate Joe copula is

$$c(u, v) = (\bar{u}^\delta + \bar{v}^\delta - \bar{u}^\delta\bar{v}^\delta)^{-2+1/\delta}\bar{u}^{\delta-1}\bar{v}^{\delta-1}[\delta - 1 + \bar{u}^\delta + \bar{v}^\delta - \bar{u}^\delta\bar{v}^\delta], \tag{B.8}$$

where $\bar{u} = 1 - u$ and $\bar{v} = 1 - v$.

$$\log c(u, v) = (-2 + \delta^{-1})\log B + (\delta - 1)\log \bar{u}\bar{v} + \log(\delta - 1 + B), \tag{B.9}$$

where $B = \bar{u}^\delta + \bar{v}^\delta - \bar{u}^\delta\bar{v}^\delta$.

Downloaded from https://www.cambridge.org/core. 16 Nov 2026 at 02:13:47, subject to the Cambridge Core terms of use.

The partial derivative of $\log f(\theta,\tau)$ w.r.t. δ is

$$\begin{aligned}\frac{\partial \log f(\theta,\tau)}{\partial \delta} &= \frac{\partial \log c(u,v)}{\partial \delta} \\ &= -\delta^{-2}\log B + (-2+\delta^{-1})B^{-1}\frac{\partial B}{\partial \delta} + \log \tilde{u}\tilde{v} + \frac{1}{\delta - 1 + B}\left(1 + \frac{\partial B}{\partial \delta}\right),\end{aligned} \tag{B.10}$$

where

$$\frac{\partial B}{\partial \delta} = \tilde{u}^{\delta}\log\tilde{u} + \tilde{v}^{\delta}\log\tilde{v} - \tilde{u}^{\delta}\tilde{v}^{\delta}\log\tilde{u}\tilde{v}. \tag{B.11}$$

And the partial derivative of $\log f(\theta,\tau)$ w.r.t. σ_τ^2 is obtained by replacing $\frac{\partial \log c(u,v)}{\partial v}$ in Equation (B.4) with

$$\frac{\partial \log c(u,v)}{\partial v} = (-2+\delta^{-1})B^{-1}\frac{\partial B}{\partial v} + (1-\delta)\tilde{v}^{-1} + \frac{1}{\delta - 1 + B}\frac{\partial B}{\partial v}, \tag{B.12}$$

where

$$\frac{\partial B}{\partial v} = -\delta(1-\tilde{u}^{\delta})\tilde{v}^{\delta-1}. \tag{B.13}$$

B.3. Partial derivatives of $\hat{Q}_i$ in Equation (A.15)

$$\begin{aligned}\frac{\partial \hat{Q}_i}{\partial a_i} &= \sum_p \sum_{(\theta,\tau)} \omega_p(a_i)\cdot \hat{p}(\theta,\tau \mid \boldsymbol{\eta}, \tilde{\mathbf{Y}}_p, \tilde{\mathbf{T}}_p), \\ \frac{\partial \hat{Q}_i}{\partial b_i} &= \sum_p \sum_{(\theta,\tau)} \omega_p(b_i)\cdot \hat{p}(\theta,\tau \mid \boldsymbol{\eta}, \tilde{\mathbf{Y}}_p, \tilde{\mathbf{T}}_p), \\ \frac{\partial \hat{Q}_i}{\partial \alpha_i} &= \sum_p \sum_{(\theta,\tau)} \omega_p(\alpha_i)\cdot \hat{p}(\theta,\tau \mid \boldsymbol{\eta}, \tilde{\mathbf{Y}}_p, \tilde{\mathbf{T}}_p), \\ \frac{\partial \hat{Q}_i}{\partial \beta_i} &= \sum_p \sum_{(\theta,\tau)} \omega_p(\beta_i)\cdot \hat{p}(\theta,\tau \mid \boldsymbol{\eta}, \tilde{\mathbf{Y}}_p, \tilde{\mathbf{T}}_p),\end{aligned} \tag{B.14}$$

and $H(z) = 1/(1+\exp(-z))$. The first-order derivatives for the item parameters are given by

$$\begin{aligned}\omega_p(a_i) &= y_{pi}(\theta - b_i) - H(a_i(\theta - b_i))\,\theta, \\ \omega_p(b_i) &= \left[H(a_i(\theta - b_i)) - y_{pi}\right]a_i, \\ \omega_p(\alpha_i) &= \alpha_i^{-1} - \alpha_i(\log t_{pi} + \tau - \beta_i)^2, \\ \omega_p(\beta_i) &= \alpha_i^2(\log t_{pi} + \tau - \beta_i).\end{aligned} \tag{B.15}$$

These derivatives are invariant to the choice of copula function and its rotation.

Appendix C. Gradient of the log joint PDF with rotated copulas

C.1. 270°-rotated Gumbel copula

The joint PDF is of θ, τ is

$$f(\theta,\tau) = c_{270}(u,v) f_\theta(\theta) f_\tau(\tau). \tag{C.1}$$

The Gumbel copula density is

$$c(u,v) = \exp\left\{-\left[x^{\delta}+y^{\delta}\right]^{1/\delta}\right\}\left[(x^{\delta}+y^{\delta})^{1/\delta} + \delta - 1\right]\left[x^{\delta}+y^{\delta}\right]^{1/\delta-2}(xy)^{\delta-1}(uv)^{-1}. \tag{C.2}$$

Let $\tilde{y} = -\log(1-v)$, $\tilde{v} = 1-v$, and $\tilde{A} = (x^{\delta}+\tilde{y}^{\delta})^{1/\delta}$. The 270°-rotated Gumbel copula density is

$$\begin{aligned}c_{270}(u,v) &= c(u,1-v) \\ &= \exp\{-\tilde{A}\}\left[\tilde{A} + \delta - 1\right]\tilde{A}^{1-2\delta}(x\tilde{y})^{\delta-1}(u\tilde{v})^{-1}.\end{aligned} \tag{C.3}$$

Downloaded from https://www.cambridge.org/core. 16 Nov 2026 at 02:13:47, subject to the Cambridge Core terms of use.

Taking the logarithm,

$$\log c_{270}(u,v) = -\bar{A} + \log(\bar{A}+\delta-1) + (1-2\delta)\log\bar{A} + (\delta-1)\log(x\bar{y}) - \log(u\bar{v}). \tag{C.4}$$

The partial derivative of $\log c_{270}(u,v)$ w.r.t. δ is

$$\frac{\partial \log c_{270}(u,v)}{\partial\delta} = \left[-1 + \frac{1}{\bar{A}+\delta-1} + \frac{1-2\delta}{\bar{A}}\right]\frac{\partial\bar{A}}{\partial\delta} + \frac{1}{\bar{A}+\delta-1} - 2\log\bar{A} + \log(x\bar{y}), \tag{C.5}$$

where

$$\frac{\partial\bar{A}}{\partial\delta} = \frac{\bar{A}}{\delta}\left(\frac{x^\delta\log x + \bar{y}^\delta\log\bar{y}}{x^\delta+\bar{y}^\delta} - \log\bar{A}\right). \tag{C.6}$$

The partial derivative of $f(\theta,\tau)$ w.r.t. σ_τ^2 is obtained by replacing Equation (B.5) with

$$\frac{\partial \log c_{270}(u,v)}{\partial v} = \left[-1 + \frac{1}{\bar{A}+\delta-1} + \frac{1-2\delta}{\bar{A}}\right]\frac{\partial\bar{A}}{\partial v} + \frac{\delta-1}{\bar{y}(1-v)} + \frac{1}{\bar{v}}, \tag{C.7}$$

where

$$\frac{\partial\bar{A}}{\partial v} = \frac{1}{\bar{v}}\bar{A}^{1-\delta}\bar{y}^{\delta-1}. \tag{C.8}$$

C.2. 90°-rotated Gumbel copula

The joint PDF is of θ, τ is

$$f(\theta,\tau) = c_{90}(u,v) f_\theta(\theta) f_\tau(\tau). \tag{C.9}$$

The Gumbel copula density is

$$c(u,v) = \exp\left\{-\left[x^\delta+y^\delta\right]^{1/\delta}\right\}\left[(x^\delta+y^\delta)^{1/\delta}+\delta-1\right]\left[x^\delta+y^\delta\right]^{1/\delta-2}(xy)^{\delta-1}(uv)^{-1}. \tag{C.10}$$

Let $\tilde{x} = -\log(1-u)$, $\tilde{u} = 1-u$, and $\tilde{A} = (\tilde{x}^\delta+y^\delta)^{1/\delta}$. The 90°-rotated Gumbel copula density is

$$\begin{aligned} c_{90}(u,v) &= c(1-u,v) \\ &= \exp\{-\tilde{A}\}\left[\tilde{A}+\delta-1\right]\tilde{A}^{1-2\delta}(\tilde{x}y)^{\delta-1}(\tilde{u}v)^{-1}. \end{aligned} \tag{C.11}$$

Taking the logarithm,

$$\log c_{90}(u,v) = -\tilde{A} + \log(\tilde{A}+\delta-1) + (1-2\delta)\log\tilde{A} + (\delta-1)\log(\tilde{x}y) - \log(\tilde{u}v). \tag{C.12}$$

The partial derivative of $\log c_{90}(u,v)$ w.r.t. δ is

$$\frac{\partial \log c_{90}(u,v)}{\partial\delta} = \left[-1 + \frac{1}{\tilde{A}+\delta-1} + \frac{1-2\delta}{\tilde{A}}\right]\frac{\partial\tilde{A}}{\partial\delta} + \frac{1}{\tilde{A}+\delta-1} - 2\log\tilde{A} + \log(\tilde{x}y), \tag{C.13}$$

where

$$\frac{\partial\tilde{A}}{\partial\delta} = \frac{\tilde{A}}{\delta}\left(\frac{\tilde{x}^\delta\log\tilde{x} + y^\delta\log y}{\tilde{x}^\delta+y^\delta} - \log\tilde{A}\right). \tag{C.14}$$

The partial derivative of $f(\theta,\tau)$ w.r.t. σ_τ^2 is obtained by replacing Equation (B.5) with

$$\frac{\partial \log c_{90}(u,v)}{\partial v} = \left[-1 + \frac{1}{\tilde{A}+\delta-1} + \frac{1-2\delta}{\tilde{A}}\right]\frac{\partial\tilde{A}}{\partial v} - \frac{\delta-1}{yv} - \frac{1}{v}, \tag{C.15}$$

where

$$\frac{\partial\tilde{A}}{\partial v} = -\frac{1}{v}\tilde{A}^{1-\delta}y^{\delta-1}. \tag{C.16}$$

Downloaded from https://www.cambridge.org/core. 16 Nov 2026 at 02:13:47, subject to the Cambridge Core terms of use.

C.3. 180°-rotated Gumbel copula

The joint PDF is of θ, τ is

$$f(\theta,\tau) = c_{180}(u,v) f_\theta(\theta) f_\tau(\tau). \tag{C.17}$$

The Gumbel copula density is

$$c(u,v) = \exp\left\{-\left[x^\delta + y^\delta\right]^{1/\delta}\right\}\left[\left(x^\delta + y^\delta\right)^{1/\delta} + \delta - 1\right]\left[x^\delta + y^\delta\right]^{1/\delta - 2}(xy)^{\delta-1}(uv)^{-1}. \tag{C.18}$$

Let $\bar{x} = -\log(1-u)$, $\bar{u} = 1-u$, $\bar{y} = -\log(1-v)$, $\bar{v} = 1-v$, and $\bar{A} = \left(\bar{x}^\delta + \bar{y}^\delta\right)^{1/\delta}$. The 180°-rotated Gumbel copula density is

$$\begin{aligned} c_{180}(u,v) &= c(1-u,1-v) \\ &= \exp\{-\bar{A}\}\left[\bar{A} + \delta - 1\right]\bar{A}^{1-2\delta}(\bar{x}\bar{y})^{\delta-1}(\bar{u}\bar{v})^{-1}. \end{aligned} \tag{C.19}$$

Taking the logarithm,

$$\log c_{180}(u,v) = -\bar{A} + \log(\bar{A} + \delta - 1) + (1-2\delta)\log\bar{A} + (\delta-1)\log(\bar{x}\bar{y}) - \log(\bar{u}\bar{v}). \tag{C.20}$$

The partial derivative of $\log c_{180}(u,v)$ w.r.t. δ is

$$\frac{\partial \log c_{180}(u,v)}{\partial \delta} = \left[-1 + \frac{1}{\bar{A} + \delta - 1} + \frac{1-2\delta}{\bar{A}}\right]\frac{\partial \bar{A}}{\partial \delta} + \frac{1}{\bar{A} + \delta - 1} - 2\log\bar{A} + \log(\bar{x}\bar{y}), \tag{C.21}$$

where

$$\frac{\partial \bar{A}}{\partial \delta} = \frac{\bar{A}}{\delta}\left(\frac{\bar{x}^\delta \log\bar{x} + \bar{y}^\delta \log\bar{y}}{\bar{x}^\delta + \bar{y}^\delta} - \log\bar{A}\right). \tag{C.22}$$

The partial derivative of $f(\theta,\tau)$ w.r.t. σ_τ^2 is obtained by replacing Equation (B.5) with

$$\frac{\partial \log c_{180}(u,v)}{\partial v} = \left[-1 + \frac{1}{\bar{A} + \delta - 1} + \frac{1-2\delta}{\bar{A}}\right]\frac{\partial \bar{A}}{\partial v} + \frac{\delta - 1}{\bar{y}\bar{v}} + \frac{1}{\bar{v}}, \tag{C.23}$$

where

$$\frac{\partial \bar{A}}{\partial v} = \frac{1}{\bar{v}}\bar{A}^{1-\delta}\bar{y}^{\delta-1}. \tag{C.24}$$

C.4. 270°-rotated Joe copula

The copula density of the bivariate Joe copula is

$$c(u,v) = \left(\bar{u}^\delta + \bar{v}^\delta - \bar{u}^\delta\bar{v}^\delta\right)^{-2+1/\delta}\bar{u}^{\delta-1}\bar{v}^{\delta-1}\left[\delta - 1 + \bar{u}^\delta + \bar{v}^\delta - \bar{u}^\delta\bar{v}^\delta\right], \tag{C.25}$$

where $\bar{u} = 1-u$ and $\bar{v} = 1-v$. The 270°-rotated copula density is

$$\begin{aligned} c_{270}(u,v) &= c(u,1-v) \\ &= \left(\bar{u}^\delta + v^\delta - \bar{u}^\delta v^\delta\right)^{-2+1/\delta}\bar{u}^{\delta-1}v^{\delta-1}\left[\delta - 1 + \bar{u}^\delta + v^\delta - \bar{u}^\delta v^\delta\right]. \end{aligned} \tag{C.26}$$

Then taking the logarithm,

$$\log c_{270}(u,v) = \left(-2 + \delta^{-1}\right)\log\tilde{B} + (\delta-1)\log(\bar{u}v) + \log(\delta - 1 + \tilde{B}), \tag{C.27}$$

with $\tilde{B} = \bar{u}^\delta + v^\delta - \bar{u}^\delta v^\delta$. The partial derivative of $\log f(\theta,\tau)$ w.r.t. δ is

$$\frac{\partial \log c_{270}(u,v)}{\partial \delta} = -\delta^{-2}\log\tilde{B} + \left(-2 + \delta^{-1}\right)\tilde{B}^{-1}\frac{\partial \tilde{B}}{\partial \delta} + \log\bar{u}v + \frac{1}{\delta - 1 + \tilde{B}}\left(1 + \frac{\partial \tilde{B}}{\partial \delta}\right), \tag{C.28}$$

where

$$\frac{\partial \tilde{B}}{\partial \delta} = \bar{u}^\delta\log\bar{u} + v^\delta\log v - \bar{u}^\delta v^\delta\log\bar{u}v. \tag{C.29}$$

The partial derivative of $f(\theta,\tau)$ w.r.t. σ_τ^2 is obtained by replacing Equation (B.5) with

$$\frac{\partial \log c(u,v)}{\partial v} = \left(-2 + \delta^{-1}\right)\tilde{B}^{-1}\frac{\partial \tilde{B}}{\partial v} + (\delta-1)v^{-1} + \frac{1}{\delta - 1 + \tilde{B}}\frac{\partial \tilde{B}}{\partial v}, \tag{C.30}$$

Downloaded from https://www.cambridge.org/core. 16 Nov 2026 at 02:13:47, subject to the Cambridge Core terms of use.

where

$$\frac{\partial \tilde{B}}{\partial v} = \delta(1-\tilde{u}^{\delta})v^{\delta-1}. \tag{C.31}$$

C.5. 90°-rotated Joe copula

The copula density of the bivariate Joe copula is

$$c(u,v) = (\tilde{u}^{\delta}+\tilde{v}^{\delta}-\tilde{u}^{\delta}\tilde{v}^{\delta})^{-2+1/\delta}\tilde{u}^{\delta-1}\tilde{v}^{\delta-1}[\delta-1+\tilde{u}^{\delta}+\tilde{v}^{\delta}-\tilde{u}^{\delta}\tilde{v}^{\delta}], \tag{C.32}$$

where $\tilde{u} = 1-u$ and $\tilde{v} = 1-v$. The 90°-rotated copula density is

$$\begin{aligned} c_{90}(u,v) &= c(1-u,v) \\ &= (u^{\delta}+\tilde{v}^{\delta}-u^{\delta}\tilde{v}^{\delta})^{-2+1/\delta}u^{\delta-1}\tilde{v}^{\delta-1}\left[\delta-1+u^{\delta}+\tilde{v}^{\delta}-u^{\delta}\tilde{v}^{\delta}\right]. \end{aligned} \tag{C.33}$$

Then taking the logarithm,

$$\log c_{90}(u,v) = (-2+\delta^{-1})\log\tilde{B} + (\delta-1)\log(u\tilde{v}) + \log(\delta-1+\tilde{B}), \tag{C.34}$$

with $\tilde{B} = u^{\delta}+\tilde{v}^{\delta}-u^{\delta}\tilde{v}^{\delta}$. The partial derivative of $\log f(\theta,\tau)$ w.r.t. δ is

$$\frac{\partial \log c_{90}(u,v)}{\partial\delta} = -\delta^{-2}\log\tilde{B} + (-2+\delta^{-1})\tilde{B}^{-1}\frac{\partial\tilde{B}}{\partial\delta} + \log u\tilde{v} + \frac{1}{\delta-1+\tilde{B}}\left(1+\frac{\partial\tilde{B}}{\partial\delta}\right), \tag{C.35}$$

where

$$\frac{\partial\tilde{B}}{\partial\delta} = u^{\delta}\log u + \tilde{v}^{\delta}\log\tilde{v} - u^{\delta}\tilde{v}^{\delta}\log u\tilde{v}. \tag{C.36}$$

The partial derivative of $f(\theta,\tau)$ w.r.t. σ_{τ}^2 is obtained by replacing Equation (B.5) with

$$\frac{\partial \log c(u,v)}{\partial v} = (-2+\delta^{-1})\tilde{B}^{-1}\frac{\partial\tilde{B}}{\partial v} + \frac{\delta-1}{v-1} + \frac{1}{\delta-1+\tilde{B}}\frac{\partial\tilde{B}}{\partial v}, \tag{C.37}$$

where

$$\frac{\partial\tilde{B}}{\partial v} = -\delta(1-u^{\delta})\tilde{v}^{\delta-1}. \tag{C.38}$$

C.6. 180°-rotated Joe copula

The copula density of the bivariate Joe copula is

$$c(u,v) = (\tilde{u}^{\delta}+\tilde{v}^{\delta}-\tilde{u}^{\delta}\tilde{v}^{\delta})^{-2+1/\delta}\tilde{u}^{\delta-1}\tilde{v}^{\delta-1}[\delta-1+\tilde{u}^{\delta}+\tilde{v}^{\delta}-\tilde{u}^{\delta}\tilde{v}^{\delta}], \tag{C.39}$$

where $\tilde{u} = 1-u$ and $\tilde{v} = 1-v$. The 180°-rotated copula density is

$$\begin{aligned} c_{180}(u,v) &= c(1-u,1-v) \\ &= (u^{\delta}+v^{\delta}-u^{\delta}v^{\delta})^{-2+1/\delta}u^{\delta-1}v^{\delta-1}\left[\delta-1+u^{\delta}+v^{\delta}-u^{\delta}v^{\delta}\right]. \end{aligned} \tag{C.40}$$

Then taking the logarithm,

$$\log c_{180}(u,v) = (-2+\delta^{-1})\log\tilde{B} + (\delta-1)\log(uv) + \log(\delta-1+\tilde{B}), \tag{C.41}$$

with $\tilde{B} = u^{\delta}+v^{\delta}-u^{\delta}v^{\delta}$. The partial derivative of $\log f(\theta,\tau)$ w.r.t. δ is

$$\frac{\partial \log c_{180}(u,v)}{\partial\delta} = -\delta^{-2}\log\tilde{B} + (-2+\delta^{-1})\tilde{B}^{-1}\frac{\partial\tilde{B}}{\partial\delta} + \log uv + \frac{1}{\delta-1+\tilde{B}}\left(1+\frac{\partial\tilde{B}}{\partial\delta}\right), \tag{C.42}$$

where

$$\frac{\partial\tilde{B}}{\partial\delta} = u^{\delta}\log u + v^{\delta}\log v - u^{\delta}v^{\delta}\log uv. \tag{C.43}$$

Downloaded from https://www.cambridge.org/core. 16 Nov 2026 at 02:13:47, subject to the Cambridge Core terms of use.

The partial derivative of $f(\theta, \tau)$ w.r.t. σ_τ^2 is obtained by replacing Equation (B.5) with

$$\frac{\partial \log c(u, v)}{\partial v} = \left(-2 + \delta^{-1}\right)\bar{B}^{-1}\frac{\partial \bar{B}}{\partial v} + \frac{\delta - 1}{v} + \frac{1}{\delta - 1 + \bar{B}}\frac{\partial \bar{B}}{\partial v}, \tag{C.44}$$

where

$$\frac{\partial \bar{B}}{\partial v} = \delta\left(1 - u^\delta\right)v^{\delta - 1}. \tag{C.45}$$

Appendix D. Simulation results

Table D1. Average log marginal likelihood in the simulation study

			True: Gumbel			True: MVN			True: Joe		
N	I	τ_K	Gumbel	MVN	Joe	Gumbel	MVN	Joe	Gumbel	MVN	Joe
500	10	0.3	−8,516.8	−8,519.1	−8,519.0	−8,511.8	−8,509.5	−8,517.5	−8,507.6	−8,513.9	−8,505.7
1,000	10	0.3	−17,058.1	−17,062.7	−17,062.6	−17,041.6	−17,036.9	−17,053.4	−17,037.3	−17,049.6	−17,033.8
500	20	0.3	−14,193.3	−14,197.1	−14,196.2	−14,188.4	−14,184.4	−14,196.5	−14,180.9	−14,190.7	−14,178.0
1,000	20	0.3	−28,431.0	−28,438.6	−28,437.1	−28,421.6	−28,413.9	−28,437.8	−28,406.6	−28,426.6	−28,400.8
500	10	0.5	−8,465.6	−8,467.8	−8,471.4	−8,455.8	−8,452.4	−8,467.4	−8,456.1	−8,464.6	−8,453.7
1,000	10	0.5	−16,953.0	−16,957.7	−16,964.3	−16,928.6	−16,921.8	−16,952.1	−16,929.3	−16,946.1	−16,924.6
500	20	0.5	−14,127.9	−14,132.7	−14,135.1	−14,113.9	−14,108.2	−14,130.7	−14,107.1	−14,122.1	−14,101.6
1,000	20	0.5	−28,293.1	−28,302.9	−28,307.4	−28,273.9	−28,262.9	−28,307.4	−28,253.6	−28,284.1	−28,242.7

Note: τ_K denotes Kendall's τ rank coefficient. The main column headings indicate the true dependence structure used to generate the data. The sub-headings indicate the fitted models.

Downloaded from https://www.cambridge.org/core. 16 Nov 2026 at 02:13:47, subject to the Cambridge Core terms of use.

Table D2. Parameter recovery under the Joe copula dependence condition

Condition			Bias						MAD					
N	I	δ	a	b	α	β	δ	σ_τ	a	b	α	β	δ	σ_τ
500	10	1.77	0.012	−0.004	0.013	0.003	−0.099	−0.003	0.149	0.230	0.071	0.022	0.117	0.014
1,000	10	1.77	0.006	0.002	0.009	0.003	−0.104	−0.002	0.103	0.131	0.050	0.016	0.112	0.010
500	20	1.77	0.014	−0.040	0.008	0.001	−0.058	−0.003	0.153	0.221	0.068	0.022	0.089	0.013
1,000	20	1.77	0.008	−0.011	0.004	0.001	−0.059	−0.002	0.105	0.130	0.048	0.016	0.079	0.009
500	10	2.86	0.013	−0.008	0.011	0.008	−0.516	−0.006	0.151	0.247	0.071	0.022	0.516	0.014
1,000	10	2.86	0.005	0.001	0.007	0.008	−0.504	−0.007	0.103	0.135	0.049	0.017	0.504	0.011
500	20	2.86	0.014	−0.021	0.008	0.003	−0.337	−0.007	0.153	0.281	0.068	0.022	0.339	0.014
1,000	20	2.86	0.007	−0.013	0.003	0.003	−0.335	−0.006	0.107	0.134	0.048	0.016	0.335	0.010
Condition			RMSE						95% coverage rate					
N	I	δ	a	b	α	β	δ	σ_τ	a	b	α	β	δ	σ_τ
500	10	1.77	0.194	1.548	0.091	0.028	0.140	0.017	0.91	0.94	0.95	0.98	0.94	0.95
1,000	10	1.77	0.135	0.300	0.064	0.020	0.129	0.012	0.91	0.94	0.95	0.97	0.83	0.95
500	20	1.77	0.259	1.083	0.087	0.028	0.109	0.016	0.96	0.98	0.96	0.97	0.98	0.97
1,000	20	1.77	0.153	0.252	0.061	0.021	0.095	0.011	0.95	0.97	0.96	0.95	0.95	0.97
500	10	2.86	0.200	1.186	0.090	0.028	0.535	0.018	0.90	0.94	0.96	0.98	0.42	0.92
1,000	10	2.86	0.134	0.362	0.063	0.021	0.516	0.013	0.89	0.94	0.95	0.96	0.13	0.89
500	20	2.86	0.244	2.716	0.087	0.028	0.366	0.018	0.95	0.98	0.97	0.97	0.78	0.96
1,000	20	2.86	0.164	0.278	0.061	0.021	0.354	0.013	0.93	0.97	0.96	0.96	0.47	0.93
Condition			SE ratio											
N	I	δ	a	b	α	β	δ	σ_τ						
500	10	1.77	0.93	1.16	1.03	1.15	1.41	1.05						
1,000	10	1.77	0.92	1.10	1.01	1.09	1.24	1.03						
500	20	1.77	1.08	1.45	1.09	1.12	1.50	1.20						
1,000	20	1.77	1.03	1.31	1.04	1.01	1.24	1.14						
500	10	2.86	0.88	1.06	1.04	1.24	1.76	1.01						
1,000	10	2.86	0.88	1.06	1.02	1.15	1.51	1.03						
500	20	2.86	1.03	1.47	1.09	1.18	1.70	1.19						
1,000	20	2.86	0.97	1.19	1.04	1.09	1.42	1.13						

Note: N represents the sample size. I represents the test length. $\boldsymbol{a}$, $\boldsymbol{b}$, $\boldsymbol{\alpha}$, and $\boldsymbol{\beta}$ represent item parameters, and δ and σ_τ represent structural parameters.

Downloaded from https://www.cambridge.org/core. 16 Nov 2026 at 02:13:47, subject to the Cambridge Core terms of use.

Table D3. Accuracy of ability estimates under the Joe copula dependence condition

Condition			Bias(θ)				RMSE(θ)				Cor($\hat{\theta}$, θ)			
N	*I*	δ	Gumbel	Joe	MVN	Indep	Gumbel	Joe	MVN	Indep	Gumbel	Joe	MVN	Indep
500	10	1.77	0.004	0.005	0.001	0.000	0.554	0.552	0.566	0.597	0.832	0.833	0.824	0.801
1,000	10	1.77	0.003	0.004	0.000	−0.001	0.551	0.549	0.563	0.595	0.834	0.836	0.826	0.803
500	20	1.77	0.003	0.003	0.001	0.000	0.451	0.449	0.460	0.479	0.892	0.893	0.887	0.878
1,000	20	1.77	0.002	0.001	0.000	−0.001	0.449	0.448	0.458	0.477	0.893	0.894	0.889	0.879
500	10	2.86	0.007	0.016	0.000	−0.001	0.501	0.497	0.518	0.598	0.865	0.867	0.855	0.801
1,000	10	2.86	0.006	0.016	−0.001	−0.002	0.498	0.493	0.514	0.595	0.867	0.869	0.857	0.803
500	20	2.86	0.005	0.008	0.000	−0.002	0.415	0.410	0.431	0.479	0.909	0.912	0.902	0.877
1,000	20	2.86	0.004	0.008	0.000	−0.002	0.412	0.408	0.428	0.477	0.911	0.913	0.903	0.878

Note: *N* represents the sample size. *I* represents the test length. The column headers (Gumbel, Joe, MVN, and Indep) indicate the estimating model, while Gumbel was the data-generating model. *Indep* column represents the baseline independence 2PL model without response time.

Table D4. Accuracy of speed estimates under the Gumbel copula dependence condition

Condition			Bias(τ)			RMSE(τ)			Cor($\hat{\tau}$, τ)		
N	*I*	δ	Gumbel	Joe	MVN	Gumbel	Joe	MVN	Gumbel	Joe	MVN
500	10	1.43	0.001	0.003	0.001	0.124	0.124	0.124	0.969	0.969	0.969
1,000	10	1.43	0.002	0.003	0.002	0.123	0.123	0.123	0.969	0.969	0.969
500	20	1.43	0.000	0.001	0.000	0.090	0.090	0.090	0.984	0.984	0.984
1,000	20	1.43	0.002	0.002	0.001	0.088	0.088	0.088	0.984	0.984	0.984
500	10	2	0.003	0.009	0.001	0.122	0.123	0.123	0.970	0.969	0.969
1,000	10	2	0.003	0.010	0.002	0.122	0.122	0.122	0.970	0.970	0.970
500	20	2	0.002	0.004	0.002	0.089	0.089	0.089	0.984	0.984	0.984
1,000	20	2	0.002	0.005	0.002	0.088	0.088	0.088	0.985	0.985	0.985

Downloaded from https://www.cambridge.org/core. 16 Nov 2026 at 02:13:47, subject to the Cambridge Core terms of use.

Downloaded from https://www.cambridge.org/core. 16 Nov 2026 at 02:13:47, subject to the Cambridge Core terms of use.

Table D5. Item parameter recovery under Gumbel copula condition ($N = 500$, $I = 18$, and $\delta = 1.43$)

	Bias								RMSE								MAD							
	Gumbel				MVN				Gumbel				MVN				Gumbel				MVN			
Item	a	b	α	β	a	b	α	β	a	b	α	β	a	b	α	β	a	b	α	β	a	b	α	β
1	0.003	0.016	0.007	0.001	0.003	0.015	0.006	0.001	0.133	0.152	0.090	0.028	0.133	0.152	0.090	0.028	0.106	0.117	0.071	0.022	0.106	0.117	0.071	0.022
2	0.005	0.282	0.011	0.000	0.005	0.282	0.011	0.000	0.107	4.353	0.080	0.029	0.107	4.353	0.080	0.029	0.084	0.920	0.061	0.023	0.084	0.920	0.061	0.023
3	0.004	−0.010	0.017	0.000	0.004	−0.011	0.014	0.000	0.156	0.147	0.082	0.030	0.156	0.147	0.081	0.030	0.122	0.113	0.065	0.024	0.122	0.113	0.065	0.024
4	0.029	−0.117	0.016	0.001	0.029	−0.116	0.014	0.001	0.250	0.710	0.090	0.030	0.250	0.710	0.089	0.030	0.200	0.491	0.072	0.024	0.200	0.491	0.071	0.024
5	0.002	0.011	0.012	0.000	0.002	0.010	0.010	0.000	0.130	0.135	0.084	0.030	0.129	0.135	0.083	0.030	0.104	0.107	0.067	0.024	0.103	0.107	0.066	0.024
6	0.014	−0.005	0.028	0.000	0.014	−0.007	0.026	0.000	0.192	0.115	0.108	0.027	0.192	0.115	0.109	0.027	0.156	0.090	0.085	0.021	0.156	0.090	0.085	0.021
7	0.009	0.000	0.015	0.001	0.009	0.000	0.014	0.001	0.129	0.174	0.091	0.027	0.129	0.174	0.091	0.027	0.102	0.132	0.072	0.022	0.102	0.132	0.071	0.022
8	0.009	0.010	0.005	0.001	0.009	0.007	0.005	0.001	0.207	0.087	0.073	0.030	0.207	0.087	0.073	0.030	0.161	0.070	0.058	0.024	0.161	0.069	0.058	0.024
9	0.007	0.003	0.008	0.000	0.007	0.002	0.007	0.000	0.155	0.130	0.067	0.030	0.155	0.130	0.067	0.030	0.123	0.100	0.053	0.024	0.123	0.100	0.052	0.024
10	0.017	−0.001	0.009	0.001	0.017	−0.003	0.008	0.001	0.217	0.099	0.074	0.029	0.217	0.099	0.074	0.029	0.170	0.078	0.060	0.023	0.170	0.077	0.059	0.023
11	0.168	−0.412	0.005	0.001	0.168	−0.410	0.005	0.001	0.892	2.473	0.088	0.028	0.892	2.473	0.088	0.028	0.569	0.849	0.070	0.022	0.569	0.851	0.070	0.022
12	0.014	0.004	0.009	0.001	0.014	0.003	0.008	0.000	0.162	0.118	0.098	0.028	0.162	0.117	0.098	0.028	0.129	0.090	0.078	0.022	0.129	0.089	0.078	0.023
13	0.018	−0.025	0.001	0.001	0.018	−0.024	0.001	0.001	0.201	0.244	0.088	0.028	0.201	0.244	0.088	0.028	0.160	0.189	0.070	0.022	0.160	0.189	0.071	0.023
14	0.017	0.011	0.013	0.002	0.017	0.009	0.011	0.002	0.187	0.117	0.074	0.030	0.187	0.118	0.074	0.030	0.145	0.091	0.058	0.024	0.145	0.092	0.058	0.024
15	0.029	0.015	0.009	0.000	0.029	0.016	0.008	0.000	0.222	0.268	0.074	0.029	0.222	0.268	0.074	0.030	0.170	0.202	0.059	0.024	0.170	0.202	0.059	0.024
16	0.005	−0.086	−0.002	0.000	0.005	−0.086	−0.001	0.000	0.192	0.485	0.091	0.027	0.192	0.485	0.092	0.027	0.155	0.355	0.073	0.021	0.155	0.356	0.073	0.021
17	0.002	0.000	−0.001	0.000	0.002	0.000	−0.001	0.000	0.123	0.142	0.102	0.027	0.123	0.142	0.103	0.028	0.100	0.111	0.083	0.022	0.100	0.111	0.083	0.022
18	0.007	−0.003	0.002	0.000	0.007	−0.005	0.001	0.000	0.147	0.110	0.078	0.029	0.147	0.110	0.079	0.029	0.117	0.085	0.063	0.023	0.117	0.084	0.063	0.023
19	0.007	−0.003	0.007	0.001	0.007	−0.004	0.007	0.000	0.150	0.151	0.064	0.032	0.150	0.151	0.064	0.032	0.120	0.120	0.051	0.025	0.120	0.120	0.051	0.025
20	0.007	−0.008	0.015	0.001	0.007	−0.009	0.014	0.001	0.190	0.140	0.083	0.029	0.190	0.140	0.083	0.029	0.150	0.112	0.065	0.023	0.150	0.112	0.065	0.023

Note: Data were simulated under the Gumbel copula condition. Results show the bias, RMSE, and mean absolute deviance (MAD) recovered using the Gumbel copula model and the MVN model. The MAD is calculated as $\text{MAD}(\eta) = \frac{1}{R}\sum_{r=1}^{R}(|\hat{\eta}^{(r)} - \eta|)$.

Downloaded from https://www.cambridge.org/core. 16 Nov 2026 at 02:13:47, subject to the Cambridge Core terms of use.

Table D6. Item parameter recovery under MVN dependence condition ($N = 500$, $I = 18$, and $\rho = 0.45$)

	Bias								RMSE								MAD							
	Gumbel				MVN				Gumbel				MVN				Gumbel				MVN			
Item	a	b	α	β	a	b	α	β	a	b	α	β	a	b	α	β	a	b	α	β	a	b	α	β
1	0.025	0.003	0.003	0.001	0.025	0.004	0.003	0.001	0.134	0.153	0.099	0.027	0.134	0.153	0.100	0.027	0.106	0.120	0.079	0.021	0.106	0.120	0.079	0.021
2	−0.002	−0.320	0.008	−0.001	−0.002	−0.320	0.008	0.000	0.108	6.946	0.084	0.028	0.108	6.946	0.084	0.029	0.084	1.334	0.067	0.023	0.084	1.334	0.067	0.023
3	0.010	−0.020	0.017	0.000	0.010	−0.020	0.016	0.001	0.169	0.160	0.082	0.029	0.169	0.160	0.082	0.029	0.132	0.121	0.064	0.024	0.132	0.121	0.064	0.024
4	0.029	−0.091	0.020	0.000	0.029	−0.091	0.019	0.001	0.236	0.670	0.092	0.028	0.236	0.671	0.091	0.028	0.187	0.461	0.073	0.022	0.187	0.462	0.072	0.022
5	0.014	−0.006	0.007	0.000	0.014	−0.006	0.005	0.001	0.136	0.133	0.086	0.031	0.136	0.133	0.086	0.031	0.107	0.103	0.070	0.024	0.107	0.103	0.070	0.024
6	0.018	0.001	0.028	0.000	0.018	0.001	0.027	0.000	0.196	0.125	0.113	0.027	0.196	0.125	0.113	0.027	0.153	0.099	0.087	0.022	0.153	0.098	0.087	0.022
7	0.003	−0.015	0.014	−0.001	0.003	−0.015	0.013	−0.001	0.131	0.173	0.095	0.028	0.131	0.173	0.095	0.028	0.103	0.134	0.074	0.023	0.103	0.134	0.074	0.023
8	0.003	0.003	0.004	0.000	0.003	0.003	0.004	0.000	0.197	0.086	0.077	0.029	0.197	0.087	0.077	0.029	0.156	0.068	0.061	0.023	0.156	0.068	0.061	0.023
9	0.027	−0.004	0.007	0.000	0.027	−0.004	0.007	0.001	0.156	0.132	0.070	0.032	0.156	0.132	0.070	0.032	0.123	0.102	0.056	0.026	0.123	0.102	0.056	0.026
10	0.018	−0.003	0.005	−0.001	0.018	−0.004	0.005	−0.001	0.217	0.094	0.070	0.028	0.217	0.094	0.070	0.028	0.171	0.075	0.055	0.023	0.171	0.075	0.055	0.023
11	0.115	−0.160	0.004	−0.001	0.115	−0.159	0.004	−0.001	0.740	2.720	0.092	0.027	0.740	2.720	0.092	0.027	0.515	0.825	0.075	0.022	0.515	0.826	0.075	0.022
12	0.007	−0.008	0.004	−0.001	0.007	−0.008	0.004	−0.001	0.159	0.119	0.092	0.027	0.159	0.118	0.092	0.027	0.127	0.093	0.074	0.022	0.127	0.093	0.074	0.022
13	0.015	−0.032	0.006	0.000	0.015	−0.031	0.006	0.000	0.197	0.244	0.089	0.028	0.197	0.244	0.089	0.028	0.152	0.183	0.072	0.022	0.152	0.183	0.072	0.022
14	0.008	0.008	0.013	0.000	0.008	0.009	0.012	0.000	0.171	0.123	0.074	0.033	0.171	0.123	0.074	0.033	0.135	0.097	0.056	0.027	0.135	0.098	0.056	0.027
15	0.019	0.029	0.007	−0.001	0.019	0.034	0.007	−0.001	0.216	0.297	0.074	0.031	0.216	0.297	0.074	0.031	0.167	0.215	0.059	0.024	0.167	0.214	0.059	0.024
16	0.007	−0.098	−0.010	−0.001	0.007	−0.097	−0.009	0.000	0.192	0.492	0.093	0.027	0.192	0.492	0.093	0.027	0.155	0.374	0.073	0.021	0.155	0.374	0.073	0.021
17	−0.001	0.003	−0.001	0.000	−0.001	0.004	−0.001	0.001	0.120	0.153	0.103	0.027	0.120	0.153	0.103	0.027	0.093	0.120	0.083	0.021	0.093	0.120	0.083	0.021
18	0.007	0.001	0.007	−0.001	0.007	0.001	0.007	0.000	0.148	0.112	0.081	0.029	0.148	0.112	0.081	0.029	0.119	0.086	0.064	0.023	0.119	0.086	0.064	0.023
19	0.006	−0.015	0.004	0.000	0.006	−0.015	0.004	0.001	0.144	0.143	0.064	0.033	0.144	0.143	0.064	0.033	0.116	0.113	0.051	0.026	0.116	0.113	0.051	0.026
20	0.037	−0.003	0.009	−0.001	0.037	−0.003	0.008	−0.001	0.209	0.148	0.088	0.029	0.209	0.147	0.088	0.029	0.164	0.118	0.072	0.023	0.164	0.118	0.072	0.023

Note: Data were simulated under the MVN dependence condition. Results show the bias, RMSE, and mean absolute deviance (MAD) recovered using the Gumbel copula model and the MVN model. The MAD is calculated as $\mathrm{MAD}(\eta) = \frac{1}{R}\sum_{r=1}^{R}(|\hat{\eta}^{(r)} - \eta|)$.

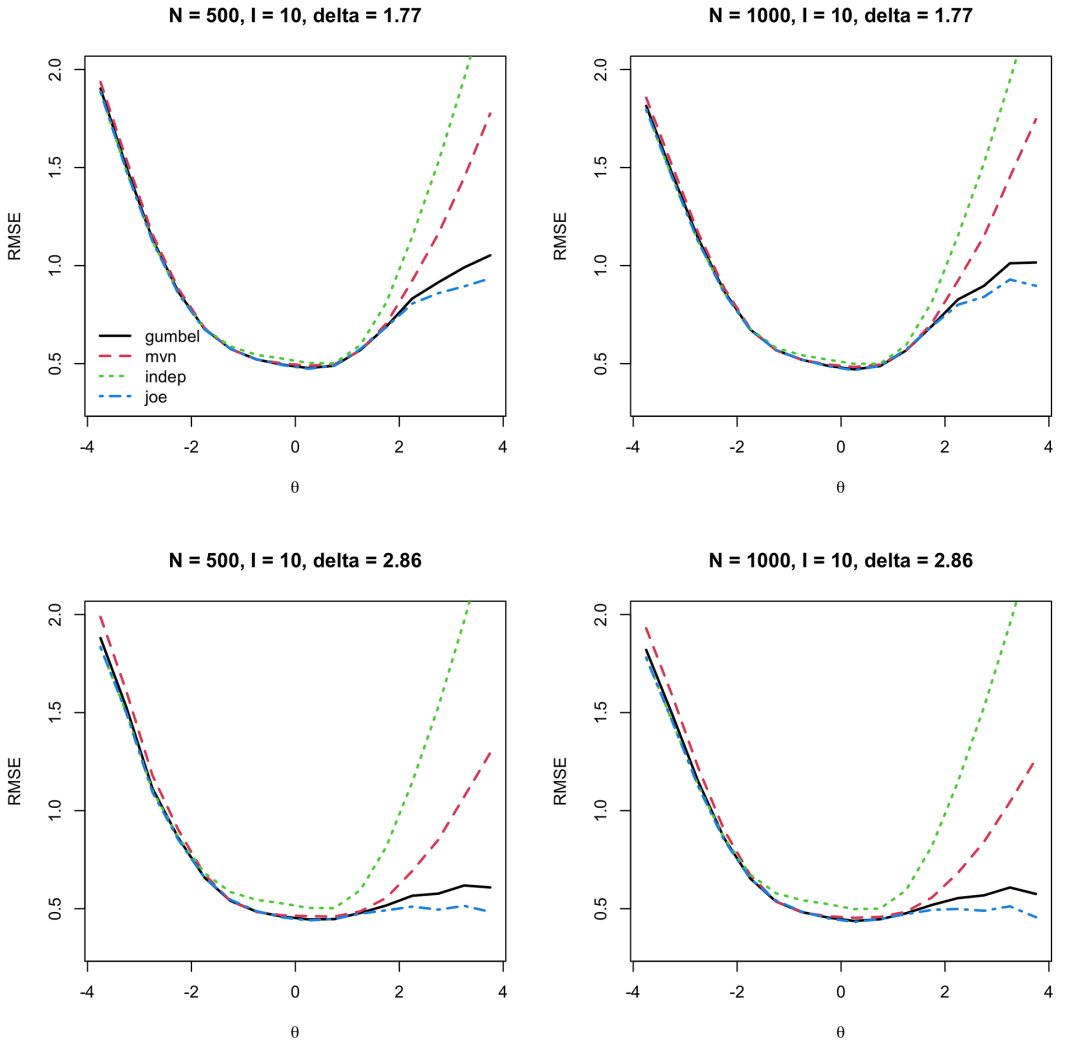


Figure D1. Conditional RMSE of ability estimates under the Joe copula dependence condition.

Downloaded from https://www.cambridge.org/core. 16 Nov 2026 at 02:13:47, subject to the Cambridge Core terms of use.

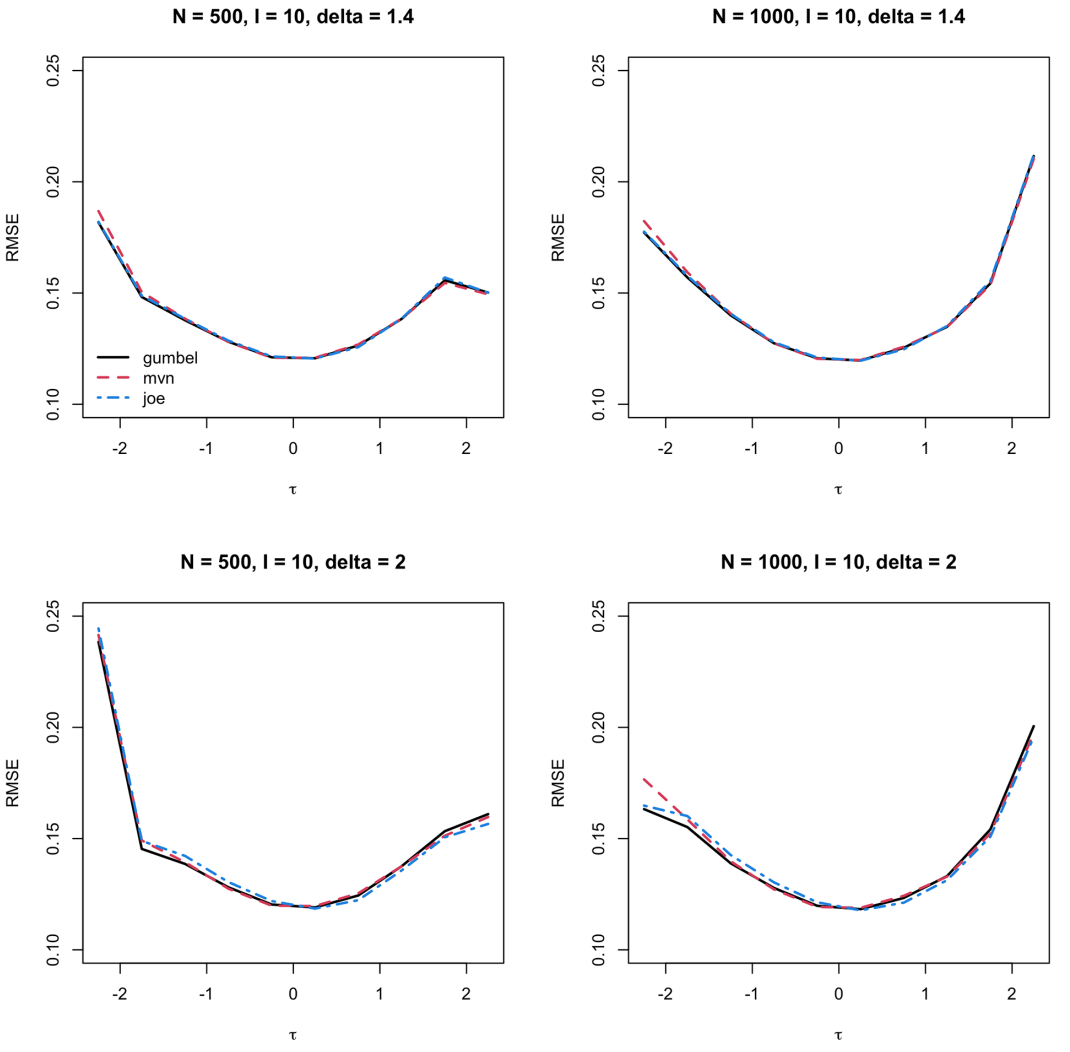


Figure D2. Conditional RMSE of speed estimates under the Gumbel dependence condition.

Downloaded from https://www.cambridge.org/core. 16 Nov 2026 at 02:13:47, subject to the Cambridge Core terms of use.

Appendix E. Additional simulation results: 270°-rotated copulas

Table E1. Model selection result under the 270°-rotated Gumbel copula

Condition			Model				
N	*I*	δ	Gumbel	Joe	MVN	270G	270J
500	10	1.43	0.00	0.00	0.15	0.71	0.14
1,000	10	1.43	0.00	0.00	0.06	0.88	0.07
500	20	1.43	0.00	0.00	0.11	0.79	0.10
1,000	20	1.43	0.00	0.00	0.03	0.94	0.04
500	10	2	0.00	0.00	0.18	0.77	0.04
1,000	10	2	0.00	0.00	0.09	0.91	0.00
500	20	2	0.00	0.00	0.06	0.92	0.02
1,000	20	2	0.00	0.00	0.01	0.99	0.00

Note: τ_K denotes Kendall's τ rank coefficient. 270G and 270J refer to the 270°-rotated Gumbel and Joe copula models, respectively.

Table E2. Model selection result under the 270°-rotated Joe copula

Condition			Model				
N	*I*	δ	Gumbel	Joe	MVN	270G	270J
500	10	1.77	0.00	0.00	0.00	0.16	0.83
1,000	10	1.77	0.00	0.00	0.00	0.11	0.89
500	20	1.77	0.00	0.00	0.00	0.12	0.88
1,000	20	1.77	0.00	0.00	0.00	0.04	0.96
500	10	2.86	0.00	0.00	0.00	0.17	0.83
1,000	10	2.86	0.00	0.00	0.00	0.12	0.88
500	20	2.86	0.00	0.00	0.00	0.05	0.95
1,000	20	2.86	0.00	0.00	0.00	0.02	0.98

Note: τ_K denotes Kendall's τ rank coefficient. 270G and 270J refer to the 270°-rotated Gumbel and Joe copula models, respectively.

Downloaded from https://www.cambridge.org/core. 16 Nov 2026 at 02:13:47, subject to the Cambridge Core terms of use.

Table E3. Parameter recovery under the 270°-rotated Gumbel copula

Condition			Bias						MAD					
N	I	δ	a	b	α	β	δ	σ_τ	a	b	α	β	δ	σ_τ
500	10	1.43	0.010	−0.028	0.014	0.000	−0.006	−0.001	0.149	0.229	0.072	0.023	0.054	0.013
1,000	10	1.43	0.003	0.002	0.009	0.001	−0.009	0.001	0.107	0.153	0.049	0.016	0.039	0.010
500	20	1.43	0.012	−0.032	0.008	0.001	−0.003	−0.001	0.154	0.210	0.067	0.023	0.051	0.013
1,000	20	1.43	0.009	−0.020	0.005	0.001	−0.004	0.001	0.107	0.137	0.048	0.016	0.034	0.009
500	10	2	0.011	−0.013	0.012	−0.001	−0.131	−0.005	0.153	0.227	0.071	0.023	0.139	0.013
1,000	10	2	0.002	−0.015	0.007	−0.001	−0.135	−0.003	0.105	0.140	0.049	0.016	0.137	0.010
500	20	2	0.010	−0.025	0.008	0.000	−0.076	−0.004	0.153	0.213	0.067	0.023	0.096	0.013
1,000	20	2	0.008	−0.016	0.004	0.000	−0.077	−0.003	0.108	0.138	0.048	0.016	0.085	0.009
Condition			RMSE						95% coverage rate					
N	I	δ	a	b	α	β	δ	σ_τ	a	b	α	β	δ	σ_τ
500	10	1.43	0.196	0.740	0.092	0.029	0.068	0.016	0.91	0.95	0.96	1.00	0.97	1.00
1,000	10	1.43	0.139	0.606	0.063	0.020	0.049	0.012	0.89	0.94	0.95	1.00	0.97	1.00
500	20	1.43	0.242	0.673	0.086	0.029	0.063	0.016	0.96	0.98	0.97	0.97	0.98	1.00
1,000	20	1.43	0.158	0.438	0.060	0.020	0.042	0.012	0.95	0.98	0.96	0.97	0.98	0.99
500	10	2	0.202	0.695	0.091	0.029	0.162	0.017	0.90	0.96	0.96	1.00	0.96	1.00
1,000	10	2	0.137	0.467	0.063	0.020	0.152	0.012	0.90	0.96	0.96	1.00	0.92	1.00
500	20	2	0.235	0.662	0.085	0.029	0.119	0.017	0.95	0.98	0.97	0.98	0.96	1.00
1,000	20	2	0.154	0.508	0.060	0.020	0.100	0.012	0.95	0.97	0.96	0.98	0.94	0.98
Condition			SE ratio											
N	I	δ	a	b	α	β	δ	σ_τ						
500	10	1.43	0.93	1.93	1.04	1.60	1.28	1.73						
1,000	10	1.43	0.90	1.30	1.03	1.55	1.22	1.60						
500	20	1.43	1.10	1.58	1.11	1.16	1.29	1.50						
1,000	20	1.43	1.06	1.36	1.05	1.10	1.27	1.39						
500	10	2	0.91	1.57	1.04	3.69	2.16	2.69						
1,000	10	2	0.91	1.41	1.03	3.58	2.05	2.54						
500	20	2	1.08	1.39	1.11	1.29	1.53	1.37						
1,000	20	2	1.01	1.26	1.05	1.21	1.46	1.26						

Note: N represents the sample size. I represents the test length. $\boldsymbol{a}$, $\boldsymbol{b}$, $\boldsymbol{\alpha}$, and $\boldsymbol{\beta}$ represent item parameters, and δ and σ_τ represent structural parameters.

Downloaded from https://www.cambridge.org/core. 16 Nov 2026 at 02:13:47, subject to the Cambridge Core terms of use.

Table E4. Parameter recovery under the 270°-rotated Joe copula

Condition			Bias						MAD					
N	*I*	δ	a	b	α	β	δ	σ_τ	a	b	α	β	δ	σ_τ
500	10	1.77	0.012	−0.004	0.013	−0.002	−0.099	−0.004	0.149	0.230	0.071	0.022	0.120	0.014
1,000	10	1.77	0.006	0.002	0.009	−0.003	−0.103	−0.002	0.103	0.131	0.050	0.016	0.111	0.010
500	20	1.77	0.014	−0.040	0.009	−0.001	−0.058	−0.002	0.153	0.221	0.068	0.022	0.090	0.013
1,000	20	1.77	0.008	−0.011	0.005	−0.002	−0.059	−0.002	0.105	0.130	0.048	0.016	0.078	0.009
500	10	2.86	0.013	−0.009	0.011	−0.007	−0.516	−0.008	0.151	0.247	0.070	0.022	0.516	0.015
1,000	10	2.86	0.005	0.001	0.007	−0.008	−0.500	−0.007	0.103	0.135	0.050	0.017	0.500	0.011
500	20	2.86	0.014	−0.021	0.008	−0.002	−0.336	−0.006	0.153	0.281	0.068	0.022	0.339	0.014
1,000	20	2.86	0.007	−0.013	0.003	−0.003	−0.336	−0.006	0.107	0.134	0.048	0.016	0.336	0.010
Condition			RMSE						95% coverage rate					
N	*I*	δ	a	b	α	β	δ	σ_τ	a	b	α	β	δ	σ_τ
500	10	1.77	0.194	1.548	0.091	0.028	0.143	0.018	0.91	0.94	0.96	0.97	0.90	0.93
1,000	10	1.77	0.135	0.300	0.064	0.021	0.129	0.012	0.91	0.94	0.95	0.96	0.83	0.93
500	20	1.77	0.259	1.083	0.087	0.028	0.110	0.017	0.96	0.98	0.96	0.97	0.98	0.97
1,000	20	1.77	0.153	0.252	0.061	0.020	0.096	0.012	0.95	0.97	0.95	0.95	0.93	0.97
500	10	2.86	0.200	1.186	0.090	0.028	0.537	0.019	0.90	0.94	0.96	0.98	0.45	0.92
1,000	10	2.86	0.134	0.362	0.063	0.022	0.514	0.014	0.89	0.94	0.95	0.96	0.14	0.87
500	20	2.86	0.244	2.716	0.087	0.028	0.367	0.018	0.95	0.98	0.97	0.97	0.77	0.96
1,000	20	2.86	0.164	0.278	0.061	0.020	0.356	0.013	0.93	0.97	0.96	0.96	0.45	0.93
Condition			SE ratio											
N	*I*	δ	a	b	α	β	δ	σ_τ						
500	10	1.77	0.93	1.16	1.04	1.14	1.36	1.00						
1,000	10	1.77	0.92	1.10	1.01	1.07	1.23	1.02						
500	20	1.77	1.08	1.45	1.09	1.10	1.49	1.17						
1,000	20	1.77	1.03	1.31	1.04	1.02	1.22	1.13						
500	10	2.86	0.88	1.06	1.04	1.22	1.67	1.02						
1,000	10	2.86	0.88	1.06	1.02	1.14	1.47	0.99						
500	20	2.86	1.03	1.47	1.09	1.19	1.66	1.18						
1,000	20	2.86	0.97	1.19	1.04	1.10	1.40	1.10						

Note: *N* represents the sample size. *I* represents the test length. $\boldsymbol{a}$, $\boldsymbol{b}$, $\boldsymbol{\alpha}$, and $\boldsymbol{\beta}$ represent item parameters, and δ and σ_τ represent structural parameters.

Downloaded from https://www.cambridge.org/core. 16 Nov 2026 at 02:13:47, subject to the Cambridge Core terms of use.

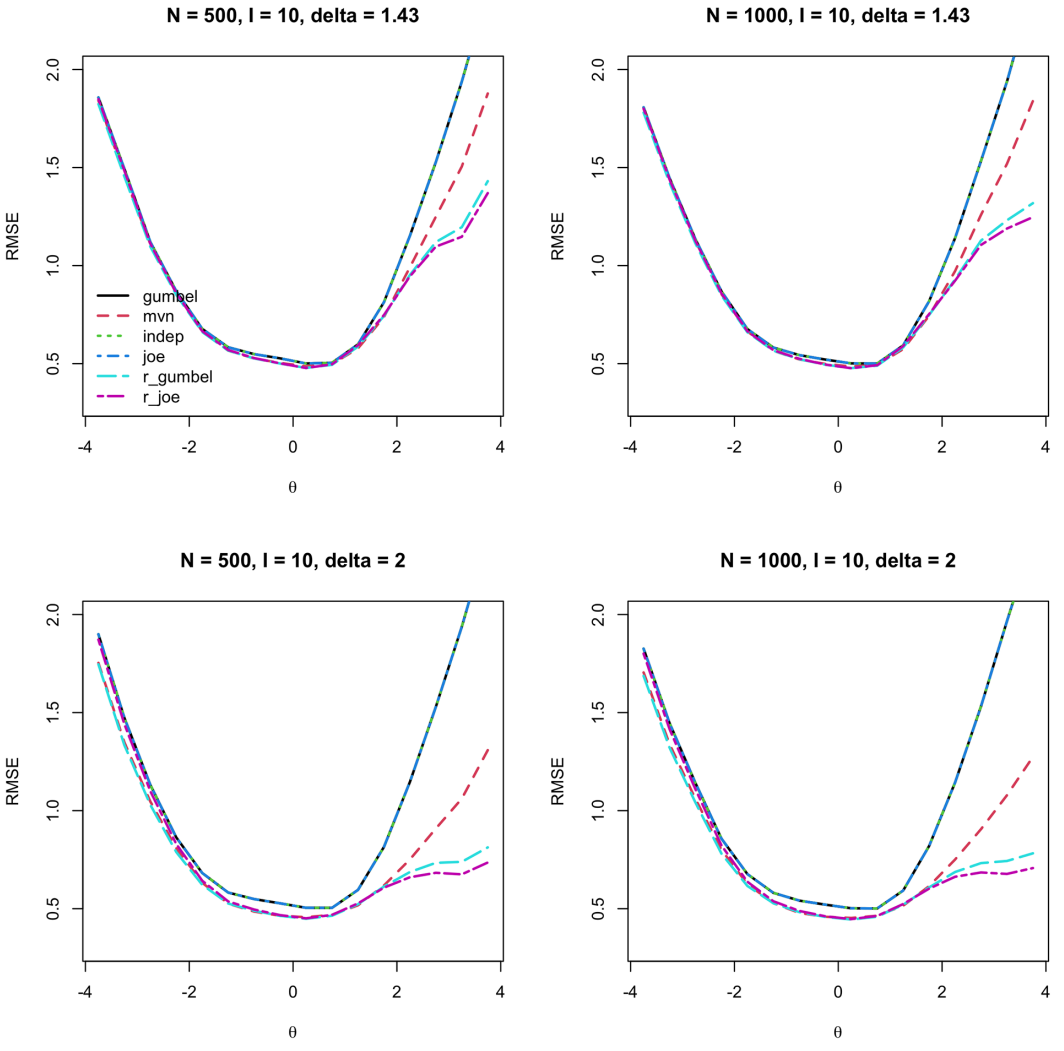


Figure E1. Conditional RMSE of ability estimates under the 270°-rotated Gumbel copula.

Downloaded from https://www.cambridge.org/core. 16 Nov 2026 at 02:13:47, subject to the Cambridge Core terms of use.

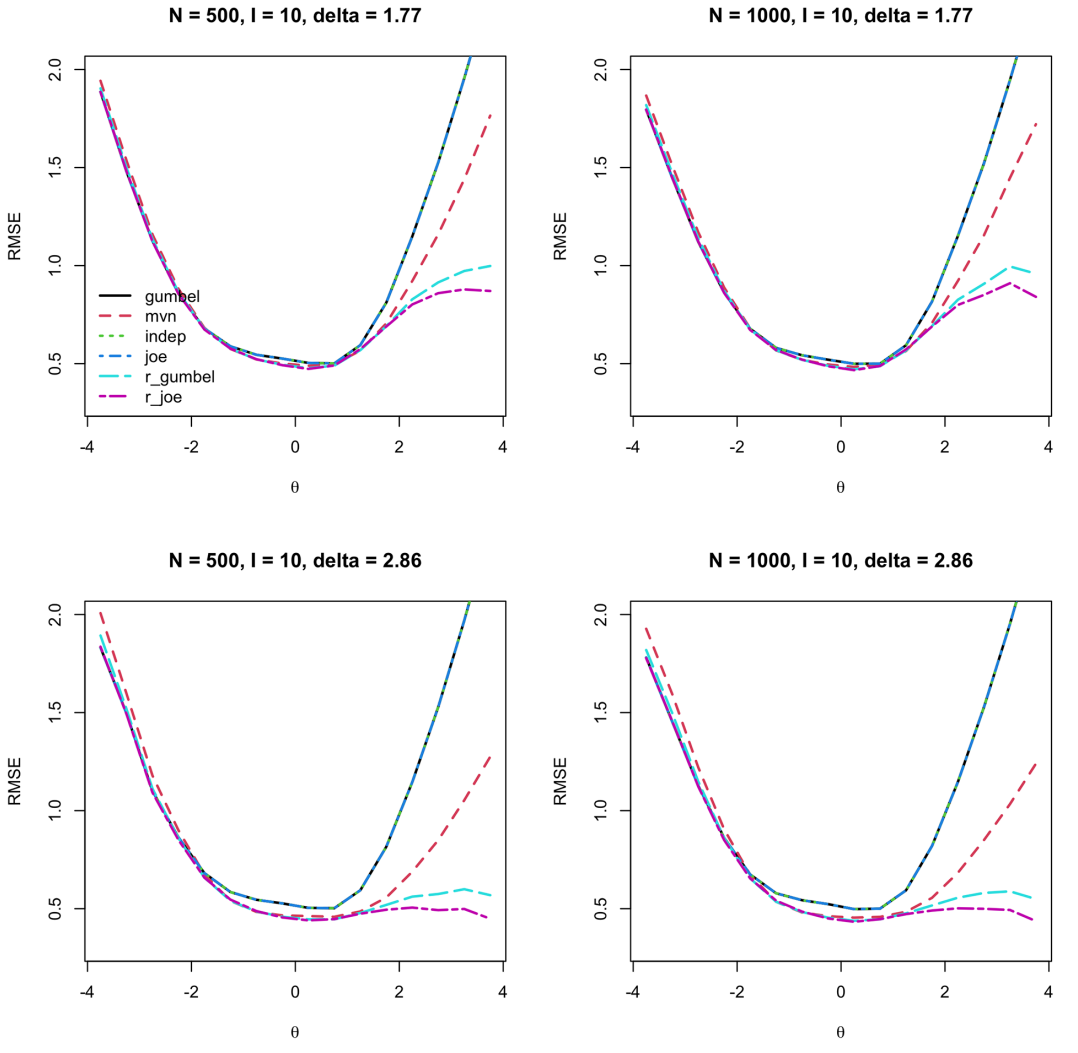


Figure E2. Conditional RMSE of ability estimates under the 270°-rotated Joe copula.

Downloaded from https://www.cambridge.org/core. 16 Nov 2026 at 02:13:47, subject to the Cambridge Core terms of use.

Appendix F. Empirical data analysis results

Table F1. Dependence parameter estimates from the empirical data analyses

Dataset	Selected model	Dependence parameter estimates								
		MVN	Gumbel	Joe	90G	90J	180G	180J	270G	270J
addition	MVN	−0.44	1.00	1.00	1.21	1.38	1.00	1.00	1.45	1.62
multiplication	MVN	−0.50	1.00	1.00	1.49	1.63	1.00	1.00	1.63	1.79
set	270G	−0.33	1.00	1.00	1.31	1.30	1.00	1.00	1.37	1.43
letterchaos	270G	−0.26	1.00	1.00	1.10	1.09	1.00	1.00	1.27	1.35
subtraction	MVN	−0.58	1.00	1.00	1.56	1.64	1.00	1.00	1.67	2.01
nomt	MVN	−0.47	1.00	1.00	1.14	1.35	1.00	1.00	1.22	1.32
pisa_math_C1_DEU	MVN	−0.17	1.00	1.02	1.29	1.19	1.04	1.00	1.00	1.19
pisa_math_C1_JPN	MVN	−0.23	1.00	1.02	1.34	1.49	1.00	1.00	1.28	1.46
pisa_math_C1_MEX	90J	−0.42	1.00	1.00	1.41	1.65	1.00	1.00	1.31	1.35
pisa_math_C1_NZL	MVN	−0.24	1.00	1.00	1.14	1.40	1.02	1.04	1.24	1.19
pisa_math_C1_USA	90J	−0.31	1.00	1.00	1.25	1.38	1.00	1.00	1.20	1.18
pisa_math_C2_DEU	MVN	−0.25	1.01	1.05	1.39	1.61	1.00	1.00	1.06	1.58
pisa_math_C2_JPN	90J	−0.45	1.00	1.00	1.46	1.82	1.00	1.00	1.53	1.76
pisa_math_C2_MEX	MVN	−0.34	1.00	1.00	1.34	1.46	1.00	1.00	1.24	1.31
pisa_math_C2_NZL	MVN	−0.24	1.00	1.00	1.35	1.59	1.00	1.00	1.21	1.15
pisa_math_C2_USA	90G	−0.42	1.00	1.00	1.33	1.53	1.00	1.00	1.36	1.40
pisa_math_C3_DEU	MVN	−0.17	1.00	1.00	1.22	1.31	1.01	1.04	1.06	1.00
pisa_math_C3_JPN	MVN	−0.31	1.00	1.00	1.29	1.41	1.00	1.00	1.29	1.15
pisa_math_C3_MEX	90J	−0.21	1.00	1.00	1.18	1.29	1.00	1.00	1.07	1.04
pisa_math_C3_NZL	270G	−0.13	1.00	1.00	1.18	1.24	1.00	1.00	1.06	1.00
pisa_math_C3_USA	90J	−0.31	1.00	1.00	1.23	1.35	1.00	1.00	1.18	1.10
pisa_science_C1_DEU	MVN	−0.36	1.00	1.00	1.35	1.42	1.00	1.00	1.27	1.17
pisa_science_C1_JPN	90J	−0.43	1.00	1.00	1.40	1.49	1.00	1.00	1.40	1.35
pisa_science_C1_MEX	90J	−0.30	1.00	1.00	1.24	1.38	1.00	1.00	1.19	1.21
pisa_science_C1_NZL	90J	−0.37	1.00	1.00	1.25	1.39	1.00	1.00	1.28	1.22
pisa_science_C1_USA	90J	−0.38	1.00	1.00	1.31	1.47	1.00	1.00	1.29	1.24
pisa_science_C2_DEU	90J	−0.38	1.00	1.00	1.26	1.36	1.00	1.00	1.31	1.25
pisa_science_C2_JPN	90J	−0.38	1.00	1.00	1.28	1.37	1.00	1.00	1.37	1.27
pisa_science_C2_MEX	90J	−0.34	1.00	1.00	1.28	1.45	1.00	1.00	1.23	1.25
pisa_science_C2_NZL	90J	−0.35	1.00	1.00	1.23	1.36	1.00	1.00	1.25	1.16
pisa_science_C2_USA	90J	−0.43	1.00	1.00	1.37	1.57	1.00	1.00	1.34	1.31
pisa_science_C3_DEU	90J	−0.29	1.00	1.00	1.22	1.26	1.00	1.00	1.21	1.12
pisa_science_C3_JPN	90J	−0.37	1.00	1.00	1.26	1.37	1.00	1.00	1.27	1.12
pisa_science_C3_MEX	90J	−0.44	1.00	1.00	1.39	1.64	1.00	1.00	1.34	1.44
pisa_science_C3_NZL	90J	−0.39	1.00	1.00	1.24	1.36	1.00	1.00	1.30	1.17
pisa_science_C3_USA	90J	−0.50	1.00	1.00	1.43	1.61	1.00	1.00	1.47	1.47

Note: C1–C3 represent clusters 1–3. The dependence parameter was ρ for the MVN model and δ for the remaining models.

Downloaded from https://www.cambridge.org/core. 16 Nov 2026 at 02:13:47, subject to the Cambridge Core terms of use.

Downloaded from https://www.cambridge.org/core. 16 Nov 2026 at 02:13:47, subject to the Cambridge Core terms of use.

Table F2. Cross-validation results from the empirical data analyses

Dataset	Selected model	Log-likelihood								
		MVN	Gumbel	Joe	90G	90J	180G	180J	270G	270J
pisa_math_C1_fold_1	90J	−34,187.3	−34,186.3	−34,188.5	−34,178.8	**−34,175.3**	−34,186.2	−34,187.9	−34,188.5	−34,188.4
pisa_math_C1_fold_2	MVN	**−34,174.2**	−34,466.5	−34,539.8	−34,598.6	−34,637.1	−34,479.3	−34,405.6	−34,465.9	−34,239.3
pisa_math_C1_fold_3	90J	−34,129.7	−34,129.6	−34,129.6	−34,124.6	**−34,121.4**	−34,127.3	−34,125.5	−34,129.6	−34,129.6
pisa_math_C1_fold_4	270J	−33,986.2	−34,423.2	−34,419.8	−34,348.6	−34,481.1	−34,491.9	−34,420.1	−34,326.4	**−33,985.9**
pisa_math_C1_fold_5	90J	−34,205.4	−34,205.0	−34,205.1	−34,198.7	**−34,194.9**	−34,205.1	−34,204.9	−34,204.9	−34,205.3
pisa_math_C2_fold_1	90J	−42,950.5	−42,960.3	−42,960.7	−42,936.7	**−42,933.3**	−42,960.7	−42,961.0	−42,958.9	−42,961.0
pisa_math_C2_fold_2	90J	−43,086.9	−43,088.0	−43,087.9	−43,082.3	**−43,080.8**	−43,087.4	−43,087.9	−43,088.1	−43,088.5
pisa_math_C2_fold_3	90J	−42,887.8	−42,895.1	−42,895.1	−42,883.6	**−42,883.4**	−42,895.0	−42,895.2	−42,894.3	−42,895.1
pisa_math_C2_fold_4	90J	−42,952.4	−43,124.1	−43,073.2	−43,030.0	**−42,951.0**	−43,069.1	−43,130.6	−42,956.5	−42,957.0
pisa_math_C2_fold_5	90J	−43,162.7	−43,172.6	−43,172.5	−43,155.0	**−43,152.8**	−43,172.7	−43,172.5	−43,170.4	−43,172.9
pisa_math_C3_fold_1	90J	−41,738.6	−41,743.4	−41,743.3	−41,723.2	**−41,716.7**	−41,743.3	−41,742.6	−41,743.1	−41,743.3
pisa_math_C3_fold_2	90J	−41,984.7	−41,984.1	−41,984.5	−41,977.6	**−41,974.9**	−41,983.1	−41,981.8	−41,984.2	−41,984.2
pisa_math_C3_fold_3	90J	−41,872.5	−41,874.8	−41,874.8	−41,866.1	**−41,862.3**	−41,874.7	−41,874.6	−41,874.7	−41,874.5
pisa_math_C3_fold_4	90J	−41,759.6	−41,759.3	−41,759.2	−41,754.2	**−41,752.3**	−41,757.1	−41,755.5	−41,759.2	−41,759.4
pisa_math_C3_fold_5	90J	−41,845.2	−41,844.6	−41,844.1	−41,835.6	**−41,832.4**	−41,844.0	−41,843.0	−41,845.1	−41,845.7
pisa_science_C1_fold_1	90J	−49,614.6	−49,623.4	−49,623.3	−49,608.6	**−49,603.9**	−49,623.3	−49,623.4	−49,622.0	−49,623.3
pisa_science_C1_fold_2	90J	−49,758.8	−49,765.8	−49,765.8	−49,756.6	**−49,755.3**	−49,765.8	−49,765.8	−49,763.8	−49,765.9
pisa_science_C1_fold_3	90J	−49,791.2	−49,802.0	−49,802.0	−49,787.0	**−49,784.1**	−49,802.0	−49,802.0	−49,798.5	−49,802.3
pisa_science_C1_fold_4	90J	−49,794.9	−49,799.3	−49,799.3	−49,787.7	**−49,783.1**	−49,799.3	−49,798.6	−49,799.3	−49,799.3

(Continued)

Downloaded from https://www.cambridge.org/core. 16 Nov 2026 at 02:13:47, subject to the Cambridge Core terms of use.

Table F2. Continued

Dataset	Selected model	Log-likelihood								
		MVN	Gumbel	Joe	90G	90J	180G	180J	270G	270J
pisa_science_C1_fold_5	90J	−49,933.2	−49,941.5	−49,941.5	−49,930.7	**−49,928.6**	−49,941.5	−49,941.5	−49,939.2	−49,941.6
pisa_science_C2_fold_1	90J	−58,473.7	−58,491.8	−58,491.8	−58,466.9	**−58,462.9**	−58,491.8	−58,491.8	−58,486.5	−58,492.2
pisa_science_C2_fold_2	90J	−58,435.9	−58,445.1	−58,445.1	−58,429.8	**−58,426.2**	−58,445.1	−58,445.1	−58,444.3	−58,445.1
pisa_science_C2_fold_3	90J	−58,648.4	−58,661.6	−58,661.6	−58,644.6	**−58,641.7**	−58,661.6	−58,661.6	−58,658.7	−58,661.6
pisa_science_C2_fold_4	90J	−58,564.5	−58,593.6	−58,594.2	−58,558.1	**−58,556.2**	−58,593.7	−58,593.8	−58,577.9	−58,592.7
pisa_science_C2_fold_5	90J	−58,537.6	−58,551.7	−58,551.7	−58,526.7	**−58,520.5**	−58,551.7	−58,551.7	−58,548.4	−58,551.7
pisa_science_3C3_fold_1	90J	−60,278.9	−60,290.8	−60,290.8	−60,270.2	**−60,264.0**	−60,290.8	−60,290.8	−60,289.8	−60,290.8
pisa_science_C3_fold_2	90J	−60,040.9	−60,049.8	−60,049.6	−60,032.1	**−60,026.1**	−60,049.7	−60,049.9	−60,049.1	−60,049.6
pisa_science_C3_fold_3	90J	−59,808.2	−59,818.1	−59,818.1	−59,801.0	**−59,796.2**	−59,818.1	−59,818.1	−59,816.7	−59,818.1
pisa_science_C3_fold_4	90J	−60,206.8	−60,227.4	−60,227.4	−60,192.2	**−60,182.7**	−60,227.4	−60,227.4	−60,222.7	−60,227.4
pisa_science_C3_fold_5	90J	−59,782.8	−59,807.3	−59,807.5	−59,778.7	**−59,776.2**	−59,807.3	−59,807.8	−59,797.7	−59,807.8

Note: C1–C3 represent clusters 1–3. Folds 1–5 refer to the five cross-validation folds.

Downloaded from https://www.cambridge.org/core. 16 Nov 2026 at 02:13:47, subject to the Cambridge Core terms of use.

Table F3. Model selection results with BIC values from the empirical data analyses

Dataset	Selected model	BIC									
		MVN	Gumbel	Joe	90G	90J	180G	180J	270G	270J	CD
addition	MVN	**141,715.4**	148,237.8	147,395.9	145,928.7	141,754.6	147,885.1	148,101.0	146,526.0	146,175.8	142,036.7
multiplication	MVN	**508,504.0**	526,665.9	523,915.9	526,630.9	526,634.3	537,508.5	517,040.4	516,385.8	523,879.2	508,692.5
subtraction	CD	396,848.9	397,194.8	397,194.5	396,920.4	396,986.7	397,194.5	397,194.5	404,556.3	405,114.0	**396,600.5**
set	CD	150,659.6	150,717.7	151,355.9	150,679.9	150,690.8	151,167.5	150,717.7	150,651.7	151,282.8	**150,578.7**
letterchaos	270G	41,486.1	41,503.7	41,503.7	41,496.6	41,500.4	41,503.9	41,503.8	**41,480.8**	41,482.0	41,780.4
nomt	MVN	**249,563.5**	255,147.7	254,530.8	263,308.8	256,939.3	254,742.2	255,570.0	255,003.8	249,659.4	253,645.8
pisa_math_C1_DEU	MVN	**55,432.8**	57,706.7	56,263.0	56,262.4	57,739.7	56,263.1	56,263.0	57,738.1	57,737.8	55,476.2
pisa_math_C1_JPN	MVN	**54,018.7**	55,840.1	54,548.6	54,547.8	54,547.7	54,548.6	54,548.6	55,920.7	54,548.3	54,084.9
pisa_math_C1_MEX	90J	80,405.4	80,456.4	80,456.4	80,390.6	**80,383.7**	80,456.6	80,456.5	80,424.5	80,443.4	80,516.4
pisa_math_C1_NZL	MVN	**67,852.0**	70,650.1	68,943.2	70,166.0	68,942.2	68,943.3	68,943.3	68,942.8	69,477.3	–
pisa_math_C1_USA	90J	81,955.8	81,986.5	81,985.9	81,936.6	**81,933.0**	81,985.9	81,985.4	1,971.3	81,985.7	82,045.7
pisa_math_C2_DEU	MVN	**72,295.7**	73,422.0	73,422.1	73,421.1	73,421.1	73,422.0	73,422.0	75,504.1	73,421.3	–
pisa_math_C2_JPN	90J	79,808.8	79,884.4	79,884.7	79,799.0	**79,797.4**	79,881.8	79,882.1	79,828.0	79,867.1	79,842.5
pisa_math_C2_MEX	CD	104,317.8	104,361.1	104,361.1	104,322.1	104,327.7	104,361.1	104,361.2	104,333.5	104,345.8	**104,302.7**
pisa_math_C2_NZL	CD	86,391.4	87,472.5	87,539.7	87,347.3	87,280.1	87,282.4	87,274.9	87,009.3	86,416.7	**86,314.6**
pisa_math_C2_USA	90G	85,557.5	85,630.4	85,630.3	**85,554.9**	85,557.6	85,630.4	85,630.4	85,582.4	85,611.1	85,630.9
pisa_math_C3_DEU	CD	65,132.9	65,140.2	65,140.5	65,579.6	65,442.0	65,141.0	65,139.7	65,141.0	65,141.5	**65,029.1**
pisa_math_C3_JPN	MVN	**78,138.6**	78,710.1	79,051.9	79,257.9	78,938.8	78,692.9	79,072.6	78,664.0	78,176.5	78,157.8
pisa_math_C3_MEX	90J	104,851.7	104,870.5	104,870.4	104,842.8	**104,837.6**	104,870.5	104,870.4	104,866.3	104,870.5	104,856.0
pisa_math_C3_NZL	CD	83,725.0	83,727.8	83,727.4	84,054.4	84,362.9	83,725.9	83,727.4	83,724.3	83,728.1	**83,581.2**
pisa_math_C3_USA	CD	84,244.4	84,280.8	84,280.2	84,214.5	84,203.9	84,280.7	84,280.6	84,265.6	84,279.9	**84,176.0**
pisa_science_C1_DEU	MVN	**103,701.9**	103,748.4	103,748.3	104,630.4	105,152.2	103,747.7	103,747.8	103,728.6	103,749.5	103,745.9
pisa_science_C1_JPN	90J	100,472.8	100,540.6	100,540.3	100,455.4	**100,447.1**	100,540.2	100,540.2	100,498.1	100,532.1	100,493.1

(Continued)

Downloaded from https://www.cambridge.org/core. 16 Nov 2026 at 02:13:47, subject to the Cambridge Core terms of use.

Table F3. Continued

Dataset	Selected model	BIC									
		MVN	Gumbel	Joe	90G	90J	180G	180J	270G	270J	CD
pisa_science_C1_MEX	90J	157,546.7	157,593.0	157,593.0	157,538.9	**157,536.1**	157,593.0	157,593.0	157,564.2	157,579.1	157,709.0
pisa_science_C1_NZL	90J	133,818.3	133,884.3	133,884.1	133,794.8	**133,786.7**	133,884.3	133,884.4	133,846.6	133,878.2	133,874.4
pisa_science_C1_USA	90J	131,639.6	131,709.7	131,709.7	131,620.4	**131,610.4**	131,709.7	131,709.7	131,666.4	131,700.6	131,721.5
pisa_science_C2_DEU	90J	87,359.6	87,409.1	87,409.1	87,347.8	**87,343.8**	87,409.0	87,409.0	87,381.1	87,406.8	87,366.4
pisa_science_C2_JPN	CD	110,413.6	110,471.3	110,471.0	110,410.4	110,406.4	110,471.4	110,471.7	110,441.5	110,470.3	**110,251.9**
pisa_science_C2_MEX	90J	144,744.0	144,804.7	144,804.7	144,741.2	**144,740.1**	144,804.6	144,804.7	144,771.8	144,794.2	144,763.8
pisa_science_C2_NZL	CD	120,547.4	120,602.4	120,602.1	120,523.2	120,513.8	120,602.1	120,602.1	120,574.0	120,601.8	**120,506.1**
pisa_science_C2_USA	90J	118,156.4	118,249.8	118,249.8	118,140.2	**118,131.8**	118,249.8	118,249.8	118,200.4	118,243.2	118,163.4
pisa_science_C3_DEU	90J	81,734.1	81,759.7	81,757.5	81,723.9	**81,719.6**	81,759.7	81,759.6	81,749.3	81,761.4	81,854.6
pisa_science_C3_JPN	90J	110,852.1	110,913.8	110,913.8	110,832.6	**110,823.8**	110,913.8	110,913.8	110,885.7	110,913.0	110,892.3
pisa_science_C3_MEX	90J	155,649.8	155,751.5	155,751.5	155,638.7	**155,631.3**	155,751.5	155,751.5	155,689.0	155,729.6	155,736.8
pisa_science_C3_NZL	90J	127,215.2	127,285.6	127,285.7	127,190.6	**127,180.4**	127,285.8	127,285.3	127,246.7	127,284.4	127,238.1
pisa_science_C3_USA	90J	120,015.8	120,143.1	120,143.1	120,008.3	**120,002.5**	120,143.1	120,143.1	120,056.3	120,116.7	–

Note: C1–C3 represent clusters 1–3.

Downloaded from https://www.cambridge.org/core. 16 Nov 2026 at 02:13:47, subject to the Cambridge Core terms of use.

Table F4. Model selection results with AIC values from the empirical data analyses

Dataset	Selected model	AIC									
		MVN	Gumbel	Joe	90G	90J	180G	180J	270G	270J	CD
addition	MVN	**141,145.5**	147,668.0	146,826.0	145,358.9	141,184.8	147,315.3	147,531.1	145,956.1	145,606.0	141,186.6
multiplication	CD	507,769.8	525,931.8	523,181.7	525,896.7	525,900.1	536,774.3	516,306.2	515,651.6	523,145.1	**507,597.2**
subtraction	CD	396,154.3	396,500.2	396,499.9	396,225.8	396,292.2	396,499.9	396,500.0	403,861.8	404,419.5	**395,564.3**
set	CD	150,412.6	150,470.6	151,108.8	150,432.9	150,443.8	150,920.5	150,470.6	150,404.7	151,035.8	**150,214.1**
letterchaos	270G	41,297.0	41,314.6	41,314.5	41,307.5	41,311.3	41,314.7	41,314.7	**41,291.7**	41,292.9	41,501.3
nomt	MVN	**247,272.6**	252,856.8	252,239.8	261,017.8	254,648.3	252,451.2	253,279.1	252,712.8	247,368.4	250,213.3
pisa_math_C1_DEU	CD	55,231.8	57,505.8	56,062.1	56,061.5	57,538.8	56,062.2	56,062.1	57,537.2	57,536.9	**55,178.8**
pisa_math_C1_JPN	CD	53,819.2	55,640.6	54,349.1	54,348.3	54,348.3	54,349.1	54,349.1	55,721.2	54,348.9	**53,789.7**
pisa_math_C1_MEX	90J	80,188.3	80,239.3	80,239.4	80,173.6	**80,166.6**	80,239.6	80,239.5	80,207.5	80,226.3	80,195.2
pisa_math_C1_NZL	MVN	**67,641.5**	70,439.7	68,732.8	69,955.5	68,731.8	68,732.9	68,732.9	68,732.3	69,266.9	–
pisa_math_C1_USA	90J	81,736.5	81,767.2	81,766.7	81,717.3	**81,713.7**	81,766.6	81,766.1	81,752.1	81,766.5	81,721.2
pisa_math_C2_DEU	MVN	**72,095.0**	73,221.3	73,221.4	73,220.4	73,220.4	73,221.3	73,221.3	75,303.4	73,220.6	–
pisa_math_C2_JPN	CD	79,604.1	79,679.7	79,680.0	79,594.2	79,592.7	79,677.1	79,677.4	79,623.3	79,662.3	**79,539.9**
pisa_math_C2_MEX	CD	104,101.6	104,144.9	104,144.9	104,105.9	104,111.5	104,144.9	104,145.0	104,117.3	104,129.6	**103,983.1**
pisa_math_C2_NZL	CD	86,182.6	87,263.6	87,330.8	87,138.5	87,071.2	87,073.5	87,066.1	86,800.4	86,207.8	**86,005.9**
pisa_math_C2_USA	CD	85,350.0	85,422.9	85,422.7	85,347.4	85,350.1	85,422.9	85,422.8	85,374.9	85,403.5	**85,324.1**
pisa_math_C3_DEU	CD	64,936.8	64,944.1	64,944.4	65,383.5	65,245.9	64,944.9	64,943.6	64,944.8	64,945.3	**64,739.2**
pisa_math_C3_JPN	CD	77,933.8	78,505.3	78,847.2	79,053.2	78,734.1	78,488.2	78,867.9	78,459.3	77,971.8	**77,855.1**
pisa_math_C3_MEX	CD	104,635.1	104,653.9	104,653.7	104,626.1	104,621.0	104,653.8	104,653.7	104,649.7	104,653.9	**104,535.7**
pisa_math_C3_NZL	CD	83,517.0	83,519.8	83,519.4	83,846.3	84,154.9	83,517.8	83,519.4	83,516.3	83,520.1	**83,273.7**
pisa_math_C3_USA	CD	84,036.8	84,073.2	84,072.7	84,006.9	83,996.4	84,073.1	84,073.1	84,058.0	84,072.3	**83,869.2**

(Continued)

Downloaded from https://www.cambridge.org/core. 16 Nov 2026 at 02:13:47, subject to the Cambridge Core terms of use.

Table F4. Continued

Dataset	Selected model	AIC									
		MVN	Gumbel	Joe	90G	90J	180G	180J	270G	270J	CD
pisa_science_C1_DEU	CD	103,357.8	103,404.3	103,404.1	104,286.3	104,808.1	103,403.6	103,403.7	103,384.5	103,405.4	**103,233.9**
pisa_science_C1_JPN	CD	100,130.0	100,197.9	100,197.5	100,112.7	100,104.3	100,197.4	100,197.4	100,155.4	100,189.4	**99,983.2**
pisa_science_C1_MEX	CD	157,169.5	157,215.9	157,215.9	157,161.7	157,158.9	157,215.8	157,215.8	157,187.1	157,201.9	**157,147.8**
pisa_science_C1_NZL	CD	133,466.9	133,532.9	133,532.6	133,443.3	133,435.3	133,532.9	133,532.9	133,495.2	133,526.8	**133,351.7**
pisa_science_C1_USA	CD	131,276.9	131,347.0	131,347.0	131,257.7	131,247.7	131,347.0	131,347.0	131,303.7	131,337.9	**131,181.9**
pisa_science_C2_DEU	CD	87,068.6	87,118.1	87,118.1	87,056.8	87,052.8	87,118.0	87,118.1	87,090.1	87,115.8	**86,934.1**
pisa_science_C2_JPN	CD	110,106.4	110,164.1	110,163.8	110,103.2	110,099.2	110,164.2	110,164.5	110,134.3	110,163.1	**109,795.5**
pisa_science_C2_MEX	CD	144,419.2	144,479.9	144,479.9	144,416.4	144,415.3	144,479.8	144,479.9	144,447.0	144,469.4	**144,281.2**
pisa_science_C2_NZL	CD	120,234.0	120,289.0	120,288.7	120,209.8	120,200.5	120,288.7	120,288.7	120,260.6	120,288.4	**120,040.5**
pisa_science_C2_USA	CD	117,845.2	117,938.6	117,938.6	117,829.0	117,820.6	117,938.6	117,938.6	117,889.2	117,932.0	**117,701.1**
pisa_science_C3_DEU	CD	81,418.6	81,444.2	81,442.0	81,408.4	81,404.0	81,444.2	81,444.1	81,433.8	81,445.9	**81,385.4**
pisa_science_C3_JPN	CD	110,509.9	110,571.6	110,571.6	110,490.5	110,481.6	110,571.6	110,571.6	110,543.5	110,570.8	**110,383.5**
pisa_science_C3_MEX	CD	155,287.9	155,389.6	155,389.6	155,276.8	155,269.3	155,389.6	155,389.6	155,327.1	155,367.7	**155,198.6**
pisa_science_C3_NZL	CD	126,865.7	126,936.2	126,936.3	126,841.2	126,831.0	126,936.4	126,935.8	126,897.2	126,935.0	**126,718.4**
pisa_science_C3_USA	90J	119,671.8	119,799.1	119,799.1	119,664.3	**119,658.5**	119,799.1	119,799.1	119,712.3	119,772.7	–

Note: C1–C3 represent clusters 1–3.

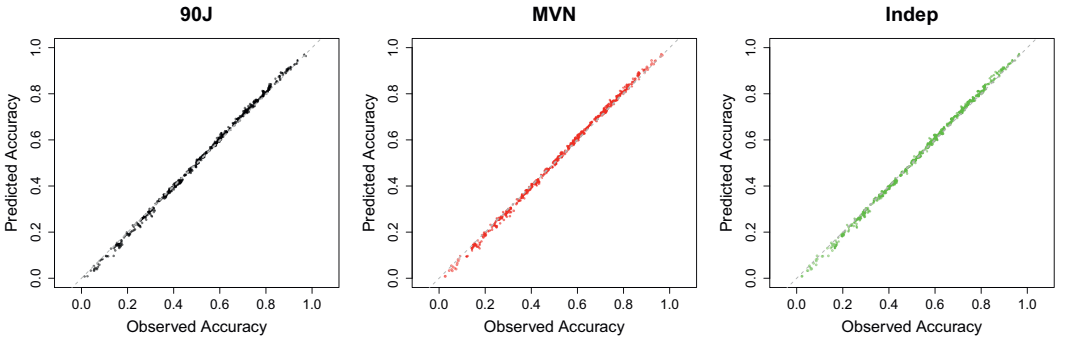


Figure F1. Item-level predicted accuracy versus observed accuracy from the 2018 PISA Math and Science Data.

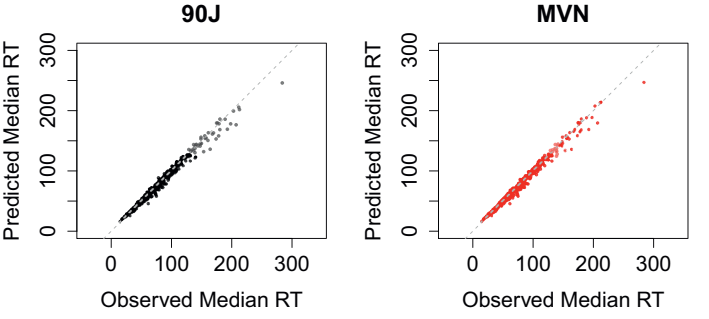


Figure F2. Item-level predicted median RT versus observed median RT from the 2018 PISA Math and Science Data.

Cite this article: Kwon, S. and Zhang, S. (2026). A Copula-Based Joint Model for Speed and Accuracy. *Psychometrika*, 1–57. https://doi.org/10.1017/psy.2026.10143

Downloaded from https://www.cambridge.org/core. 16 Nov 2026 at 02:13:47, subject to the Cambridge Core terms of use.